H_2 PRODUCTION IN PALLADIUM & PALLADIUM–COPPER MEMBRANE REACTORS AT 1173K IN THE PRESENCE OF H_2S

by

Osemwengie Uyi Iyoha

B.S. in Chemical Engineering, Clark Atlanta University, 2002

M.S. in Chemical Engineering, University of Pittsburgh, 2005

Submitted to the Graduate Faculty of

the School of Engineering in partial fulfillment

of the requirements for the degree of

Doctor of Philosophy

University of Pittsburgh

2007

UNIVERSITY OF PITTSBURGH

SCHOOL OF ENGINEERING

This dissertation was presented

by

Osemwengie Uyi Iyoha

It was defended on

March 05, 2007

and approved by

Irving Wender, Professor, Chemical and Petroleum Engineering Department

Anthony Cugini, Professor, U.S. DOE, National Energy Technology Laboratory

Götz Veser, Assistant Professor, Chemical and Petroleum Engineering Department

Gerald Meier, Professor, Mechanical Engineering and Materials Science Department

Dissertation Director: Robert Enick, Chairman, Chemical and Petroleum Engineering Department

H_2 PRODUCTION IN PALLADIUM & PALLADIUM–COPPER MEMBRANE REACTORS AT 1173K IN THE PRESENCE OF H_2S

Osemwengie Uyi Iyoha, Ph.D.

University of Pittsburgh, 2007

The efficacy of producing high-purity H_2 from coal-derived syngas via the high-temperature water-gas shift reaction (WGSR) in catalyst-free Pd and 80wt%Pd-Cu membrane reactors (MRs) was evaluated in the absence and presence of H_2S. The impetus for this study stems from the fact that successfully integrating water-gas shift MRs to the coal gasifier process has the potential of increasing the efficiency of the coal-to-H_2 process, thereby significantly reducing the cost of H_2 production from coal.

To this end, the effect of the WGSR environment on 80wt%Pd-Cu MRs was studied over a wide range of temperatures. Results indicate minimal impact of the WGSR environment on the 80wt%Pd-Cu membrane at 1173K. Subsequently, using pure reactant gases (CO and steam), the rapid rate of H_2 extraction from the reaction zone, coupled with the moderate catalytic activity of the Pd-based walls was shown to enhance the CO conversion beyond the equilibrium value of 54% at 1173K, in the absence of additional heterogeneous catalysts in both Pd and 80wt%Pd-Cu MRs.

The effect of H_2S contamination in the coal-derived syngas on Pd and 80wt%Pd-Cu membranes at 1173K was also studied. Results indicate that the sulfidization of Pd-

based membranes is strongly dependent on the H_2S-to-H_2 ratio and not merely the inlet H_2S concentration. The Pd and 80wt%Pd-Cu MRs were shown to maintain their structural integrity at 1173K in the presence of H_2S-to-H_2 ratios below 0.0011 (~1,000 ppm H_2S-in-H_2).

A COMSOL Multiphysics model developed to analyze and predict performance of the water-gas shift MRs in the presence of H_2S indicated that the MRs could be operated with low H_2S concentrations. Finally, the feasibility of high-purity H_2 generation from coal-derived syngas was investigated using simulated syngas feed containing 53%CO, 35%H_2 and 12%CO_2. The effect of H_2S contamination on MR performance was investigated by introducing varying concentrations of H_2S to the syngas mixture. When the H_2S-to-H_2 ratio in the MR was maintained below 0.0011 (~1,000 ppm H_2S-in-H_2), the MR was observed to maintain its structural integrity and H_2 selectivity, however, a precipitous reduction in CO conversion was observed. Increasing H_2S concentrations such that the H_2S-in-H_2 ratio increased above about 0.0014 resulted in MR failure within minutes.

TABLE OF CONTENTS

LIST OF TABLES

LIST OF FIGURES

ACKNOWLEDGEMENTS

I would like to express my sincere gratitude to my advisor, Dr. Robert Enick, for his wit and candor in guiding me through my Ph.D. work. I am forever indebted to you. I would also like to acknowledge my committee members, Drs. G. Meier, I. Wender, G. Veser and A. Cugini for their insightful discussions.

My colleagues at the National Energy Technology Laboratory, Bryan Morreale, Bret Howard, Richard Killmeyer and Mike Ciocco. I sincerely appreciate your time and helpful discussions over the years.

I wish to express my gratitude to the National Energy Technology Lab for funding this project. I am very grateful for the opportunity to have worked in this field.

I would also like to acknowledge the technical prowess and support of the engineering technicians and computer personnel of Parsons Project Services, Paul Dieter, Bill Brown, Ron Hirsh, Jack Thoms and Russell Miller who operate and maintain the Hydrogen Membrane Test Units. Thanks for all your support.

Finally, this work is dedicated to my family for their love, prayers and encouragement that motivated me and kept me focused throughout my academic career. To my mother, Efe Iyoha, for her endless love and words of wisdom. To my father and role model, Wilson Iyoha, for his mentorship and support. For teaching me that with hard work, everything is possible. My siblings, Egaugie, Ifueko, Otabor and Amenze, you were my inspiration.

1.0 CHAPTER ONE: INTRODUCTION

The H_2 economy is an ambitious technological goal that envisions major segments of the American economy, especially power generation and transportation, being fueled by H_2 rather than fossil fuels. Ideally, upon combustion of H_2 in an engine or in a fuel cell, only water vapor is emitted. By contrast, the combustion of fossil fuels releases CO_2, thereby elevating the concentration of this greenhouse gas in the atmosphere. Unlike fossil fuels, however, H_2 is not a natural resource and must therefore be produced from other available resources (e.g. coal, biomass, natural gas or water) that contain H_2 bound to carbon and oxygen. The costs and technical challenges associated with the production, storage and distribution of H_2 are daunting. Although methods of employing nuclear power or renewable resources to make H_2 without consuming fossil fuels or releasing CO_2 are currently being researched, such techniques are not yet economically and technically feasible. Therefore, fossil fuels are expected to be the near-term feedstock for H_2 generation. With coal being a cheap, abundant, natural resource, coal-to-H_2 technologies are expected to play a crucial role as we transition to the H_2 economy.

Coal gasification plants produce an effluent stream that is rich in CO, CO_2 and H_2. This high pressure effluent is then combined with steam in a water-gas shift (WGS) reactor that converts the CO and steam to additional H_2 and CO_2. H_2 currently produced from coal gasification is mostly used as an intermediate in chemical synthesis. The issues

of greenhouse gas emission and capture, however, remain concerns during the generation of H_2 from fossil fuels. Nevertheless, it is certainly more realistic to envision the capture and sequestration of CO_2 from these large, central, H_2-generating facilities than from a multitude of vehicles. DOE is sponsoring the development of a suite of CO_2 capture and sequestration technologies that will be closely integrated with H_2-from-coal plants. Successful advances in gasification, carbon capture and sequestration technologies may result in a cost-effective method of H_2 production from coal to fuel the H_2 economy.

A major component of prospective coal-to-H_2 plants is the WGS membrane reactor (WGSMR) which combines the WGS reaction and the CO_2–H_2 separation processes in a single unit operation. If the membrane is H_2-selective, the product streams would consist of a low pressure, high-purity H_2 stream and a high pressure CO_2-steam stream that could be dehydrated and sequestered. System studies of conceptual coal gasification plant configurations have suggested that enhanced plant efficiency can be achieved by integrating H_2-selective membrane reactors (MR) into the process (Bracht et al. 1997; Chiesa et al. 2005). This would result in enhanced reactant conversion due to the selective extraction of one of the products, in this case H_2. The MR would shift the equilibrium conversion toward the products (CO_2 and H_2), with the level of CO conversion being limited by MR length and/or permeate concentration of H_2. Furthermore, the use of a MR obviates the need for traditional H_2 purification processes, such as pressure-swing adsorption, because dense metal, H_2-selective, diffusion membranes could result in H_2 recovery and purity levels as high as 99% and 99.9999%, respectively (Grashoff et al. 1983). The high pressure CO_2-steam retentate stream would then be directed towards potential sequestration processes, most of which (e.g. injection

into coal seams or oil or gas reservoirs, or deep sea disposal) require compressed CO_2. In summary, the successful integration of a MR into the gasification process has the potential to enhance high purity H_2 production from an abundant domestic natural resource (coal), while simultaneously producing a high pressure CO_2-rich retentate stream which is amenable to sequestration strategies.

1.1 WATER-GAS SHIFT REACTION

The water-gas shift reaction (WGSR) is present in several industrial processes including: coal gasification, steam reforming, and ammonia production. It is the reaction between CO and steam to produce CO_2 and H_2 as shown in Equation (1).

$$CO + H_2O \leftrightarrow CO_2 + H_2 \qquad \Delta H^0_{298} = -41.1 \text{ kJ/mol} \tag{1}$$

The WGSR is a slightly exothermic reaction, with equilibrium constant decreasing with increasing temperature. Since the 1960s, the WGSR has mainly been used in H_2 production for ammonia synthesis, hydrotreating of petroleum and coal processing. Typically, when high purity H_2 is required, the WGSR is carried out in two stages. A low-temperature reaction stage operated at about 473 – 523K and a high-temperature reaction stage operated at about 593 – 723K.

Many metals, metal oxides and mixed oxides have been shown to catalyze the WGSR including Fe, Cu, Ni Cr and Co. However, binary copper oxide/zinc oxide and

ternary copper/zinc oxide/alumina mixed oxides have been almost exclusively used since the early 1960s to catalyze the low-temperature WGSR, while the Iron Oxide/Chromium oxide type catalysts have been used to catalyze the high-temperature WGSR. The high-temperature iron oxide-based catalyst is promoted with chromium oxide which increases catalyst life by suppressing sintering. Iron oxide catalysts can tolerate low sulfur concentrations and can effectively reduce inlet CO concentrations from about 40 mol% down to the equilibrium CO value dictated by the operating temperature (i.e. ~3% at about 723K) (Copperthwaite et al. 1990). The Cu-based WGSR catalysts which typically operate in plants for about 2-4 years (C. Rhodes, 1995) can effectively reduce CO concentrations down to about 0.1%. In addition to their high catalytic activity, the low temperature Cu-based catalysts exhibit higher reaction selectivity and fewer side reactions at elevated pressures compared to the high-temperature shift catalysts. A disadvantage of the Cu-based catalysts, however, is their lack of sulfur tolerance, being poisoned by very low sulfur concentrations (Copperthwaite et al. 1990).

1.2 MEMBRANE REACTORS

1.2.1 Pd-based Membranes

Metallic membranes, especially Pd and its alloys, have gained a great deal of attention in the recent years because they exhibit extremely high selectivity towards H_2, are fairly robust (exhibit mechanical and chemical stability), can be operated for

prolonged periods at high temperatures, and posses relatively high rates of H_2 permeation. Pd alloys are widely used as membranes for the production of ultra-pure H_2 (<1 ppm impurity) (Ali et al. 1994). H_2 permeates through Pd-based membranes via a solution-diffusion mechanism involving the following sequential steps: (1) adsorption of H_2 molecules on the membrane surface; (2) dissociation of H_2 molecules into atoms; (3) diffusion of H_2 atoms through the bulk membrane material; (4) recombination of H_2 atoms into molecules; and (5) desorption of H_2 molecules from the membrane (Musket 1976). For thick membranes (i.e. > 20 μm) the limiting resistance to H_2 transport is expected to be the diffusion of H_2 through the bulk of the membrane (i.e. steps 1 & 5 are in equilibrium) (Hurlbert et al. 1961).

A disadvantage of dense Pd membranes, however, is the high cost of Pd. In an attempt to lower the membrane cost, Pd is typically alloyed with various elements including Ag, Cu and Au. In addition to decreasing cost, alloying Pd has been reported to enhance membrane performance with respect to increased H_2 flux, eliminate H_2 embrittlement, and increase mechanical strength. The Pd-Cu alloy membrane is one of such alloys currently being studied for their potential as H_2 membrane material by the US DOE NETL using both experimental and computational tools. This is because Pd-Cu exhibits greater mechanical strength than Pd, smaller though comparable H_2 permeance (Howard et al. 2004), and possible sulfur resistance under certain conditions (McKinley 1967; Morreale et al. 2004).

1.2.2 Water-gas Shift Membrane Reactors

The equilibrium of reversible reactions can be shifted toward more product formation by changing reaction conditions such as pressure and temperature. The equilibrium of such reactions may also be shifted by removing any of the products selectively by using a membrane. Michaels (Michaels 1968) and Shah (Shah 1970) first pointed out that the selective removal of products from the reaction zone could result in a favorable chemical equilibrium shift toward more product formation. In the case of the WGSR which has a decreasing equilibrium CO conversion with increasing temperature, H_2 yield can be appreciably enhanced at high reaction temperatures at which the equilibrium CO conversion would otherwise be low, by extracting either CO_2 or H_2 from the reaction mixture.

A membrane reactor is a device in which reaction and separation is carried out simultaneously. The principle of the WGSMR is illustrated in Figure 1. The membrane continuously removes the produced H_2 from the reaction zone, shifting the chemical equilibrium to more CO_2 and H_2 formation. When the membrane used is highly selective to the product of interest, the product can be directly recovered during the reaction, eliminating the need for additional product purification steps. In the case where a Pd-based membrane is used, the extracted high-purity H_2 is recovered at a lower pressure than the process stream pressure because the rate of H_2 transport is proportional to the square root of the H_2 partial pressure in the process-side minus the square root of the H_2 partial pressure on the permeate-side.

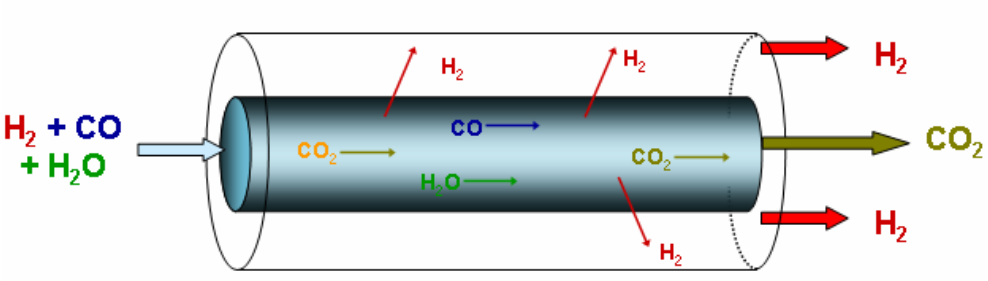

Figure 1. Principle of WGSMR. H_2 is continuously extracted from the tube-side reaction zone into the permeate-side, shifting the equilibrium to higher product CO_2 and H_2 formation.

Currently, one of the challenges of MR application is fabricating high H_2-flux membranes by the formation of uniform, thin, metallic films on commercial ceramic membrane supports. Such composite membranes in which a thin film of Pd or Pd-alloy (1-5 μm thick) is deposited onto a porous support, have been developed for MR applications (Tosti et al. 2000). However, these membranes suffer from delamination or defect formation (i.e. formation of pinholes) on the membrane surfaces during thermal and hydrogenation-dehydrogenation cycling (Tosti et al. 2003), and, therefore, cannot be used for high-purity H_2 production. In order to obtain membranes with good, long-term stability and permselectivity, this work focuses on the use of dense films of 100wt% Pd and 80wt%Pd-Cu ($Pd_{80wt\%}Cu$) alloy.

1.3 ADVANTAGES OF MEMBRANE REACTOR INTEGRATION TO THE COAL GASIFICATION PROCESS

In addition to making coal-to-H_2 a more environmentally friendly process as a result of the high carbon capture efficiency of the MR (100% carbon in syngas removed in the retentate stream as high-pressure CO_2) reducing greenhouse gas emissions to the atmosphere, successful integration of the high-temperature MR to the coal gasifier is expected to increase the efficiency of the coal-to-H_2 process, thereby appreciably decreasing the cost of H_2 production from coal (Gray et al. July 2002). The increased process efficiency arises as a result of: 1) obviating the need to cool the high-temperature coal derived syngas stream to lower temperatures in an attempt to attain higher CO conversion, 2) significantly reducing the steam-to-CO ratio requirement of the WGSR (i.e. reduce steam-to-CO ratio requirement from ~9:1 for conventional low temperature WGSR to approximately 2:1), 3) the MR integrates chemical reaction with product separation into a single unit, eliminating the need for additional pressure swing adsorption (PSA) purification equipment, 4) the MR shifts the CO conversion above the equilibrium value, resulting in higher H_2 production, and 5) it significantly reduces the power needed to recompress CO_2 due to the complete selectivity of the membrane, retaining the CO_2 at the high operating pressure.

1.4 PROJECT OBJECTIVES

The overall goal of this project was to investigate a proof-of-concept Pd and $Pd_{80wt\%}Cu$ MRs for efficient, cheap H_2 production from coal-derived syngas, while simultaneously capturing the produced CO_2. The Pd MR served as a baseline for comparison, while the $Pd_{80wt\%}Cu$ membrane was selected because it was anticipated that this alloy may exhibit potential sulfur (H_2S) tolerance under certain conditions (Morreale et al. 2004; Mundschau et al. April, 2005). Sulfur tolerance would allow the MR to be integrated into the plant prior to H_2S removal of the gasifier effluent, perhaps even at the gasifier outlet (after particulate removal). The ability to integrate the MR into the plant immediately after the gasifier would benefit from the extremely rapid kinetics attainable at high reaction temperature and the increased H_2 permeance of Pd-based membranes at elevated temperature. Furthermore, the Pd and $Pd_{80wt\%}Cu$ H_2-selective membranes are expected to enhance the rate of reaction beyond that associated with the homogeneous fWGSR. This is because the surface of the Pd and $Pd_{80wt\%}Cu$ membranes have been previously shown to exhibit modest catalytic activity, as evidenced by increases in CO conversions relative to a quartz reactor (Bustamante et al. 2005).

In light of the potential promise of $Pd_{80wt\%}Cu$ dense metal membranes, Chapter 2 explores the effects of the WGSR atmosphere (CO, CO_2 and H_2O) on the permeance and surface morphology of the $Pd_{80wt\%}Cu$ over the 623 to 1173K temperature range and 0.62 to 2.86 MPa retentate total pressure range. The objective of this chapter was to determine if any of the WGS components would be deleterious to the MR at conditions of interest.

In Chapter 3, a literature review of previous investigations involving the WGSR in a Pd-based MR is presented. Further, results from proof-of-concept Pd and $Pd_{80wt\%}Cu$

MRs operated at1173K, in the absence of heterogeneous catalyst particles are also presented. The objective of this study was to investigate the synergy between the inherent catalytic activity of the membrane walls toward the WGSR and the rapid rate of H_2 transport through Pd-based membranes to enhance CO conversions and high-purity H_2 recovery.

In Chapter 4, the sulfidization of Pd-based membranes by H_2S was investigated from a thermodynamic and experimental approach. Based on the feed composition (i.e. H_2S-to-H_2 ratio) and the thermodynamic stability of the Pd_4S, regions at which the Pd and $Pd_{80wt\%}Cu$ membrane would be expected to experience sulfidization or be safely operated are predicted. A literature review of previous investigations involving Pd membranes exposed to H_2S was conducted and correlated to the developed thermodynamic model.

In Chapter 5, a COMSOL Multiphysics model was developed to analyze and predict MR performance in the absence and presence of varying concentrations of H_2S. The effect of increasing the H_2 permeance and catalytic activity of the Pd membrane on CO conversion are investigated. Using information of the H_2S-to-H_2 ratio required to sulfidize Pd determined in Chapter 4, H_2S-in syngas concentrations below which the Pd MR may be safely operated was predicted.

Chapter 6 explored the feasibility of the Pd and $Pd_{80wt\%}Cu$ MRs for H_2 production from simulated coal syngas in the absence and presence of varying concentrations of H_2S. The MRs were operated at 1173K to be representative of a MR positioned just downstream from a coal gasifier. H_2S was introduced along with the feed to simulate H_2S

contamination in the coal-derived syngas. Control experiments involving the effect of 1000 ppm H_2S-in-H_2 on H_2 permeance of Pd and $Pd_{80wt\%}Cu$ are also presented.

Finally, Chapter 7 presents a summary of the results in this thesis and gives suggestions for further research involving Pd MRs.

2.0 CHAPTER TWO: THE EFFECTS OF H_2O, CO AND CO_2 ON THE H_2 PERMEANCE AND SURFACE CHARACTERISTICS OF 1 MM THICK $PD_{80WT\%}CU$ MEMBRANES

Abstract

The hydrogen permeance of 1 mm-thick $Pd_{80wt\%}Cu$ foils was measured in the presence of equimolar mixtures of H_2 with CO, CO_2 or H_2O over the temperature and total pressure ranges of 623 to 1173K and 0.62 to 2.86 MPa, respectively. In all cases, permeance losses at 623 and 738K were very modest. At higher temperatures, more significant decreases in membrane permeance were observed with the highest reduction of about 50% occurring when macroscopic carbon deposition occurred on the membrane surface during H_2 - CO exposure at 908K. The more worrisome effects of exposure to these gases, however, were the micron-scale surface defects observed at 908 and 1038K. Although the 1 mm thick disk membranes retained their mechanical integrity, such defects could cause catastrophic failure of ultra-thin, Pd-Cu membranes (1-5 μm thick) deposited on porous substrates.

2.1 INTRODUCTION

Pd alloys, such as Pd-Cu, are currently being studied for their potential as H_2 membrane material by various investigators including the US DOE NETL, using both experimental and computational tools. This is because Pd-Cu exhibits greater mechanical strength than Pd, smaller though comparable H_2 permeance (Howard et al. 2004), and possible sulfur resistance under certain conditions (McKinley 1967; Morreale et al. 2004). For example, transient experiments to determine the permeance of 100 μm Pd-Cu fcc alloys in the presence of 1,000 ppm H_2S suggested that the fcc Pd-Cu alloy retains a much higher percentage of its permeance than the B2 alloys (Morreale et al. 2004). Further, recent evaluation of the effects of temperature, pressure, alloy composition, and alloy phase behavior on steady-state H_2 permeance of 100 μm Pd-Cu disk membranes (Howard et al. 2004) revealed several trends that are also useful for the design of WGSMRs. For example, Howard et al. showed that increasing the palladium concentration of a B2 or fcc Pd-Cu alloy increases H_2 permeance. Further, the B2 phase exhibits high permeance relative to the fcc phase, allowing some B2 alloys with lesser amounts of Pd (e.g. $Pd_{60wt\%}Cu$) to be more permeable than fcc alloys with greater amounts of Pd (i.e. $Pd_{80wt\%}Cu$) at the same temperature (e.g. 623K). The US DOE NETL has also used ab initio calculations and coarse-grained modeling to predict H_2 permeance through Pd-Cu alloys as functions of alloy composition and temperature without the need for experimental data apart from knowledge of bulk crystal structures (Kamakoti et al. 2005). Pd-Cu surfaces have also been shown to moderately enhance the reaction rate of the forward water-gas shift reaction (fWGSR), especially at temperatures above 873K (Flytzani-Stephanopoulos et al. 2003; Bustamante et al. 2005).

However, previous investigators have reported H_2 permeance reduction of Pd-based membranes in the presence of the main components of the WGSR, CO, H_2O and CO_2. Typically, this reduction has been attributed to the blocking of available H_2 dissociation sites by the adsorption of CO or H_2O on the membrane surface and the reduction of the active area available of H_2 permeation (Ali et al. 1994; Amandusson et al. 2000; Li et al. 2000; Paglieri et al. 2002). Furthermore, it was observed that steam has a more marked effect on H_2 permeance reduction than CO in both Pd and Pd-Ag membranes, possibly due to the greater adsorption of H_2O on the membrane surface (Li et al. 2000; Hou et al. 2002). Li et al. (Li et al. 2000) observed a reversible 22% H_2 permeance reduction of Pd at temperatures up to 653K using a 12% CO – 88% H_2 mixture flowing over a 10 μm-thick Pd film deposited on a stainless steel support. A similar observation relating to H_2 permeance was reported by Hou et al. (Hou et al. 2002) using a Pd-Ag membrane. They observed that H_2O resulted in a more dramatic decrease in H_2 permeance at 548K, 70%, compared to the 10% and 40% decreases caused by CO_2 and CO, respectively. Wang et al. (Wang et al. 2004) studied H_2 permeation through pre-oxidized Pd membranes. An approximately 75% reduction of H_2 permeance for a 200 μm thick Pd membrane was associated with CO at 373K, with this effect decreasing with increasing temperature. Sakamoto et al. (Sakamoto et al. 1996) studied the effect of 10% CO on H_2 permeance in various Pd-based membranes. They observed a permeability reduction effect for the range of Pd-alloys involved in the study. This decrease in permeance was less significant with increasing temperature for the Pd-Gd-Ag alloy series, while the effect of CO on permeance reduction became more pronounced with increasing temperature for the Pd-Y-Ag and Pd-Ag alloy series in their experiments.

In addition to permeance changes, metallic surfaces may experience thermally induced (thermal etching) or reaction-induced (catalytic etching) morphological changes, depending on the composition of the environment to which they are exposed. Thermal etching occurs in non-reactive atmospheres or in vacuum and often results in the formation of boundary grooves and faceted surfaces (Wu et al. 1985). Reaction-induced surface modification, however, occurs in the presence of a reactive atmosphere and results in highly irregular surface structures different from those formed as a result of exposure to inert atmospheres (Wei et al. 1995).

In light of the potential promise of $Pd_{80wt\%}Cu$ dense metal membranes and the lack of a systematic investigation of the effect of H_2O, CO, and CO_2 on this membrane composition at post-gasifier conditions, the objective of this study was to determine the effects of these gases on the permeance and surface morphology of the $Pd_{80wt\%}Cu$ over the 623 to 1173K temperature range and 0.62 to 2.86 MPa retentate total pressure range. This alloy composition was selected because its permeance is reasonably high relative to Pd, and preliminary results have indicated that this fcc alloy may be sulfur tolerant. In this study, relatively thick (1 mm) membranes were used in order to ensure the precision and uniformity of the alloy composition, to improve weldability (membranes were welded between two Inconel 600® tubes) and to enhance the durability of the membrane upon changes in surface morphology. Because the permeance of thick membranes is more strongly influenced by bulk diffusion through the membrane than surface effects, the changes in permeance noted in this study were expected to be conservative. More significant changes in permeance (on a percentage basis) would be expected for thinner membranes that are more strongly influenced by surface phenomena.

2.2 EXPERIMENTAL

2.2.1 Permeance Apparatus

The 1 mm thick $Pd_{80wt\%}Cu$ alloy foils used in the present study were manufactured by ACI Alloys using 99.9% purity (metals basis) Pd and Cu. **Figure 2** shows a schematic of the H_2 permeance apparatus used to determine the permeance of these foils. Membranes were fabricated by punching 19 mm disks from as-received Pd-Cu foil sheets. The membrane was welded between two 19.1 mm OD Inconel 600 tubes with a thin porous aluminum oxide disk placed between the membrane and the porous Hastelloy® support to prevent intermetallic diffusion. After welding, the active membrane was 13.5 mm in diameter yielding 1.43 cm^2 of active membrane area. The membrane assembly consisted of two 9.5 mm OD Inconel 600 tubes placed concentrically inside the 19.1 mm OD Inconel 600 extension tube as shown in the magnified portion of Figure 2. The coaxial tube configuration allowed the feed and effluent gas streams to enter through the annulus of the 19.1 and 9.5 mm OD Inconel tubes, contact the membrane, and exit through the inside of the 9.5 mm OD tube. Initially, experiments were conducted using one membrane throughout the entire temperature and pressure cycle. Subsequent experiments were conducted with a fresh membrane sample at each individual temperature.

The gases used in this study were H_2, He, 90%H_2-He, CO, CO_2 and Ar. All gases used were 99.999% certified calibration gases. Equimolar feed streams of H_2 with H_2O, CO, or CO_2 were prepared in the NETL Hydrogen Membrane Test (HMT) unit, **Figure 2**. The He-containing mixture was used as a check for membrane leaks because He cannot diffuse through Pd-Cu. Ar was used as the permeate sweep gas. The flow rate of each gas was controlled by Brooks mass flow controllers. The feed and permeate pressures were regulated by pneumatically actuated stainless steel control valves. A dual element thermocouple was placed on both sides of the membrane, about 3 mm from the membrane surface. The average of the thermocouple readings (typically about a 10K difference) was used for temperature indication and control. For experiments involving steam, water was injected into the flowing gas stream by a calibrated ISCO 500D syringe pump and was vaporized in the heated feed line before entering the reactor. A trap was placed on the exit line to collect the unreacted water before the effluent gases were directed to a Hewlett-Packard 5890 Series II gas chromatograph equipped with a 3 m long by 3.2 mm OD zeolite-packed column and thermal conductivity detector for quantification. The water trap was used because high water concentrations could saturate the column resulting in inaccurate quantification of the components in the gas stream.

The membrane was heated to the desired temperature at a rate of 120K/hr under a constant flow of He in the feed side and Ar in the sweep side using a 152 mm long cylindrical resistance heater placed concentrically around the membrane assembly. At the selected operating temperature, a 90%H_2-He feed was introduced to the feed side, maintaining constant flow of Ar in the permeate side. Typical values of retentate-side total flow rates were 150 sccm. The Ar flow rate was adjusted to a value of about 110

sccm which resulted in the H_2 permeate concentration being less than 5%. The 90%H_2-He flow was maintained until steady state H_2 permeance values were attained, after which the feed was switched to an equimolar mixture of H_2 with CO, H_2O or CO_2 that was prepared by metering equivalent volumetric flow rates of the individual gases to the membrane. This flow was once again maintained until steady state H_2 permeance values were attained after which the feed was reverted to 90%H_2-He and the test conditions changed. Permeance values for all membranes were reproducible to within 3%. For studying the effect of WGS reaction components on membrane surface morphology, a fresh membrane sample was used for each temperature condition unless otherwise specified.

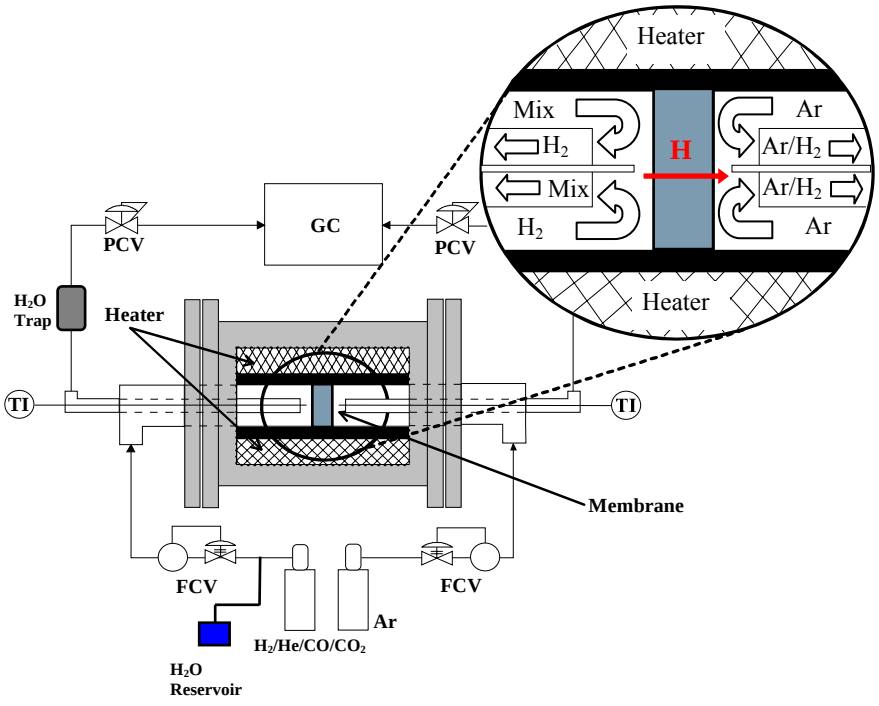

Figure 2. Schematic of Hydrogen Membrane Test unit (HMT unit)

2.2.2 SEM Analysis

Membrane surface morphology was examined prior to and following WGS testing via scanning electron microscopy (SEM). Compositional information was obtained through energy dispersive X-ray spectroscopy (EDS). Two SEM systems were used in the analyses- an Aspex PSEM 2000 and a Philips XL30 FEG, both equipped with EDS. Membranes were removed from the reactor test assembly for characterization following testing by carefully cutting them out of the extension tubes, taking care to limit surface contamination as much as possible. In cases where the remaining tube wall restricted examination, the wall height was reduced by carefully hand filing. The membranes were typically examined using an Olympus stereomicroscope to observe any large scale morphologies or deposits prior to SEM examination.

2.2.3 Determination of Permeance

H_2 permeance was calculated by the Richardson equation, using a pressure exponent of 0.5 which is consistent with diffusion limited membranes:

$$N_{H2} = k'\left(P_{H2,\mathrm{Re}t}^{0.5} - P_{H2,Per}^{0.5}\right) \tag{2}$$

$P_{H2,\mathrm{Re}t}$ and $P_{H2,Per}$ are the H_2 partial pressures on the retentate and permeate sides, respectively. k′ is the H_2 permeance (mol H_2/(m^2·s·$Pa^{0.5}$)) which is equivalent to the permeability divided by the membrane thickness. In this study, when three or more

experimental retentate pressure values were available (H_2 – H_2O mixtures), plots of steady state values of H_2 flux versus the difference between the square roots of the retentate and permeate partial pressures constrained though the origin resulted in a linear trend line with a slope equal to k′. Alternately, if only two retentate pressure values were available (mixtures of H_2 with CO or CO_2), permeance was solved for at each pressure using Equation (2).

The temperature dependence of k′ is typically reflected in an Arrhenius-type relation between k′ and inverse absolute temperature (K^{-1}), Equation (3), yielding an activation energy (E, J/mol) and a pre-exponential constant (k_0) for the Pd-Cu alloy membrane.

$$k' = k_0 \exp\left(\frac{E}{RT}\right) \tag{3}$$

2.3 RESULTS AND DISCUSSION

2.3.1 Determination of Hydrogen Permeance

H_2 permeance of the $Pd_{80wt\%}Cu$ membrane was calculated using the Richardson equation, Equation (2). **Figure 3** shows the plot of H_2-permeance of a 1 mm $Pd_{80wt\%}Cu$ membrane and a 1 mm Pd membrane versus inverse temperature over the 623 to 1173K temperature range. Concerns about superficial decreases in membrane permeance due to mass transfer limitations as opposed to the presence of contaminant species for tests employing mixed feed streams were addressed by conducting experiments using a feed

stream comprising 50%H_2-He. H_2-permeance results obtained for such experiments were within 3% of the results obtained using the 90%H_2-He feed. Arrhenius expressions for the permeance of the 1 mm thick palladium and $Pd_{80wt\%}Cu$ foils are presented below, where temperature is in Kelvin, and R is the universal gas constant, 8.314 J/mol K:

For the 1 mm Pd membrane (Morreale et al. 2003):

$$k' = 1.92 * 10^{-4} \exp\left(\frac{-13{,}810\ (J/mol)}{RT}\right) \left(mol\ H_2 / (m^2 s\ Pa^{0.5})\right) \tag{4}$$

For the 1 mm $Pd_{80wt\%}Cu$ membrane:

$$k' = 4.854 * 10^{-4} \exp\left(\frac{-24{,}767(J/mol)}{RT}\right) \left(mol\ H_2 / (m^2 s\ Pa^{0.5})\right) \tag{5}$$

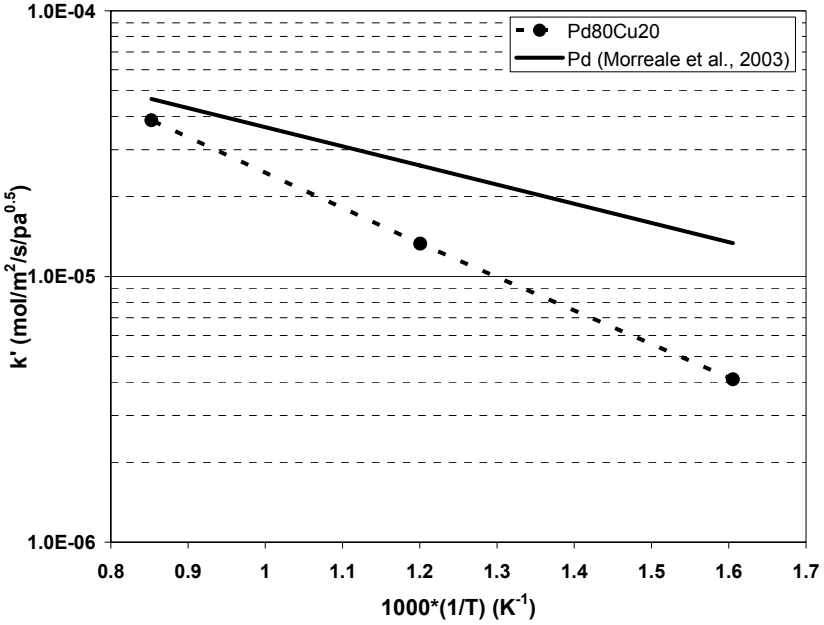

Figure 3. H_2-permeance of a 1 mm Pd and a 1 mm $Pd_{80wt\%}Cu$ membrane obtained in the presence of a 90%H_2-He feed.

2.3.2 Effect of H_2O on H_2-Permeance and Surface Morphology

2.3.2.1 Effect of H_2O on H_2-Permeance

H_2 production via the WGSR in a conventional reactor typically employs a H_2O:CO ratio greater than or equal to 2:1 to mitigate carbon formation (Xue et al. 1996) via carbon depositing mechanisms such as the Boudouard reaction and the CO-reduction reactions, in addition to favoring higher CO conversions. Hence, our experiments were conducted using a 1:1 H_2O:H_2 feed ratio as this was considered to be roughly representative of the ratio of these gases in a WGS membrane reactor. The effect of temperature and feed pressure was determined over the 623 – 1173K temperature range and feed pressures of 0.62, 1.55, 2.86 MPa (absolute). **Figure 4** shows the H_2 flux versus

the trans-membrane H_2 partial pressure for the $Pd_{80wt\%}Cu$ membrane at 623, 738, 908, 1038 and 1173K in the presence and absence of steam. The figure presents the raw data used to solve for k′ using the Richardson equation (Equation (2)). The r^2 value for the best fit lines through the origin for the flux vs. ($P_{H2,ret}^{0.5} - P_{H2,perm}^{0.5}$) data were greater than 0.99. **Figure 4** and **Table 1** illustrate that very modest decreases in permeance occurred due to the addition of steam.

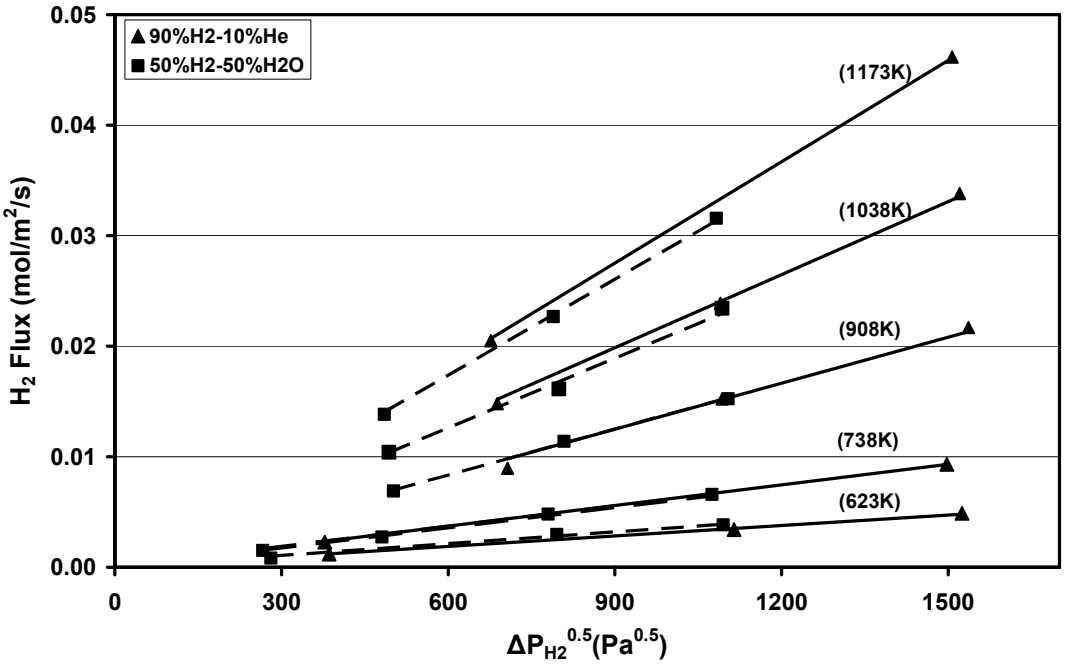

Figure 4. H_2 flux versus the difference between the square roots of H_2 partial pressures on the retentate- and permeate-sides as a function of temperature for a 90%H_2-He (solid lines) and 50%H_2-H_2O (dashed lines) feed.

Table 1. H_2-permeance values obtained for the $Pd_{80wt\%}Cu$ membrane in the presence of the 90%H_2-He and 50%H_2-H_2O feed streams.

T (K)	k′ (90%H_2-He)	k′ (50%H_2-H_2O)	% difference
623	3.149E-06	3.560E-06	+11.54
738	6.215E-06	6.075E-06	-2.253
908	1.388E-05	1.388E-05	0
1038	2.206E-05	2.10E-05	-4.805
1173	3.057E-05	2.897E-05	-5.234

Figure 5 illustrates the permeance results in the form of normalized H_2-permeance (permeance in gas mixture divided by the ideal permeance based on 90%H_2-He retentate) at total unit pressures of either 0.62 or 1.55 MPa. (Equation (2) was used to solve for permeance at each of these conditions). Only at the lowest temperature, 623K, was there an increase in permeance. This slight increase could possibly be attributable to the initial removal of surface contaminants from the membrane by steam. At all higher temperatures either no significant change or a slight decrease in permeance was observed, perhaps due to the competitive adsorption of H_2 and steam on membrane active sites. The data suggests that steam reduces the H_2-permeance of the 1 mm thick $Pd_{80wt\%}Cu$ membrane by no more than 7%, which is in good agreement with a prior study (Flytzani-

Stephanopoulos et al. 2003) that also reported very modest decreases in permeance attributable to steam on a 10-µm, B2 $Pd_{60wt\%}Cu$ membrane at 623 -723K.

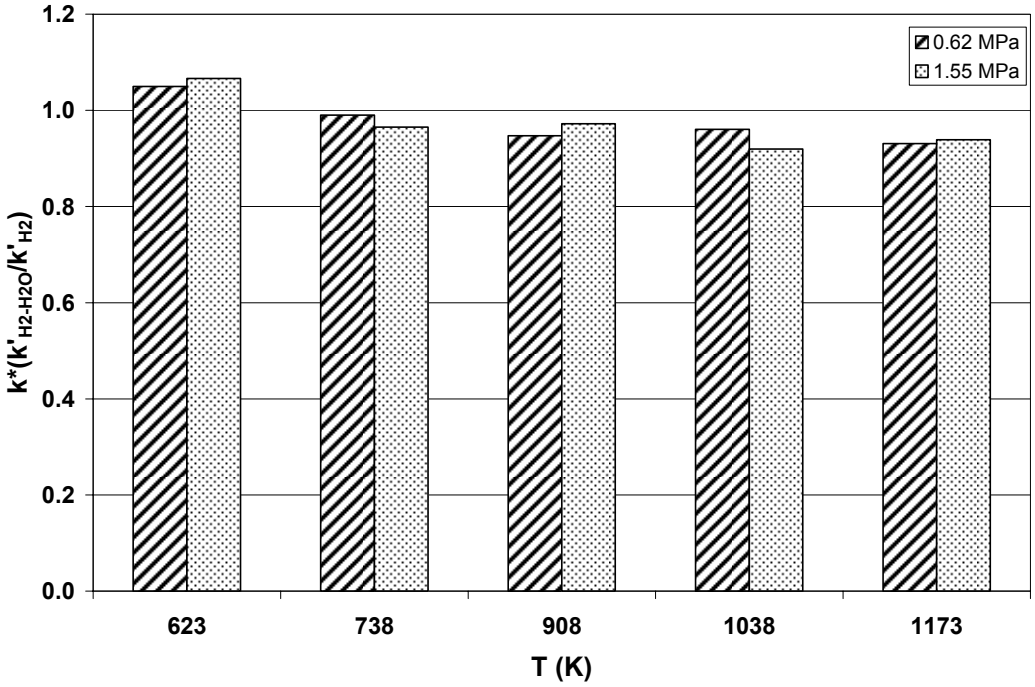

Figure 5. Effect of 50%H_2O concentration on the H_2-permeance of 1 mm $Pd_{80wt\%}Cu$ at 0.62 and 1.55 MPa total unit pressure. k* is equal to the permeance (mol $H_2/(m^2 \cdot s \cdot Pa^{0.5})$) for the 50%$H_2$-$H_2O$ feed mixture divided by permeance of the 90%H_2-He feed mixture.

2.3.2.2 Effect of H_2O on the $Pd_{80wt\%}Cu$ Surface Morphology

Although H_2O did not appear to influence the macroscopic integrity of the bulk membrane, SEM analysis of the 1-mm membrane after the H_2O exposure over a temperature range of 623 to 1173K and pressure of 0.62 to 2.86 MPa revealed significant roughening of the membrane surface (not shown). A control experiment was conducted in which a fresh $Pd_{80wt\%}Cu$ membrane at ambient temperature (**Figure 6**a) was heated up

to 1173K in a 90%H_2-He environment (**Figure 6**b). **Figure 6**b shows distinct grain boundary grooves after the H_2-He treatment that may be attributed to thermal etching. By contrast, exposure of the $Pd_{80wt\%}Cu$ membrane to the 50%H_2-H_2O at 908 and 1173K resulted in membrane surface modification (**Figure 6**c to **Figure 6**f). At 908K (**Figure 6**c), a highly irregular surface was observed and magnification of the membrane surface (**Figure 6**d) revealed the apparent initiation of a porous metal structure. However, H_2-H_2O exposure at 1173K resulted in less dramatic roughening of the membrane surface (**Figure 6**e and **Figure 6**f); slight surface modification was observed but it was not as severe as the pitting observed at 908K. This membrane also exhibited dispersed nodules protruding from the membrane surface, mostly apparent in depressions (**Figure 6**f). Although this pitting phenomenon did not result in failure of the relatively thick membranes used in this study (1 mm), similar pitting could easily lead to catastrophic failure of ultra-thin film (1-5 μm) membrane units in the presence of steam.

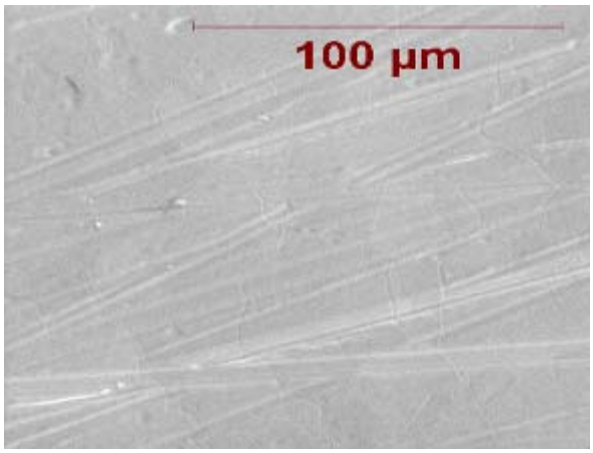

(a)

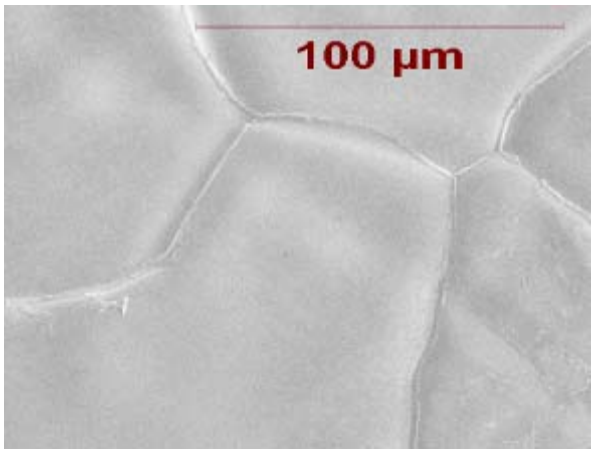

(b)

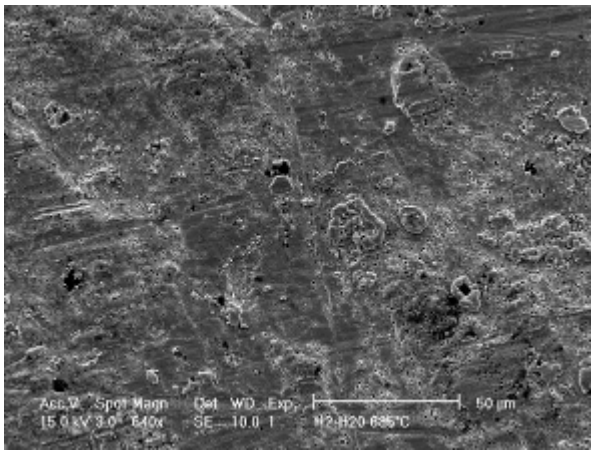

(c)

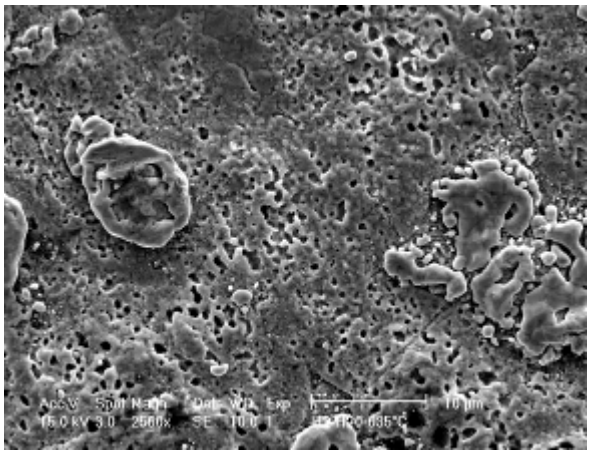

(d)

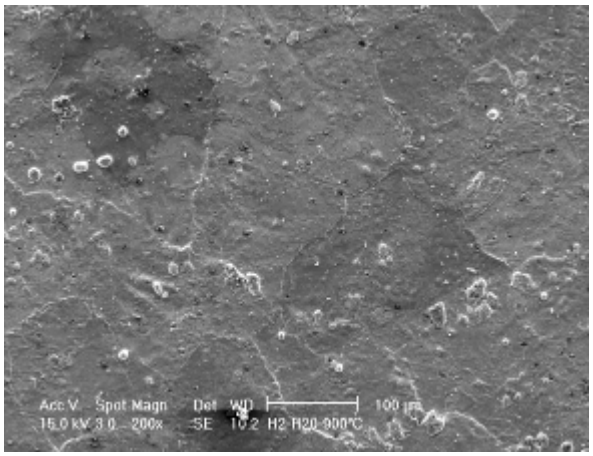

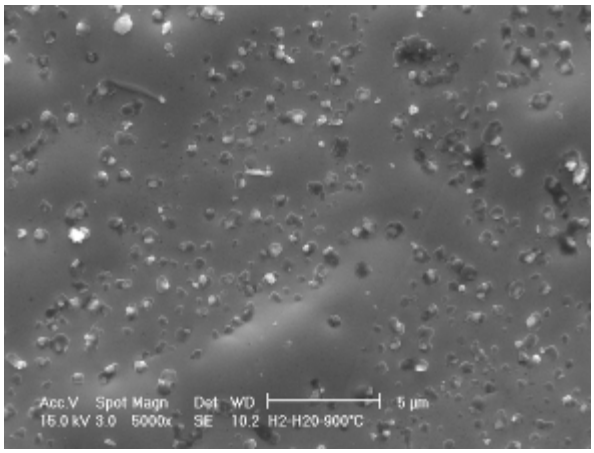

(e) (f)

Figure 6. SEM micrographs of a (a) fresh $Pd_{80wt\%}Cu$ membrane polished with 1200 grit silicon carbide paper, (b) $Pd_{80wt\%}Cu$ membrane after H_2 exposure at 623–1173K and pressure of 0.62-2.17 MPa, (c & d) $Pd_{80wt\%}Cu$ membrane after exposure to 50%H_2-H_2O feed stream at 908K and total unit pressure of 1.55 MPa for 24hrs, (e & f) $Pd_{80wt\%}Cu$ membrane after exposure to 50%H_2-H_2O feed stream at 1173K and total unit pressure of 1.55 MPa for 24hrs.

2.3.3 Effect of CO on H_2-Permeance and Surface Morphology

2.3.3.1 Effect of CO on H_2-Permeance

CO is a major component in gasifier effluent streams, ranging from about 40 to 70% (Golden et al. 1991). CO can be further reacted with H_2O in a shift reactor to produce H_2 and CO_2. **Figure 7** illustrates the effect of high concentrations of CO on the H_2 permeance of $Pd_{80wt\%}Cu$ at two retentate pressure values.

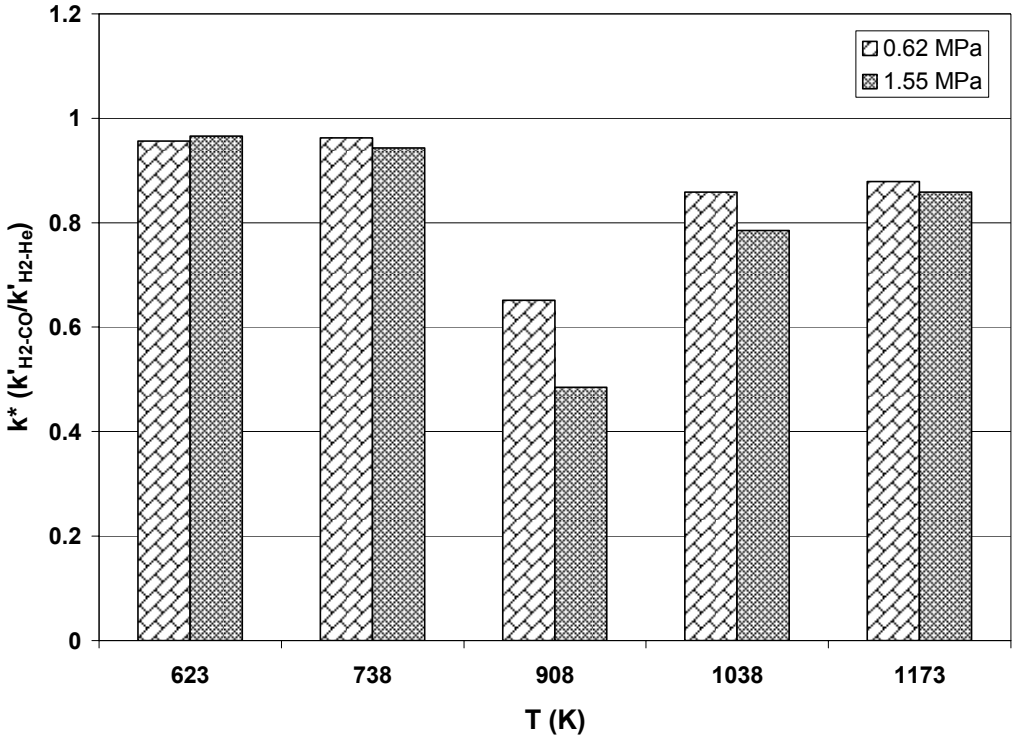

Figure 7. Effect of 50%CO concentration on the H_2 permeance of 1 mm $Pd_{80wt\%}Cu$ at 0.62 and 1.55 MPa. k* is equal to the permeance (mol $H_2/(m^2 \cdot s \cdot Pa^{0.5})$) for the mixed feed stream (H_2-CO) divided by permeance of the neat 90%H_2-He feed mixture.

Figure **7** shows that decreases of 5-7% occurred at the lowest temperatures of 623 and-738K. The permeance decreases of 15-22% at 1038 and 1173K were slightly more significant. At 908K, however, a pronounced reduction in H_2 permeance is observed resulting in 35% and 52% reductions of H_2 permeance at 0.62 and 1.55 MPa, respectively. It is apparent from the raw data in **Figure 8** that the introduction of the equimolar H_2-CO feed mixture at 908K resulted in a gradual decline of H_2 permeance which took several hours to reach steady-state. The gradual decrease in H_2 permeance as opposed to an instantaneous attainment of a new steady state permeance value in the presence of the H_2-CO feed suggests that carbon deposition on the membrane surface may have been responsible for the permeance reduction. This is further discussed in

section 2.3.3.2. The membrane, however, nearly regained its original permeance value within an hour of re-introduction of the 90%H_2-He feed, possibly due to H_2 reacting with the carbon on the membrane surface to produce methane (**Figure 8**).

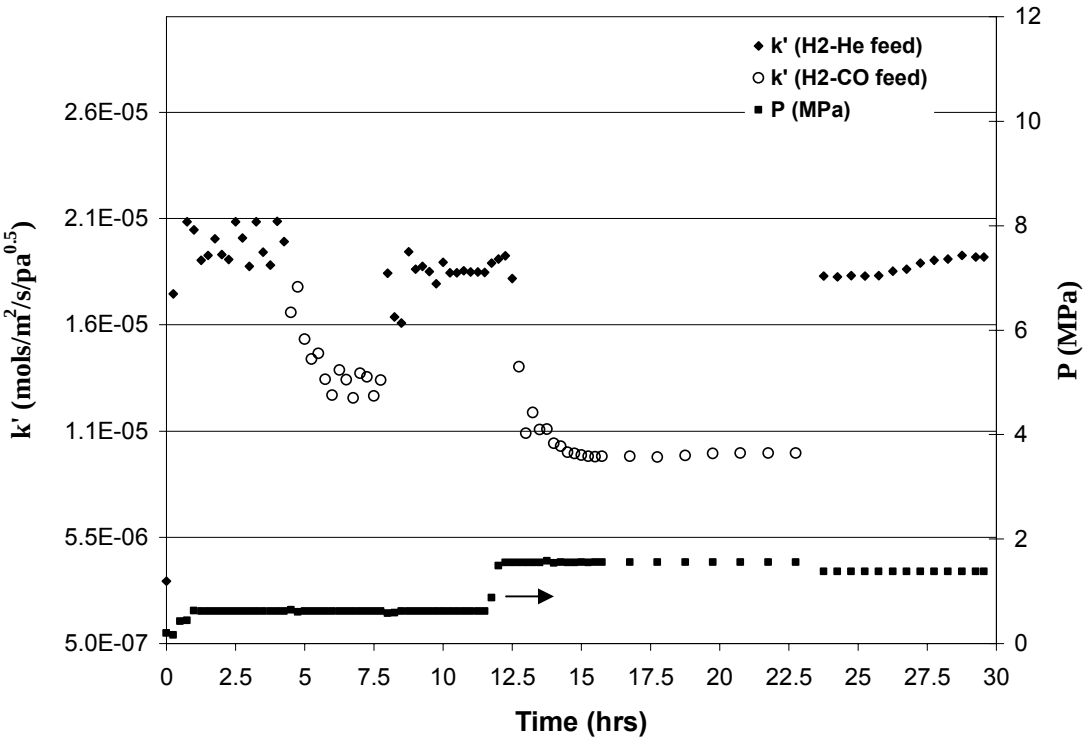

Figure 8. Raw H_2 permeance data for the $Pd_{80wt\%}Cu$ membrane at 908K with a 90%H_2-He retentate feed (diamonds) and a 50%H_2-CO retentate feed (open circles) stream at pressures of 0.62 and 1.55 MPa.

2.3.3.2 Effect of CO on $Pd_{80wt\%}Cu$ Surface Morphology

An experiment was conducted at 908K in which a fresh membrane was exposed to the 50%H_2-CO feed for 12 hours. After the H_2-CO feed was turned off, a 100% He feed was used to purge the CO and H_2 from the system. The heater was turned off to

rapidly cool the membrane unit. Disassembly of the apparatus after the completion of this experiment revealed that carbon was accumulating on and near the membrane, completely covering the membrane surface. The presence of carbon on the membrane surface (**Figure 9**) further supports the carbon induced permeance reduction mechanism.

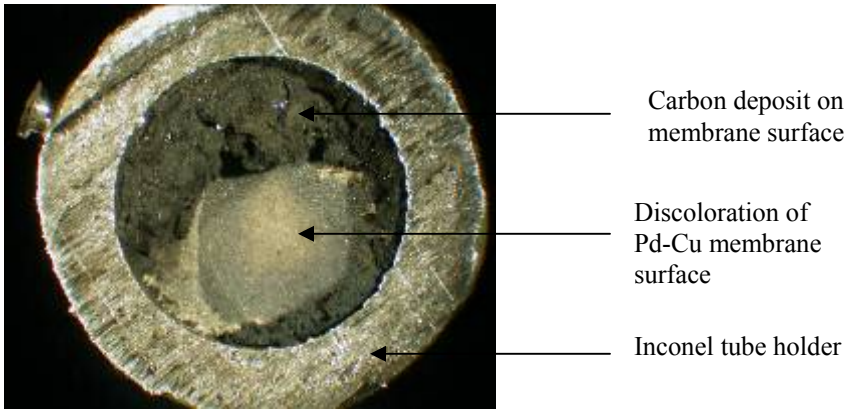

Figure 9. Photograph of the $Pd_{80wt\%}Cu$ membrane after exposure to CO. Conditions: 623 – 1173K, 0.62 and 1.55 MPa. Testing concluded after re-exposure of membrane to 50%H_2-CO feed at 908K and 0.62 MPa.

Several mechanisms for H_2 permeance reduction due to carbon interaction with Pd are possible. Prior studies of Pd have suggested that carbon can block active sites and thereby appreciably reduce H_2 permeance (Antoniazzi et al. 1989). Surface-adsorbed carbon can also be transported into the metal lattice by an activated diffusion mechanism resulting in the formation of an interstitial Pd-C phase which results in permeance reduction for Pd (Ziemecki et al. 1985). This Pd-C phase was reported to be metastable and converted back to Pd at 873K. Furthermore, carbon formation on the membrane surface could present mass transfer limitations, resulting in diffusion limited H_2 starvation at the membrane surface, which may also be responsible for the H_2 permeance

reduction. The blocking of active sites by the carbon, however, has been reported to be a more dominant mechanism of H_2 permeance reduction than the reduction due to dissolved carbon atoms in the membrane lattice (Jung et al. 2000). It is reasonable that all of these mechanisms could have contributed to the $Pd_{80wt\%}Cu$ membrane permeance losses observed at 908K in this study.

SEM was used to investigate the effect of CO exposure and carbon deposition on the $Pd_{80wt\%}Cu$ membrane surface morphology (**Figure 10** to **Figure 12**). No notable surface modification of the membrane was observed after exposure to the H_2-CO feed at 623 and 738K. **Figure 10**a and b depict the membrane exposed to the H_2-CO feed at 908K. It should be noted that small concentrations of CO_2 (<5%), H_2O (<2%) and CH_4 (<5%) were also detected in the membrane unit effluent stream by GC at this condition. It is possible that these components may have also contributed to the observed surface modification. The images reveal carbon (light appearing particles) deposited on the membrane surface.

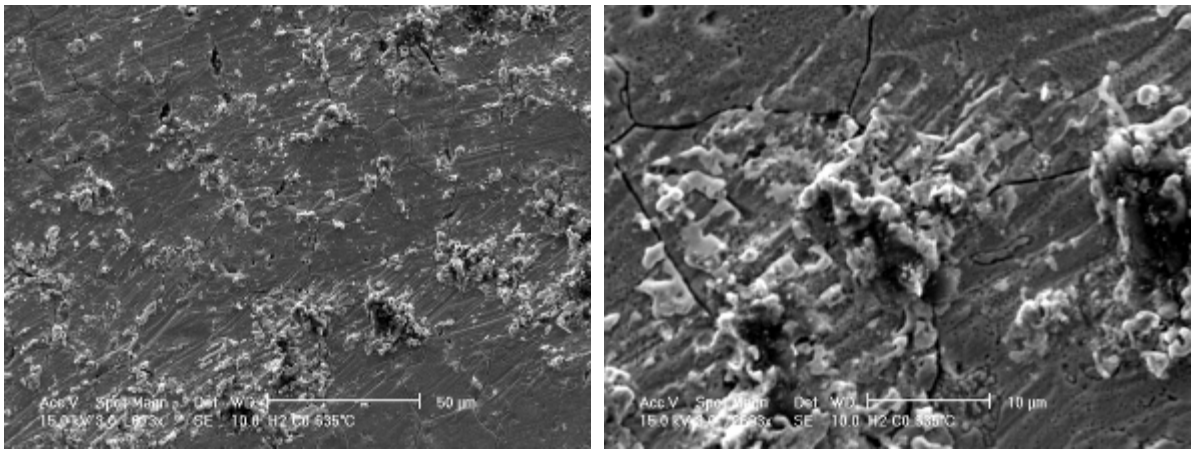

(a) (b)

Figure 10. SEM micrographs of the feed-side surface of $Pd_{80wt\%}Cu$ membrane after exposure to 50%H_2-CO feed at 908K showing deposited carbon on the surface. The membrane was exposed to feed stream for 24 hrs. The surface was also exposed to small amounts (<5% each) of CO_2, H_2O and CH_4 reaction products.

Testing at 1038K resulted in negligible carbon deposition on the membrane surface. However, severe roughening of the membrane was observed (**Figure 11**a and b). The CO_2 and CH_4 concentrations in the membrane effluent stream were as high as 30% and 25%, respectively. (Water also formed but it was difficult to quantify.) Typical membrane surface pits ranged from about 0.25 to 2µm.

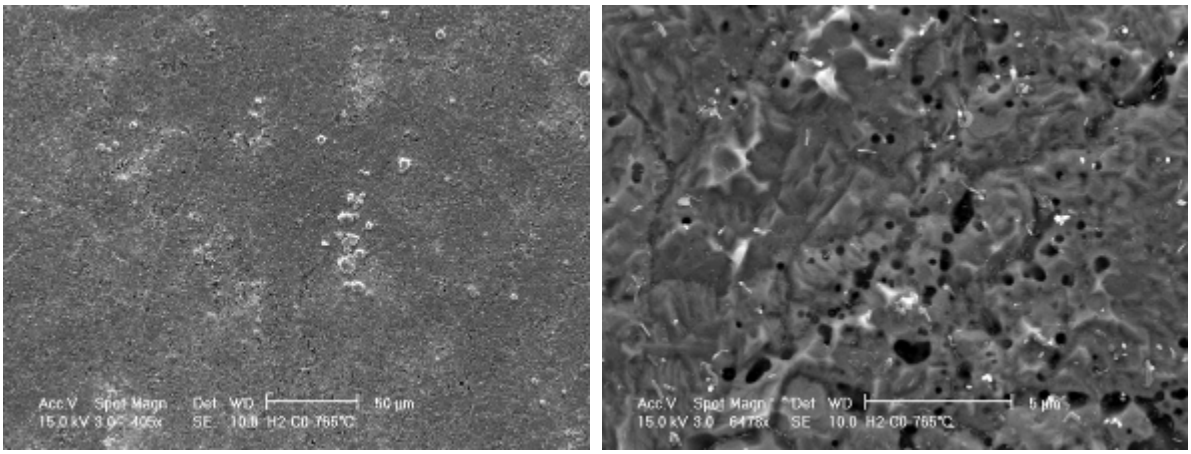

(a) (b)

Figure 11. SEM micrographs of the feed-side surface of the $Pd_{80wt\%}Cu$ membrane after exposure to 50%H_2-CO feed at 1038K and 1.11 MPa. The membrane was exposed to the feed stream for 24hrs. CO_2, CH_4 and steam were also present as a result of side reactions.

Interestingly, exposure of the $Pd_{80wt\%}Cu$ membrane to the mixed gas stream at 1173K (**Figure 12**a and b) resulted in neither membrane pitting nor carbon deposition on the membrane surface. Typical CO_2 and CH_4 concentrations in the membrane effluent stream were less than 0.7% in both cases. The membrane was relatively smooth, with visible grain boundary grooves on the surface, similar to the control experiments in which a membrane was thermally etched in H_2.

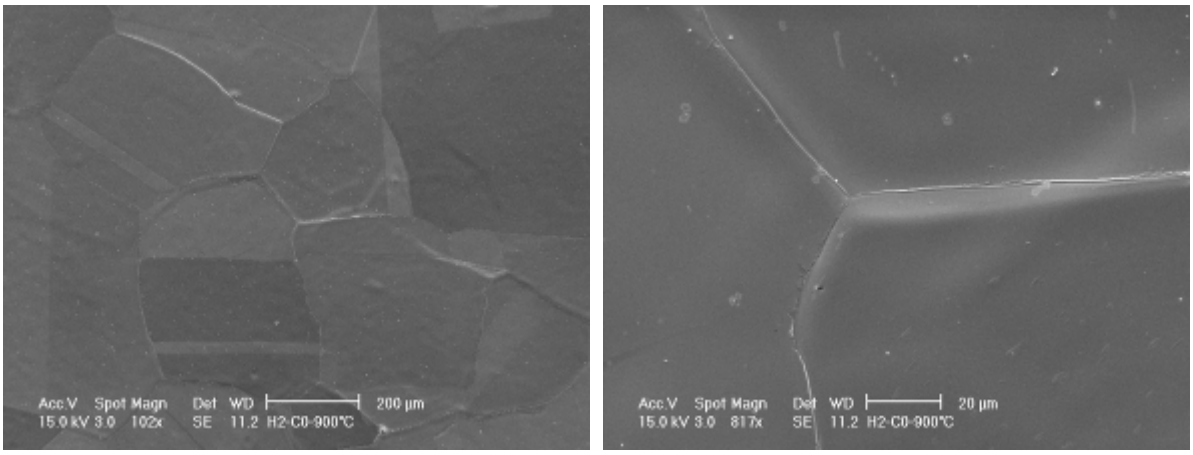

(a) (b)

Figure 12. SEM micrographs of the feed-side surface of the $Pd_{80wt\%}Cu$ membrane after exposure to 50%H_2-CO feed at 1173K and 1.11 MPa. The membrane was exposed to feed stream for 24hrs.

2.3.4 Effect of CO_2 on H_2-Permeance and Surface Morphology

2.3.4.1 Effect of CO_2 on H_2-Permeance:

CO_2, one of the products of the forward WGSR, would be present in substantial quantities in a WGSMR, especially if high conversions of CO were attained. However, because H_2 and CO_2 are the reactants of the reverse water-gas shift reaction (rWGSR), CO and H_2O were formed in the retentate stream when the H_2-CO_2 mixture was introduced to the unit. In some cases methane was also observed as a result of side reactions. For example at 908K, CO concentrations in the effluent stream were less than 3% and no CH_4 was detected. At 1038K, CO concentrations were as high as 20% and CH_4 concentrations were less than 2%, while at 1173K, CO concentrations were as high

as 26% and CH_4 concentrations were also less than 2%. It was anticipated, based on a previous study of the rWGSR in an Inconel reactor (Bustamante et al. 2004), that significant conversion of CO_2 would occur at elevated temperature, especially with the Pd-Cu membrane surface present. Permeance values were therefore calculated using the average H_2 concentration in the retentate.

Figure 13 illustrates that changes in permeance due to CO_2 varied from +2 to -5% at temperatures between 623 – 908K, with the least change occurring at 738K. Increasing temperature resulted in more substantial decreases in permeance, however. At 1173K, for example, the permeance decreased to 67-75% of its original value. Because competitive adsorption is known to decrease with increasing temperature, it is unlikely at this elevated temperature that the reduction in H_2-permeance was a result of competitive adsorption of CO_2 and H_2 on the membrane surface.

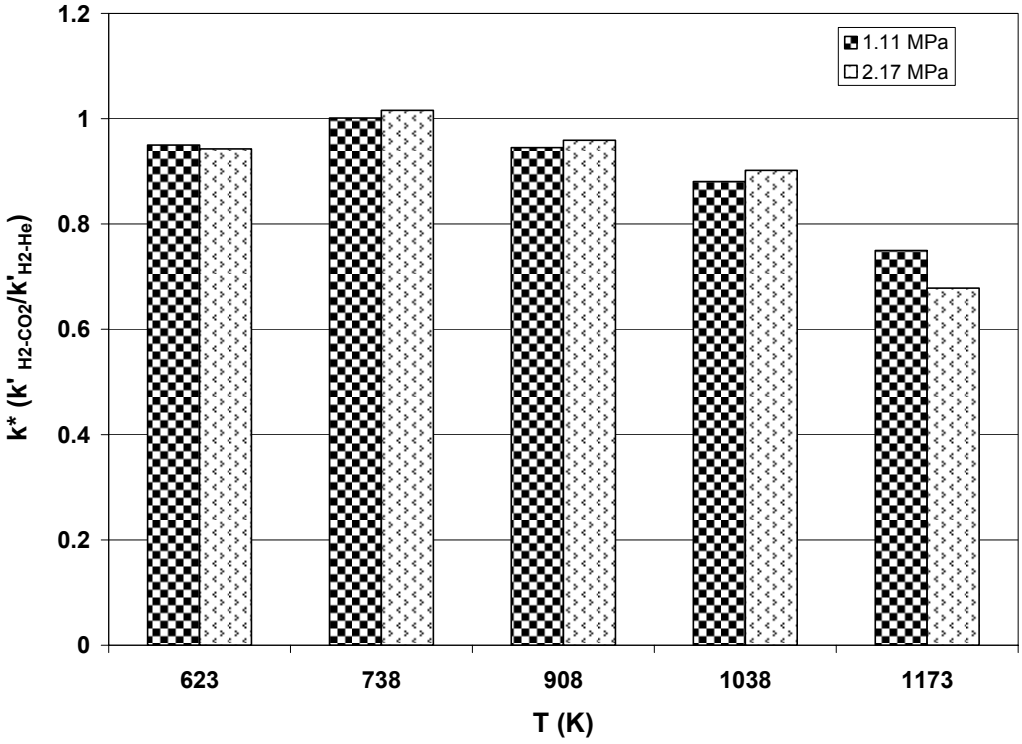

Figure 13. Effect of 50%CO_2 concentration on the H_2 permeance of 1 mm $Pd_{80wt\%}Cu$ at 1.11 and 2.17 MPa. k* is equal to the permeance (mol $H_2/(m^2 \cdot s \cdot Pa^{0.5})$) for the mixed feed stream (H_2 - CO_2) divided by permeance of the neat 90%H_2-He feed. Driving force for flux was based on the average H_2 retentate composition.

A comparison of the equilibrium conversions calculated using the temperature dependent equation for the equilibrium constant of the fWGSR, $Keq_{,f}$ (Equation (6)) given by Moe (Moe 1962) with the experimentally observed conversions in the present study is shown in Figure 13.

$$K_{eq,f} = \exp\left(\frac{4577.8}{T} - 4.33\right) \tag{6}$$

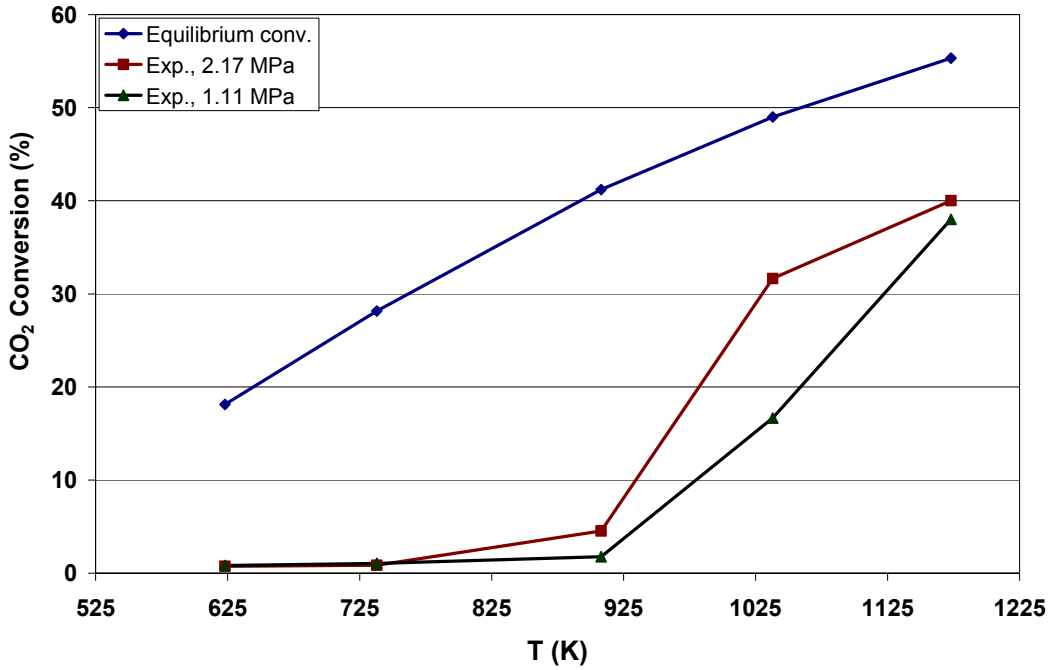

Figure 14. Comparison of equilibrium rWGSR conversion versus observed experimental conversions at total reactor pressures of 1.11 and 2.17 MPa for various temperatures, for an equimolar CO_2:H_2 inlet feed mixture.

Comparing the H_2 permeance losses shown in **Figure 13** with the observed CO_2 conversions in Figure 14, it is evident that at conditions of low CO_2 conversion, the drop in H_2-permeance is minimal. However, at temperatures greater than 908K at which more significant CO_2 – and thereby H_2 - conversion was observed, an appreciable permeance decrease was also apparent. The correlation between CO_2 conversion and permeance reduction may indicate that the observed permeance reduction may be the result of the reduced ability of the Pd-Cu membrane to dissociate and transport H_2 due to competition between the catalysis of the rWGSR and H_2 dissociation on the membrane surface.

2.3.4.2 Effect of CO_2 on $Pd_{80wt\%}Cu$ Surface Morphology

Figure 15, **Figure 16** and **Figure 17** are SEM images of the membranes following their exposure to the CO_2 - H_2 environment at 908K, 1038K and 1173K, respectively. Similar to the H_2O and CO exposure experiments, membrane roughening was observed at 908 (**Figure 15**a and b) and 1038K (**Figure 16**a and b). At 1173K less severe roughening and little pitting was observed (**Figure 17**a and b), with the appearance being similar to the H_2O – H_2 exposure at the same temperature. Hills of about 10 μm diameter are apparent which could be indicative of grain location. Sub-micron particles of unknown composition as well as some minor pitting roughly outline the hills, suggesting grain boundaries. The particles were too small to accurately ascertain their composition by EDS.

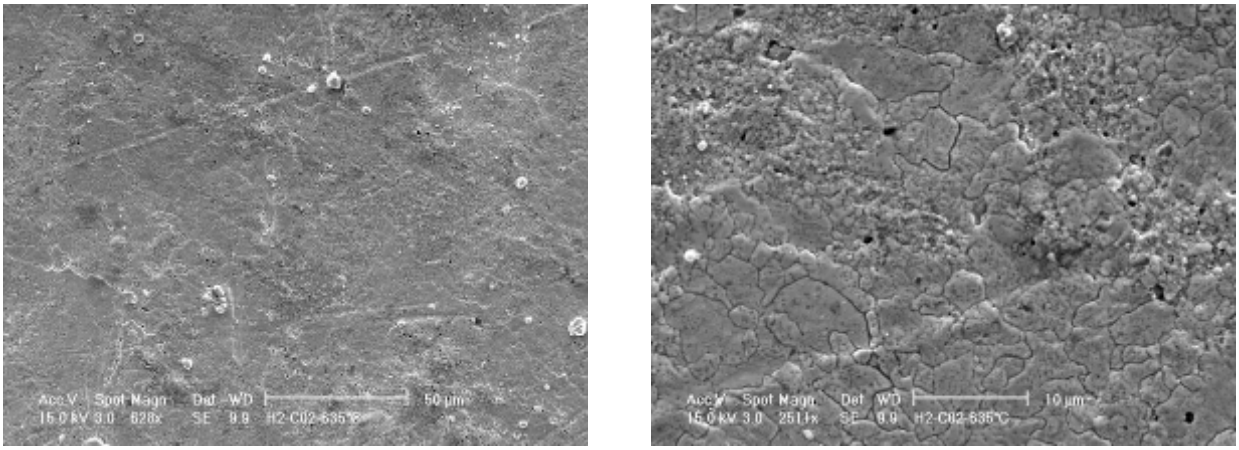

(a) (b)

Figure 15. SEM micrographs of the feed-side surface of the $Pd_{80wt\%}Cu$ membrane after exposure to 50%H_2-CO_2 stream at 908K. The membrane was exposed to 50%H_2-CO_2 at 1.11 MPa for 6 hrs and then 2.17 MPa for another 6 hrs.

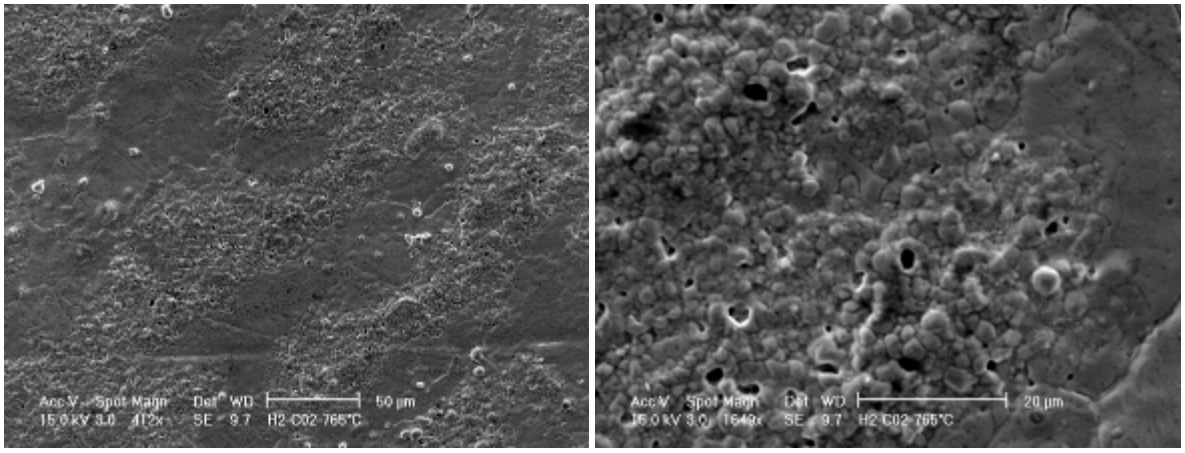

(a) (b)

Figure 16. SEM micrographs of the feed-side surface of the $Pd_{80wt\%}Cu$ membrane after exposure to 50%H_2-CO_2 stream at 1038K. The membrane was exposed to H_2-CO_2 at 1.11 MPa for 6 hrs and then 2.17 MPa for another 6 hrs.

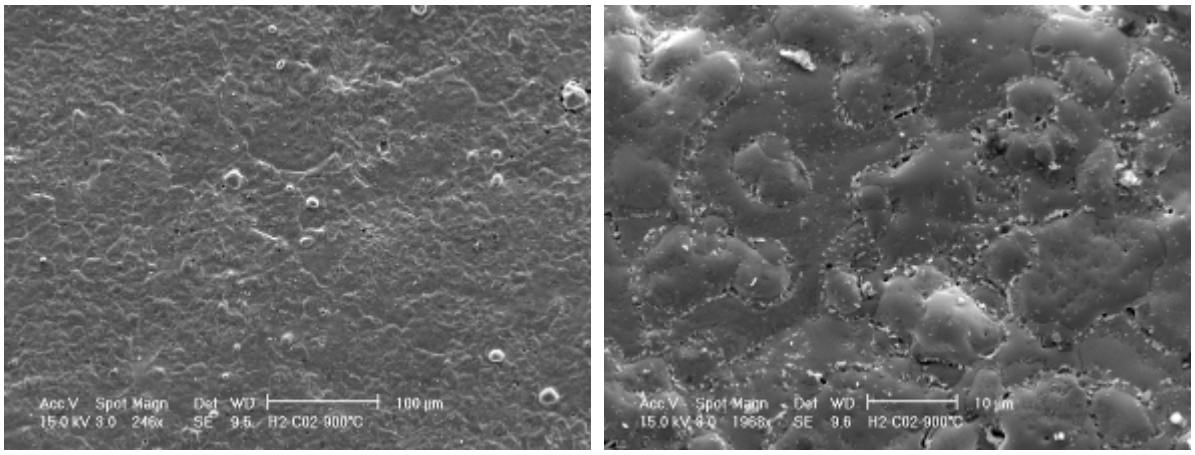

(a) (b)

Figure 17. SEM micrographs of the feed-side surface of the $Pd_{80wt\%}Cu$ membrane after exposure to 50%H_2-CO_2 stream at 1173K. The membrane was exposed to H_2-CO_2 at 1.11 MPa for 12 hrs and then 2.17 MPa for another 8 hrs.

The mechanism responsible for surface roughening and its dependence on temperature cannot be conclusively derived from these results. However, it is apparent

that for mixtures of H_2 with CO, CO_2 or H_2O, this effect is most prominent at temperatures of 908K to 1038K. This seems to point to a free radical mechanism as proposed by Dean et al. (Dean et al. 1988) and Wu et al. (Wu et al. 1985) which attributed significant surface modification of platinum foils to the interaction of homogeneously formed radicals and the metal surface. They suggest that under reaction conditions the interaction of free radicals formed via gas-phase reactions and the metal surface may result in volatile, meta-stable, intermediates which subsequently decompose at some other location, resulting in the observed surface modification.

2.4 CONCLUSIONS

The permeance of $Pd_{80wt\%}Cu$ alloy membranes in the presence of H_2 and equimolar mixtures of H_2 and either CO, H_2O or CO_2 has been determined over the 623 – 1173K temperature range at total pressures of 0.62 to 2.86 MPa in an attempt to determine the effect of the constituents of the water-gas shift reaction on a potential WGSMR membrane material. Relatively thick 1 mm membranes were used in order to ensure the precision and uniformity of the membrane composition and to improve the weldability and durability of the membrane. The relative changes in permeance noted in this study would probably be much less than those associated with thinner, higher permeance membranes.

Permeance decreases of 7% or less were noted for equimolar mixtures of H_2 and H_2O over the entire temperature range, with the smallest effects occurring at the lowest

temperatures. Significant micron-scale pitting on the $Pd_{80wt\%}Cu$ surface occurred at 908K, but the membrane surface was relatively smooth at 1173K.

The addition of CO resulted in permeance decreases of only 5% with no detectable change in surface morphology at temperatures of 623 and 738K. Permeance decreases as high as 50% occurred at 908K, the temperature in this study that carbon would be expected to form most readily via the Boudouard reaction. Permeance decreases of 15-20% occurred at 1038 and 1173K, where carbon deposition was negligible. CH_4, CO_2 and H_2O were produced at temperatures at and above 908K, reaching their greatest concentrations at 1038K. Membrane pitting and surface roughening occurred, especially at 1038K, but not at 1173K.

Although relatively small decreases in permeance occurred at temperatures of 908K or less due to the addition of CO_2, permeance reduction increased from 10 to 35% as temperature increased from 1038 to 1173K. The reverse WGS reaction also occurred over this temperature range, with conversions increasing from 15 to 40%. Competition for the catalytic Pd-Cu surface for H_2 dissociation and the rWGSR may have diminished permeance. Surface roughening was most prevalent at 908 and 1038K but a smoother membrane surface was realized at 1173K.

Although the surfaces defects associated with each of the gases did not diminish the mechanical integrity of the 1 mm membranes used in this study, comparable pitting and roughening evident at temperatures above 908K for the Pd-Cu membranes in this study, could prove catastrophic for ultra-thin (1-5 μm thick) membranes supported by porous substrates.

3.0 CHAPTER THREE: WALL-CATALYZED WATER-GAS SHIFT REACTION IN MULTI-TUBULAR, Pd AND 80WT%Pd-20WT%Cu MEMBRANE REACTORS AT 1173K

Abstract

The high-temperature, water-gas shift reaction was conducted in 100wt% Pd and 80wt%Pd-20wt%Cu ($Pd_{80wt\%}Cu$) shell-and-tube membrane reactors at 1173K with a 241 kPa (35 psig) trans-membrane pressure differential in the absence of heterogeneous catalyst particles. The tube bundle consisted of four parallel 15.25 cm long, 3.175 mm OD Pd-based tubes with a wall thickness of 125 μm. The modest catalytic activity of the Pd-based membrane surface for the forward WGS reaction, the high rate of hydrogen extraction through the Pd-based membranes, and the long residence times (1 – 5 s) resulted in a dramatic shift in carbon monoxide conversions of 93% at 1173K and a 1.5:1 steam-to-carbon monoxide feed ratio -- a value well above the equilibrium value of ~54% associated with a conventional (non-membrane) reactor. Carbon monoxide conversions decreased from 93% to 66% and hydrogen recovery from 90% to 85% at a residence time of 5 seconds when the Pd was replaced with $Pd_{80wt\%}Cu$, due to the lower permeance of the $Pd_{80wt\%}Cu$ alloy. SEM-EDS analysis of the membrane tubes suggested that the water-gas shift environment caused pinhole formation in the retentate surfaces of the Pd and $Pd_{80wt\%}Cu$ after approximately 8 days of operation.

3.1 INTRODUCTION

With the increasing demand for H_2 as an energy carrier in fuel cells and an energy source for combustion, efficient and economical methods of high-purity H_2 production are being assessed. H_2 production from coal remains one of the most promising near-term strategies for the generation of large volumes of this gas because coal is the nation's most abundant fossil fuel. Domestic recoverable coal reserves have been recently estimated at 270 billion short tons, about one-fourth of the world's total (DOE/IEA-0219(2003)). H_2 production from coal begins with gasification, which yields a syngas mixture composed predominantly of CO and H_2. The H_2 content of syngas can be increased by directing the syngas stream to a shift reactor in which the CO reacts with added steam to produce additional CO_2 and H_2 via the forward water-gas shift reaction (fWGSR).

System studies of conceptual coal gasification plant configurations have suggested that enhanced plant efficiency can be achieved by integrating H_2-selective membrane reactors (MR) into the process (Bracht et al. 1997; Chiesa et al. 2005). This would result in enhanced reactant conversion due to the selective extraction of one of the products. The MR would shift the equilibrium conversion toward the products (CO_2 and H_2), with the level of CO conversion being limited by MR length and/or permeate concentration of H_2. Furthermore, the use of a MR obviates the need for traditional H_2 purification processes, such as pressure-swing adsorption, because dense metal, H_2-selective, diffusion membranes could result in H_2 recovery and purity levels as high as 99% and 99.9999%, respectively (Grashoff et al. 1983). The high pressure CO_2-steam retentate stream would then be directed towards potential sequestration processes, most of which (e.g. injection into coal seams or oil or gas reservoirs, or deep sea disposal)

require compressed CO_2. In summary, the successful integration of a MR into the gasification process has the potential to enhance high purity H_2 production from an abundant domestic natural resource (coal), while simultaneously producing a high-pressure, CO_2-rich retentate stream which is amenable to sequestration strategies.

Several of the more promising high temperature H_2-selective membrane materials include porous ceramics, dense cermets and dense metals. This work focuses on the use of dense films of 100wt% Pd and $Pd_{80wt\%}Cu$ alloys. Pd and its alloys exhibit complete H_2 permselectivity, are fairly robust, can be operated for prolonged periods at high temperatures, and have been reported to exhibit catalytic activity for dehydrogenation and hydrogenation reactions (Gryaznov 1986) and the WGSR (Bustamante et al. 2005). As a result, dense Pd-based membranes have been used in research-scale reaction systems including dehydrogenation (Itoh et al. 1992; Abdalla et al. 1993; Ali et al. 1994; Gobina et al. 1994; Itoh 1995; Gobina et al. 1996; Lin et al. 2004), H_2S decomposition (Edlund 1996), steam reforming (Aasberg-Petersen et al. 1998; Kikuchi 2000; Lin et al. 2001), dry reforming (Ferreira-Aparicio et al. 2002) and the WGSR (Kikuchi et al. 1989; Criscuoli et al. 2000); (Basile et al. 1996; Basile et al. 1996; Tosti et al. 2003). In some cases, the investigators claim to have achieved better reaction selectivity and to have exceeded equilibrium conversion limitations in their respective reaction systems as a result of the presence of the MR (Uemiya et al. 1991; Tosti et al. 2003). Furthermore, in the case of the WGSR, complete conversion was reported (Uemiya et al. 1991; Basile et al. 1995; Criscuoli et al. 2000). **Table 2** summarizes operation temperature, MR material, catalyst type, equilibrium CO conversion, and the maximum CO conversion attained in WGSMRs. From the table, the efficacy of membrane reactors for facilitating the WGSR

is evident. However, all of the aforementioned WGSMR studies were conducted in the presence of heterogeneous catalyst particles and at reaction temperatures below 675K; conditions where high CO conversion is thermodynamically favored.

Table 2. Summary of membrane-assisted WGSRs, also known as water-gas shift membrane reactors, WGSMR.

Author	Max. conversion achieved with a MR (%)	Equilibrium conversion in non-membrane reactor (%)	T (K)	Membrane type	Catalyst type
(Basile et al. 1995)	~98	83-96	595	10 μm Pd on ceramic	Low-temp. shift catalyst LK-821-2
(Basile et al. 1996)	99.89	99.1	595	0.2 μm Pd on ɣ-Al_2O_3	Low-temp. shift catalyst
(Basile et al. 2001)	100	84	605-625	50-70 μm Pd-Ag	Low-temp. shift catalyst LK-821-2
(Basile et al. 1996)	~95	~93	595	0.1 μm Pd on ɣ-Al_2O_3	Low-temp. shift catalyst LK-821-2
(Criscuoli et al. 2000)	100	85	595	70 μm Pd	Low-temp. shift catalyst

Table 2 (continued).

Author	Max. conversion achieved with a MR (%)	Equilibrium conversion in non-membrane reactor (%)	T (K)	Membrane type	Catalyst type
(Kikuchi et al. 1989)	92	76	673	20 μm Pd on microporous-glass	Fe_2O_3-Cr_2O_3
(Seok et al. 1990)	85	99	430	Porous glass	Ruthenium (III) chloride trihydrate
(Tosti et al. 2003)	98.2	~80	598	50-70 μm Pd-Ag foil	Low-temp. shift catalyst LK-821-2
(Tosti et al. 2000)	~100	80%	605	10 μm Pd-23at.%Ag	Catalyst obtained from Haldor Topdoe, DK
(Uemiya et al. 1991)	98	75	673	20 μm Pd on porous glass	Iron-chromium oxide
(Flytzani-Stephanopoulos et al. 2004)	~94	93	623	10 μm $Pd_{60wt\%}Cu$	Cu-Ce(30%La)-Ox

The desire to integrate Pd-based membranes into various reaction environments which would expose the membrane to a wide composition of feed gases has led to studies

of the effects of these gas-phase constituents on the membrane integrity and performance. Gaseous components that have been studied for their effect on the permeability and durability of Pd-based membranes include: CO (Hara et al. 1999; Amandusson et al. 2000; Li et al. 2000; Chapter 2), H_2O (Li et al. 2000; Chapter 2), CO_2 (Chapter 2), H_2S (Hurlbert et al. 1961; McKinley 1967; Edlund et al. 1994; Kajiwara et al. 1999; Bryden et al. 2002; Morreale et al. 2004; Kulprathipanja et al. 2005; Mundschau et al. April, 2005), O_2 (Bustamante et al. 2005) and CH_4 (Chen et al. 1996; Jung et al. 2000).

In low concentrations, CO, H_2O, CO_2 and CH_4 were reported to present minimal adverse effects on membrane performance at temperatures greater than approximately 823K. Chapter 2 explored the morphological and performance changes of the $Pd_{80wt\%}Cu$ membrane associated with the presence of the various WGS components over a wide range of temperatures and pressures when present in high concentration. Chapter 2 showed that at temperatures between 908 and 1038K exposure of $Pd_{80wt\%}Cu$ membranes to either high steam or CO_2 concentrations resulted in pitting of the membrane surface. The introduction of a H_2-CO feed stream resulted in CO cracking on the $Pd_{80wt\%}Cu$ membrane surface at 908K, depositing carbon, which resulted in H_2 permeance reduction, but the carbon deposition was not observed at 1038K. By contrast, exposure of the $Pd_{80wt\%}Cu$ membrane to the binary mixture of H_2 and each of the WGS components at 1173K resulted in a negligible impact on the membrane characteristics. Therefore, it was expected that the $Pd_{80wt\%}Cu$ MR could be successfully operated at 1173K in the water-gas shift environment.

H_2S and O_2 were reported to adversely affect membrane characteristics, however, even when present at ppm levels of concentration. Bustamante et al., (Bustamante et al.

2005) suggested that prolonged exposure of solid Pd and $Pd_{80wt\%}Cu$ rods to O_2 induced surface porosity in the samples. Hurlbert et al. (Hurlbert et al. 1961) reported that in addition to a reduction in permeability, exposure of Pd to H_2S may result in the formation of an irreversible grey surface scale, presumably a palladium sulfide. Furthermore, H_2S exposure to Pd-based membranes was observed to result in dramatic pitting of the membrane surfaces (Kulprathipanja et al. 2005; Mundschau et al. April, 2005).

The objective of this study was to assess the performance of Pd and $Pd_{80wt\%}Cu$ MRs at an elevated temperature of 1173K in the absence of a bed of heterogeneous catalyst particles. This temperature, which is significantly greater than the temperature range associated with prior investigations detailed in **Table 2**, was selected to be representative of a MR positioned just downstream of the coal gasifier. High conversions of CO can be attained at this temperature if a MR that is selective to one of the products, CO_2 or H_2, is used, because the WGS reaction is not thermodynamically favored at these conditions. It was expected that this elevated temperature would enhance homogeneous fWGS reaction rate and increase the permeance of the Pd-based membranes. Further, it was anticipated that the Pd-based membrane surfaces would modestly catalyze the reaction at 1173K. Thick-walled tubes (125 μm) were selected to facilitate the construction of robust MRs that could yield reproducible results. However, the wall thickness used in this study would not be considered viable for commercial application. Rather, this investigation was designed to be a proof-of-concept assessment of the prospects of using Pd and $Pd_{80wt\%}Cu$ materials at elevated temperatures in a WGSMR to achieve high conversions of CO.

3.2 EXPERIMENTAL

The gases used in this study were He, CO, and Ar. All gases used were 99.999% certified calibration gases. He and Ar were used during heat-up of the various reaction systems to the desired reaction temperature of 1173K. The flow rate of each gas was controlled by Brooks mass flow controllers. The feed and permeate pressures were regulated by pneumatically actuated stainless steel control valves.

3.2.1 Experimental Apparatus

Four different WGS reactor systems were investigated in the current work: a conventional (non-membrane) reactor made of stainless-steel, a conventional quartz-lined stainless-steel reactor, a Pd MR, and a $Pd_{80wt\%}Cu$ MR. The first two reactors were designed for control experiments, while the latter two reactors enabled the influence and performance of the membrane reactor to be evaluated. All reactors were shell and tube configuration, with the reaction taking place in the tube-side and an inert gas sweeping away the permeated H_2 in the shell-side. The experimental apparatus used was described in Chapter 2, with the exception of the improved heating system. In this study, a three-zone heater was designed to maintain an isothermal temperature profile along the length of the reactors. (Single zone heating elements commonly produce a parabolic profile with the maximum temperature in the middle of the reactor and with a substantial temperature

gradient along the tube length.) The reactors were heated to the desired temperature at a rate of 120K/hr under a constant flow of He in the feed side and Ar in the sweep side using a 23 cm-long, three-zone cylindrical resistance heater placed concentrically around the membrane assembly. An eight-element, 3.175 mm thermocouple was used to determine the temperature profile of the reaction zone prior to conducting the WGS reaction experiments. There was a ±5K temperature change from the desired set point along the length of reactor tube at a nominal temperature of 1173K. A 1.5875 mm OD thermocouple with three sensor points located three inches apart was then used to monitor and control the membrane temperature during membrane reactor experiments.

At the experimental temperature of 1173K, CO and steam were introduced at flow rates of 80 and 120 sccm, respectively. The desired amount of steam was introduced by injecting distilled water into the flowing gas stream by a calibrated ISCO 500D syringe pump; the water was vaporized in the heated feed line before entering the reactor. Excess steam was used to prevent carbon formation in the membrane tubes. Prior control studies suggested that the 1.5 steam-to-CO ratio was adequate to suppress carbon formation in the reactor systems.

A trap was placed on the exit line to collect the unreacted steam before the effluent gases were directed to a Hewlett-Packard 5890 Series II GC equipped with a 3 m long by 3.2 mm OD zeolite-packed column and thermal conductivity detector for quantification. The water trap was used to mitigate inaccurate quantification of the components in the effluent gas stream which could result from a water-saturated column or films of liquid water in the flow lines.

Equations (7) to (10) were used to calculate the CO conversion and the H_2 recovery from the reaction zone. The amounts/concentrations of H_2, CO and CO_2 in the reactor effluent were determined by gas chromatography. These expressions are based on a feed of only CO and H_2O to the reactor. The CO conversion, X, calculated by Equation (7) was assumed to have taken place only within the reactor. Negligible CO conversion occurred in the tubing leading to and from the reactor because of the steep temperature changes before and after the reaction zone. Further, the feed lines were lined with quartz to minimize interaction of the reactant gases with the stainless-steel walls (the kinetic rate of the WGSR is extremely slow in quartz-lined empty vessels at temperatures below about 1000 K).

In order to determine the effect of residence time on CO conversion experiments, the residence times of the reactor systems were varied by changing the operating pressure, while keeping the inlet feed flow rate and reaction temperature constant. Note that previous work conducted by Bustamante et al. (Bustamante et al. 2005) provides a rate expression for the forward WGSR based on high pressure data obtained at NETL. Increasing the reaction pressure in our experiments therefore increased the residence time, increased the H_2 partial pressure driving force for H_2 flux, and also increased the rate of reaction.

$X = \left(\frac{[CO_2]}{[CO]+[CO_2]} \right)$	(7)
H_2 total (sccm) = $X*Q_{CO,0}$	(8)

H_2 extracted (sccm) $= \frac{[H_2]_{sweep}}{1-[H_2]_{sweep}} * Q_{Ar,sweep}$	(9)
H_2 recovery (%) $= \frac{H_{2\ extracted}}{H_{2\ total}} * 100$	(10)

where X is the molar CO conversion, $[H_2]$ is the molar concentration of H_2, and Q_i is the molar flow rate (sccm) of either the inlet CO ($CO,0$) or the Ar sweep (Ar_{sweep}). $[CO_2]$ and $[CO]$ are the molar concentrations of CO_2 and CO in the reactor effluent stream measured by GC, respectively.

3.2.2 Non-membrane Reactors for Control Experiments

Control experiments in a quartz-lined reactor and a stainless-steel reactor were conducted to compare CO conversions in conventional reactor systems with those in catalytic, H_2-permeable MRs. For the quartz-lined vessel, a quartz tube with an OD just less than the ID of the stainless-steel tube was carefully inserted into the stainless-steel tube. This quartz-lined reactor was designed to provide a control experiment with essentially H_2-impermeable walls (relative to Pd) and minimal sites for catalytic wall effects of the stainless steel to influence the homogeneous gas phase reaction. The reactor was a single 14 cm-long stainless-steel tube, 0.87 cm ID, lined with a 14 cm-long, 0.6 cm ID quartz lining. This resulted in a reactor volume within the quartz tube of 3.96 cm^3.

The stainless-steel reactor was of identical geometry, but without a quartz liner. This reactor served as a control experiment in that it also had essentially H_2-impermeable walls, but was likely to wall-catalyze the WGS reaction more significantly that the quartz-lined vessel. The stainless-steel reactor used had an ID of 0.46 cm, a length of 25.4 cm, and a reactor volume of 4.17 cm^3. Although the volumes of the quartz-lined stainless-steel reactor and the stainless-steel reactors differed from the MR volume, the residence time values were maintained at a comparable range by varying the operating pressure.

3.2.3 Membrane Reactors

The 3.175 mm OD, 125-μm thick Pd and $Pd_{80wt\%}Cu$ alloy tubes used in the present study were manufactured by Goodfellow using 99.9% purity (metals basis) Pd and Cu. We recognize that this thickness of Pd-based tubes is not viable for commercial-scale reactors. Numerous research efforts are being directed at the reproducible manufacture of sub-micron to 5-micron thick films of Pd or Pd-alloys of precise composition supported on a porous substrate or on a dense metal with extraordinarily high H_2 permeance but poor surface qualities (e.g. vanadium, niobium). Our goal, however, is to assess whether a specified alloy composition is appropriate for the reaction conditions of interest. Our results would enable those involved in the time-consuming task of identifying a method for reproducibly manufacturing commercial-scale membranes to select the appropriate alloy for the operating conditions of interest. Our selection of 125-micron thick tube walls 1) enabled us to quickly access Pd-based

materials of precise composition in large amounts, 2) facilitated the fabrication of the MR, 3) enhanced the robustness of the reactor at extreme conditions, 4) enabled us to assemble several reactors, and 5) permitted us to conduct experiments for long periods of time without being plagued with operational problems associated with ultra-thin membranes, such as leaks at seals and defects in membranes.

A four-tube MR (Figure 18), rather than a single tube of larger diameter, was designed to increase the catalytic surface area to reaction volume ratio of the MR. This was accomplished by designing a flange in which a 4.572 mm ID x 6.35 mm OD stainless steel tube fed four 2.925 mm ID membrane tubes, each 15.25 cm in length. The effective surface area of the four tubes for H_2 transport was about 51.9 cm^2 and the total reactor volume was 3.5 cm^3. In addition to coupling the four membrane tubes, the flange also served as a static mixer for the CO and steam feed. The membrane assembly was inserted into a 3.2 cm ID Inconel® shell. This inside-outside H_2 diffusion configuration allowed the feed gas stream to enter through the inside of the 3.175 mm OD membrane tube, allowing H_2 to diffuse through the membrane, into the Inconel shell in which an Ar sweep gas was introduced at a flow rate high enough to ensure that the H_2 concentration in the sweep was less than 3%. Typically, an Ar flow of 1800 sccm was adequate to achieve these concentration levels. The high-pressure retentate gases retained in the membrane tubes, and the low concentration H_2-Ar sweep permeate were then directed to the gas chromatograph (G.C.) for composition analysis.

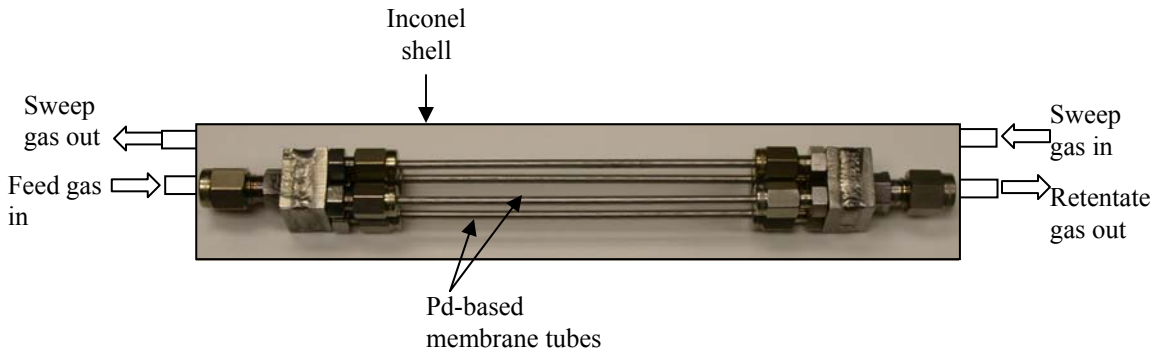

Figure 18. Detail of the NETL four-tube Pd-based membrane reactor.

3.2.4 SEM-EDS Analysis

Membrane surface morphology was examined prior to and following exposure to the mixed feed stream via SEM. Compositional information was obtained through EDS. A Philips XL30 FEG SEM equipped with EDS was used for the analyses. Membranes were removed from the test assembly for characterization following testing by carefully cutting a small section of each tube using a jeweler's saw, taking care to limit surface contamination as much as possible. For outer surface analysis, the cylindrical samples were carefully rinsed with acetone before mounting into the SEM. For inner surface analysis, the sample was carefully split in half with a surgical scissors, ensuring that the sample maintained its curvature, thereby preventing the introduction of superficial surface defects.

3.3 RESULTS AND DISCUSSION

3.3.1 Control Experiments

Figure 19 depicts the conversions attained in all four reactor systems investigated in the current work, in addition to the CO equilibrium conversion. This conversion of ~54% for the specified operating conditions was calculated using the temperature dependent equation for the fWGSR equilibrium constant given by (Moe 1962). The MR results are discussed in section 3.3.2. In the case of the H_2-impermeable stainless steel and quartz-lined stainless-steel control reactors, the figure illustrates increasing CO conversions with increasing residence time. The reaction selectivity to H_2 and CO_2 was essentially unity in both systems with no detectable side reaction products. The maximum CO conversions of about 33% and 15% were attained at a residence time of about 5 s in the traditional stainless steel and quartz-lined stainless-steel reactors, respectively. As expected, both reactor systems resulted in CO conversions appreciably lower than the equilibrium CO conversion of ~54%, with the stainless-steel reactor resulting in slightly higher conversions because of the catalytic effect of the stainless steel walls.

3.3.2 Membrane Reactor Studies

The WGSR was conducted in both Pd and $Pd_{80wt\%}Cu$ MRs operated in counter current mode, i.e. with the reactant gases and the sweep gas flowing in opposite directions. It was anticipated that both of these MRs would yield greater conversions than the control experiments because the Pd and $Pd_{80wt\%}Cu$ reactor walls were catalytically

active and perfectly perm-selective to H_2. The effect of feed-side residence time on CO conversion was investigated by varying the feed-side pressure while keeping the inlet feed flow rate and trans-membrane pressure drop of 241 kPa constant.

CO conversions attained with Pd-based MRs were greater than the equilibrium conversion of 54% associated with non-membrane reactors. The maximum CO conversions attained (Figure 19) were 65% and 93% at a residence time of 5 s for the $Pd_{80wt\%}Cu$ and Pd MRs, respectively. Although $Pd_{80wt\%}Cu$ surfaces were previously reported to exhibit slightly greater catalytic activity toward the WGSR than Pd surfaces (Bustamante et al. 2005), the lower conversions associated with the $Pd_{80wt\%}Cu$ MR are probably the result of the decrease in permeance with increasing Cu content for fcc alloys. At 1173K, the H_2 permeance of Pd and $Pd_{80wt\%}Cu$ were measured to be $3.1*10^{-4}$ and $1.42*10^{-4}$ mol H_2 /($m^2 \cdot s \cdot Pa^{0.5}$), respectively. These values suggest about a 54% lower H_2 permeance of the $Pd_{80wt\%}Cu$ membrane relative to Pd at 1173K.

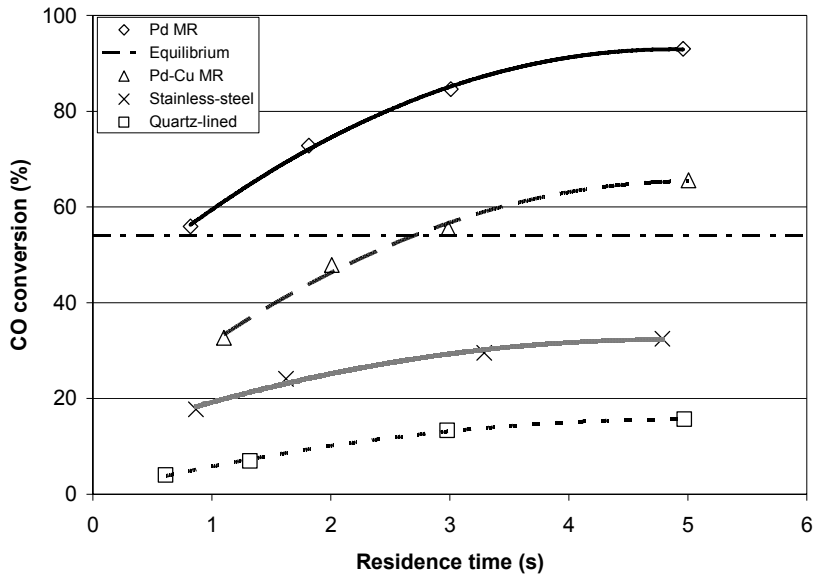

Figure 19. CO conversion at 1173K for Steam-to-CO ratio of 1.5 in quartz-lined stainless-steel, stainless-steel, Pd and $Pd_{80wt\%}Cu$ reactors as a function of residence time. Equilibrium conversion at these conditions is ~54%.

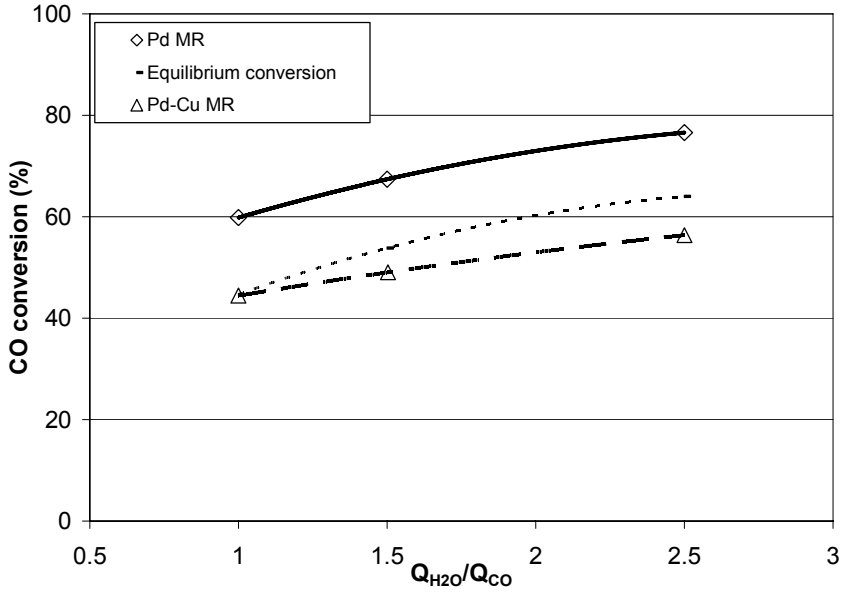

Figure 20. CO conversion at 1173K and 2 s residence time for various steam-to-CO ratios in Pd and $Pd_{80wt\%}Cu$ four-tube reactors.

Figure 20 shows the effect of steam-to-CO ratio on CO conversion for the Pd and $Pd_{80wt\%}Cu$ membrane systems at 1173K and 2 s residence time. The figure illustrates an enhancing effect of increasing steam-to-CO ratio on CO conversion for the Pd MR, surpassing equilibrium limitations over the conditions of study. Although the CO conversion in the $Pd_{80wt\%}Cu$ system also increases with increasing steam-to-CO ratio, CO conversion remained below the equilibrium limit with increasing steam-to-CO ratios. This is probably due to the diminished extraction of H_2 from the reaction zone caused by the reduction in the membrane permeance.

The H_2 recoveries from both MR systems determined using Equation 4 and are shown in **Figure 21**. These results suggest that at residence times greater than 1 s, 75 - 90% of the generated H_2 was extracted by the Pd MR system with extremely high purity, leaving a high-pressure, CO_2-rich stream on the retentate side of the MR. Although the H_2 recovery at a similar residence time in the $Pd_{80wt\%}Cu$ system is slightly lower, 72 - 86%, the results indicate that the MR system could potentially be used in the absence of additional heterogeneous catalysts to simultaneously attain high CO conversions and ultra-high purity H_2 streams at elevated temperatures.

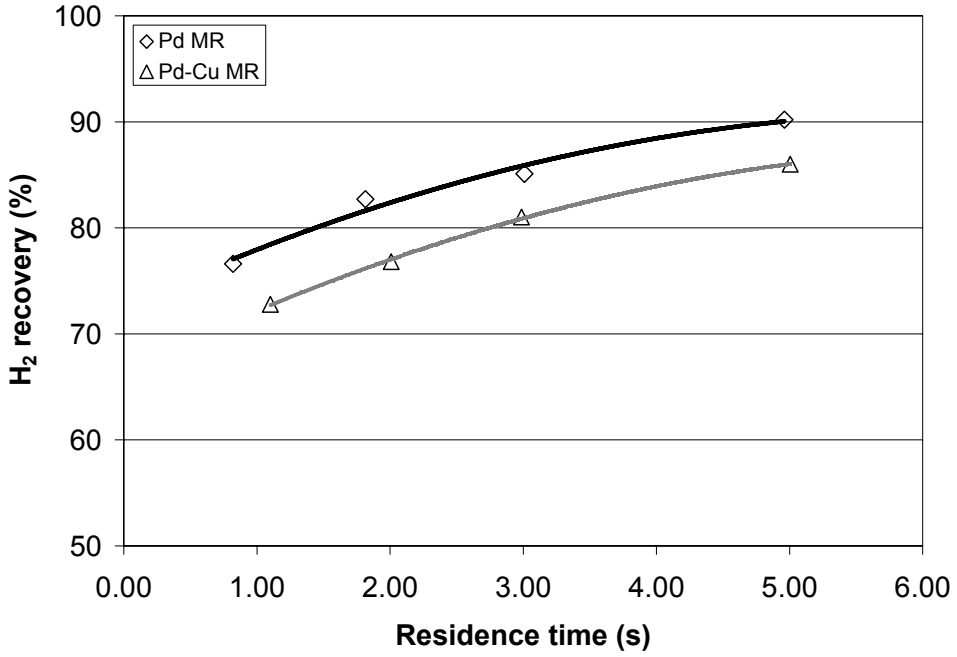

Figure 21. High purity H_2 recovery as a function of residence time for Pd and $Pd_{80wt\%}Cu$ four-tube reactors at 1173K and H_2O:CO ratio of 1.5.

3.3.3 SEM-EDS Analyses of Pd-based Membrane Reactors

Figure 22 and Figure 23 are SEM images of the as-received Pd and $Pd_{80wt\%}Cu$ membrane tubes, respectively, revealing surface defects, i.e. surface grooves and dimples on the Pd and $Pd_{80wt\%}Cu$ samples, respectively. The figures to the right (b) are higher magnifications of a selected area of the figures on the left (a). Although the Pd sample (Figure 22) did not exhibit apparent contamination on the surface, a roughened surface is evident in the SEM image (Figure 22b), probably the result of the fabrication technique for manufacturing the Pd tubes. The SEM image of the as-received $Pd_{80wt\%}Cu$ membrane (**Figure 23**) reveals a slightly less roughened surface compared to the fresh Pd sample, in addition to dimples on the sample (**Figure 23**b). Figure 24 is an EDS spectrum of the

image shown in **Figure 23**b. The EDS spectrum reveals Fe, Al, and Si contamination in the membrane sample. The Fe observed in the EDS spectrum resulted from metal shavings from the jeweler's saw used to cut the $Pd_{80wt\%}Cu$ sample and are visible on the surface of the $Pd_{80wt\%}Cu$ sample (shiny particles in **Figure 23**b).

Figure 25 to Figure 27 depict SEM images of the Pd and $Pd_{80wt\%}Cu$ membrane samples after exposure to the WGS reaction at 1173K for about 10 days. It is evident from the various images that the membranes experienced surface modification after extended exposure to the WGSR environment. Surface modification such as the formation of grain boundaries, faceted surfaces, and pits on exposure of metals to gaseous environments has been previously reported for various metals (Wu et al. 1985). **Figure 25** depicts the outer (permeate) surface of the Pd membrane which was exposed to the Ar/H_2 sweep stream. In contrast to **Figure 26**a and b which show the inner (retentate) surface of the Pd membrane that was directly exposed to the WGS environment, the outer surface is relatively smooth with no apparent pitting on the membrane surface. This contrast suggests a direct influence of the WGS environment on the formation of surface pits observed on the inner surface of the Pd MR. In light of this, control experiments were designed to ascertain if the pinhole formation may have resulted from sintering of the membrane after prolonged operation of the MR at 1173K. This was accomplished by exposing Pd and $Pd_{80wt\%}Cu$ membrane tubes to $90\%H_2$-He environments for about 240 hours. SEM analysis of the membrane surfaces following the $90\%H_2$-He exposure tests showed no pinholes on the membrane surface. The formation of surface pits in the current experiments after prolonged operation of the MRs in the

WGSR environment resulted in CO and CO_2 penetration of the permeate stream. Note that all results reported in this manuscript were recorded prior to leak detection.

Figure **27** depicts SEM images of the inner surface of the $Pd_{80wt\%}Cu$ membrane after exposure to the WGS environment for approximately 10 days. Although pits were not evident in the inner surface images, a He leak test of the MR after reaction testing revealed pinhole leaks toward the outlet of three of the four membrane tubes. The presence of pinholes resulted in the infiltration of CO and CO_2 into the permeate stream, compromising H_2 purity. A magnification of the $Pd_{80wt\%}Cu$ sample (**Figure 27**b) revealed particles preferentially segregated at the grain boundaries of the membrane. EDS analysis of the grain boundary region containing these particles (**Figure 28**) detected some Al and O_2 content. Al was also detected in the fresh $Pd_{80wt\%}Cu$ sample (Figure 24).

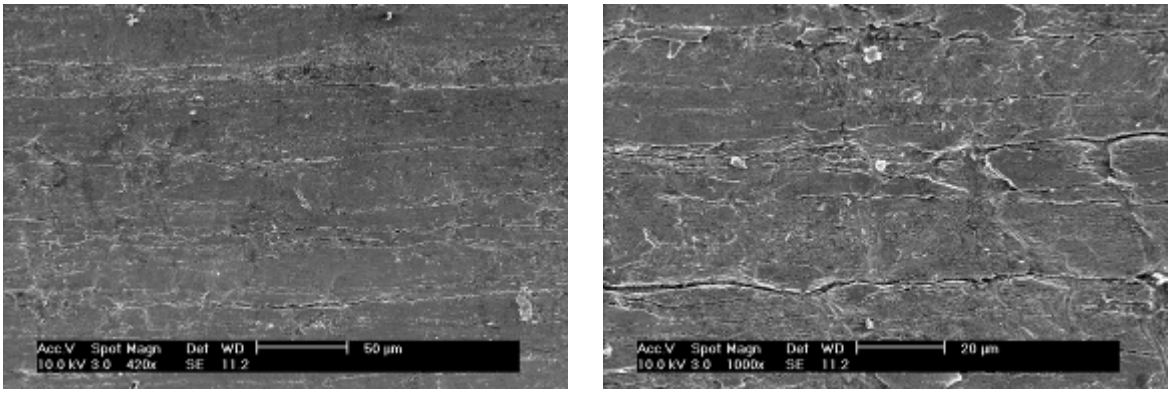

(a) (b)

Figure 22. SEM image of the inner (retentate) surface of the as-received Pd tube showing grooves on the membrane surface.

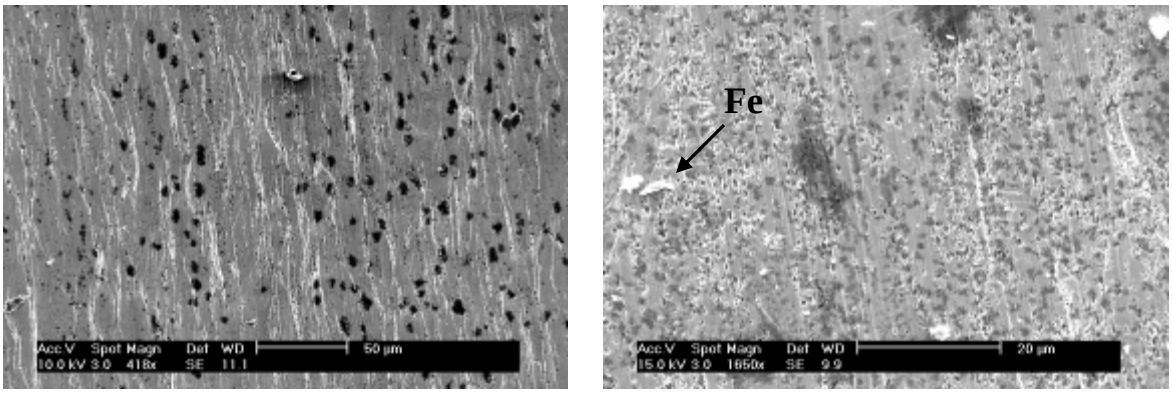

(a) (b)

Figure 23. SEM image of the inner (retentate) surface of the as-received $Pd_{80wt\%}Cu$ tube showing surface contamination (black patches) and dimples on membrane surface.

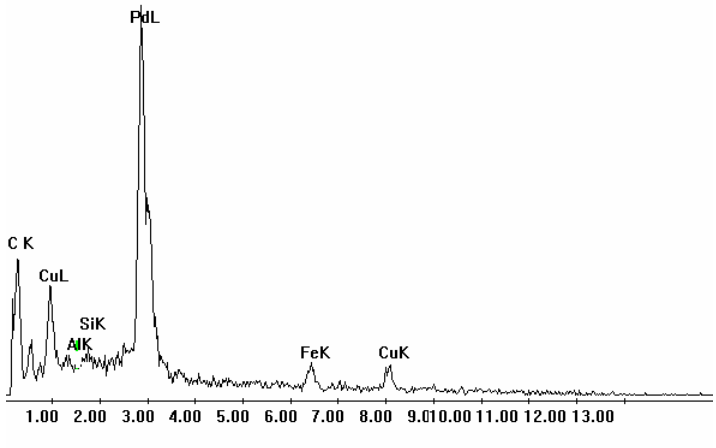

Figure 24. EDS spectrum of fresh $Pd_{80wt\%}Cu$ surface showing metal shaving on membrane surface (Fe) in addition to Al and Si contamination in membrane sample.

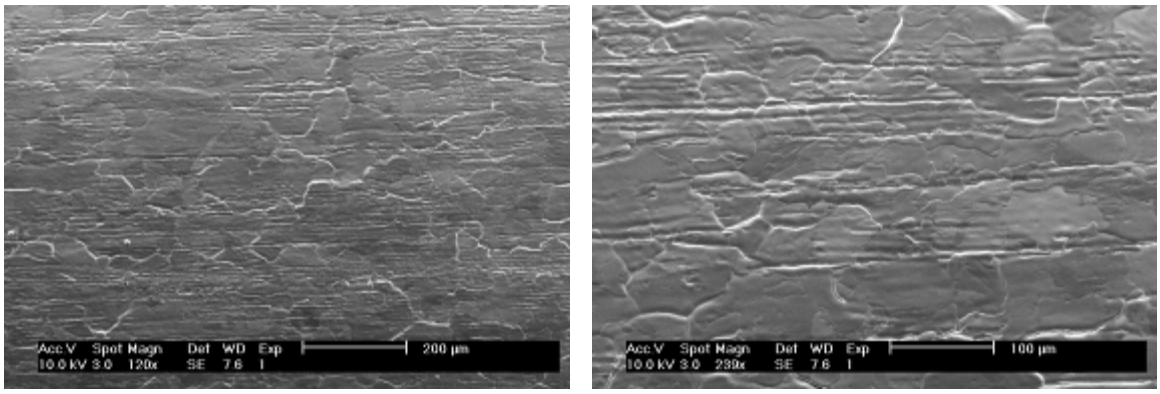

(a) (b)

Figure 25. SEM images of the outer (permeate) surface of Pd MR after 10 days of WGSR at 1173K.

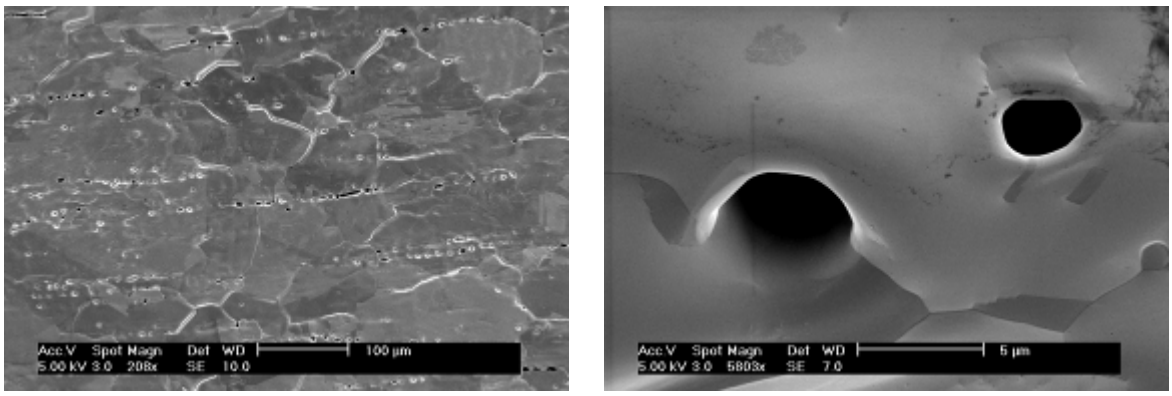

(a) (b)

Figure 26. SEM image of inner (retentate) surface of Pd MR after 10 days of WGSR at 1173K depicting holes on membrane surface.

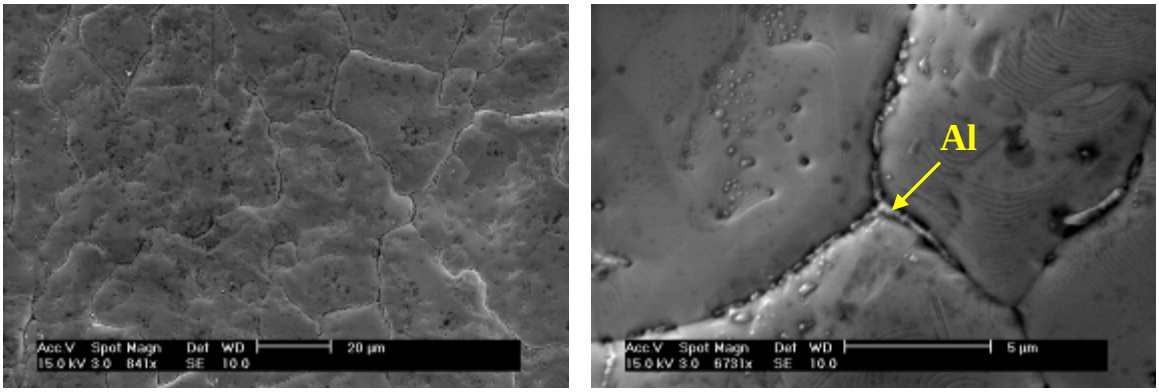

(a) (b)

Figure 27. SEM image of inner (retentate) surface of $Pd_{80wt\%}Cu$ MR after 10 days of WGSR testing at 1173K.

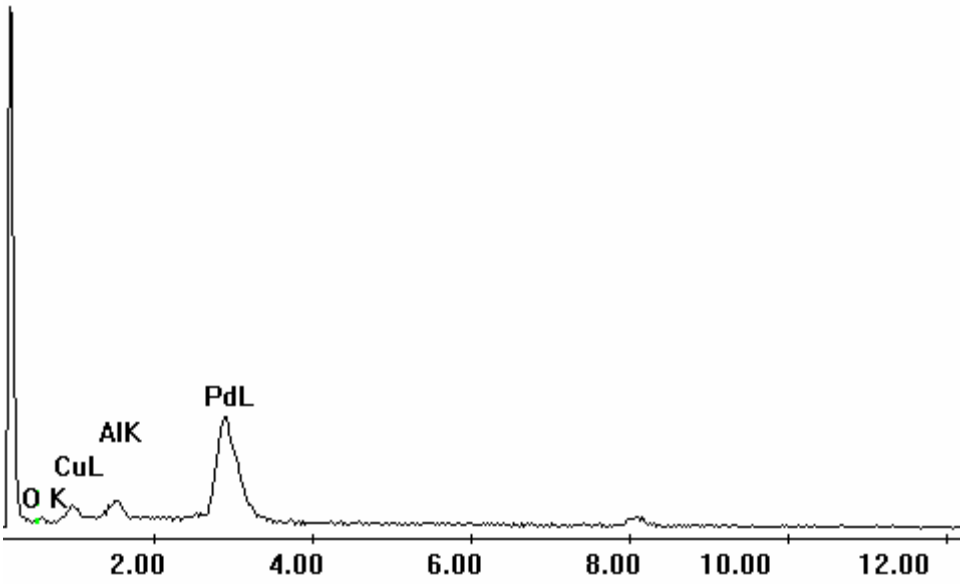

Figure 28. EDS spectrum of grain boundary location of $Pd_{80wt\%}Cu$ sample above revealing Al contamination within the grain boundary.

3.4 CONCLUSIONS

The high-temperature WGSR in the absence of additional heterogeneous catalysts was successfully demonstrated in catalytic Pd and 80wt%Pd20wt%Cu membrane reactors at 1173K in the absence of H_2S. The rapid rate of reaction coupled with the catalytic activity of the membrane reactor surface, in addition to the rapid rate of H_2 extraction, resulted in CO conversions greater than the approximately 54% equilibrium CO conversion at the operating conditions.

A maximum CO conversion of 93% was attained in the Pd membrane reactor system, while the $Pd_{80wt\%}Cu$ membrane reactor attained a maximum CO conversion of approximately 66%. The markedly lower conversion attained in the $Pd_{80wt\%}Cu$ membrane reactor system was attributed to the lower H_2 permeance of the $Pd_{80wt\%}Cu$ membrane reactor.

Increasing the steam-to-CO ratio resulted in higher CO conversions in the Pd membrane reactor system. Although a similar trend was observed for the $Pd_{80wt\%}Cu$ membrane reactor system, the CO conversions remained below the equilibrium conversion value for increasing steam-to-CO ratios probably due to the lower rate of H_2 extraction relative to the Pd membrane reactor.

Both membrane systems resulted in high H_2 recovery at residence times as low as 1 s. At a residence time of 5 s, approximately 90 and 85% of the generated H_2 was recovered through the Pd and $Pd_{80wt\%}Cu$ membranes, respectively.

Both the Pd and $Pd_{80wt\%}Cu$ membrane reactor systems were observed to form surface pits after about 10 days of reaction testing at 1173K, compromising their ability to produce ultra-high purity H_2 for prolonged periods of time.

4.0 CHAPTER FOUR: THE INFLUENCE OF H_2S-TO-H_2 PARTIAL PRESSURE RATIO ON THE SULFIDIZATION OF Pd AND 80WT%Pd-Cu MEMBRANES

Abstract

The influence of H_2S-to-H_2 partial pressure ratio on Pd and 80wt%Pd20wt%Cu ($Pd_{80wt\%}Cu$) membrane alloys was studied at 1173K using 1,000 ppm H_2S-10%He-H_2, 2,000 ppm H_2S-in-H_2 and 5,000 ppm H_2S-in-H_2 gas mixtures. Neither membrane formed sulfides when exposed to the 1,000 ppm H_2S-He-H_2 gas mixture at this temperature. According to thermodynamic calculations, the Pd should have been sulfidized when exposed to the gas mixtures containing 2,000 and 5,000 ppm H_2S-in-H_2, while the $Pd_{80}Cu$ alloy should have tolerated (not formed sulfides) the H_2S at these conditions due to the reduced activity of Pd in the alloy. However, both membranes formed sulfide scales when exposed to the mixtures with H_2S concentrations greater than 2,000 ppm H_2S-in-H_2. The unanticipated sulfidization of the $Pd_{80wt\%}Cu$ membrane exposed to the 2,000 ppm H_2S-in-H_2 was attributed to Cu segregation at the membrane surface. This resulted in the formation of Cu-S islands surrounded by regions of unsulfidized Pd-Cu for the $Pd_{80wt\%}Cu$ membrane exposed to the 2,000 ppm H_2S-in-H_2 gas mixture. Cu_2S is thermodynamically stable at 1173K in the presence of H_2S-in-H_2 concentrations above about 2,000 ppm.

4.1 INTRODUCTION

Despite growing concerns about greenhouse gases, hydrocarbons are expected to remain a major source of H_2 in the foreseeable future. H_2 production from coal gasification, in particular, has gained renewed interest in recent years because of the vast amount of domestic coal which can be gasified to produce a syngas stream with a relatively high concentration of H_2 (~35vol%), as well as CO (~51%) which can be further reacted with steam via the water-gas shift reaction to increase the H_2 concentration in the syngas. At the same time, this reaction produces a concentrated stream of CO_2 that can be more easily captured and sequestered to mitigate the greenhouse effect.

Conventionally, coal gasification occurs at high temperatures (above 1173K) and pressures (above 2,000 kPa) in the presence of O_2 and steam. The produced CO/H_2-rich (about 86% by volume) syngas is scrubbed, cooled to low temperature, and then directed to a two-stage shift reactor where the high temperature (593–723K) and subsequent low temperature (473-523K) water gas shift reactors (WGSRs) are used to increase the H_2 concentration by reacting the syngas with steam. The low temperature WGSR allows high levels of CO conversion to be attained because CO conversion of this exothermic reaction is thermodynamically favored at low temperature. Alternatively, high CO conversions can be realized at elevated temperatures (>~ 973K) if membrane reactors (MRs) that are selective to one of the products, CO_2 or H_2, are used.

Pd-based membranes have gained a great deal of attention for MR application because Pd-based membranes are highly permeable to H_2, are virtually impermeable to other gases and are stable at relatively high temperatures. It has also been shown that

when Pd is used as a MR at high temperatures in the absence of heterogeneous catalyst particles (Chapter 3), its modest catalytic activity toward the WGSR can be combined with its high rate of H_2 transport to enhance CO conversions at otherwise unfavorable conditions. Therefore, water-gas shift membrane reactors (WGSMRs) can potentially be applied to the high-temperature gasification cycle, obviating the need to cool the high-temperature, coal-derived syngas streams to lower temperatures in an attempt to attain higher CO conversions. The impetus to develop high temperature, Pd MRs stems from system studies that have suggested that integrating MRs just downstream of the coal gasifier would increase the efficiency of the coal-to-H_2 process (Gray et al. July 2002), ultimately resulting in a decreased cost of H_2 production. An additional advantage of the MR concept is that the generated CO_2 is retained at high pressure, making it more amenable to sequestration technologies, thereby mitigating any greenhouse effect. However, a major limitation of Pd membranes for post-gasifier application is their susceptibility to rapid poisoning by the sulfur-containing gaseous impurities in the syngas.

H_2S is a common contaminant present in coal-derived syngas and is a known poison of Pd-based membranes. Conventionally, H_2S is removed from syngas via the Selexol® process. Selexol is a liquid physical absorbent used for the removal of CO_2 and H_2S, possessing a higher selectivity for H_2S over CO_2 (Breckenridge et al. Feb. 2000). This solvent is a mixture of dimethyl ethers of polyethylene glycol, with a chemical formula $CH_3(CH_2CH_2O)_nCH_3$, where n is 3-9. The advantage of the Selexol solvent is that unlike amine solvents that react chemically with the acid gas, Selexol is essentially inert to the acid gas. The Selexol unit is capable of reducing H_2S levels in the syngas to

below 1 ppm, H_2S concentration levels at which Pd-based membranes may be successfully operated. However, the Selexol process is a low-temperature process that requires cooling down the high temperature syngas during absorption, and heating the H_2S-rich stream during regeneration, resulting in high utility consumption, high energy losses, and reduced overall thermal efficiency. For the MR technology to be a feasible alternative to Selexol-based absorption, sulfur-tolerant membrane materials capable of operating at high temperatures will have to be developed, as sulfidization of potential membrane materials would prove catastrophic to MRs, i.e. resulting in loss of membrane selectivity and/or H_2 permeability.

The desire to enhance H_2 generation and separation from mixed gas streams that may contain varying concentrations of H_2S has led to numerous studies on the effect of H_2S on H_2 permeability of dense Pd-based membranes (Hurlbert et al. 1961; Ali et al. 1994; Kajiwara et al. 1999; Bryden et al. 2002; Morreale et al. 2004; Kulprathipanja et al. 2005; Morreale 2006). In addition to a loss of H_2 permeability due to adsorption on the membrane surface, H_2S has been shown to result in morphological changes, including pitting of Pd-based membranes within seconds of contact.

Hurlbert et al., (Hurlbert et al. 1961) observed about an 85% reduction in H_2 permeability through Pd after exposure of a 24 μm Pd membrane to 50 ppm H_2S-in-H_2 at 623K. They attributed this to the formation of an irreversible grey surface scale, presumably a palladium sulfide, on the membrane surface. Kajiwara et al. (Kajiwara et al. 1999) observed rapid failure of a composite Pd membrane after exposure to 6,200 ppm H_2S-in-H_2 at 673K. This was evidenced by severe cracks on the surface of the membrane which they attributed to the structural stress in the membrane due to the increased lattice

constant of the resulting Pd sulfide. A similar experiment by Kulprathipanja et al. (Kulprathipanja et al. 2005) involving the effect of H_2S on Pd and Pd-Cu alloys observed pit and crack formation on the Pd and Pd-Cu alloy membrane surfaces exposed to H_2S concentrations between 500 and 1,000 ppm H_2S. EDAX analysis of a 25 μm, $Pd_{60wt\%}Cu$ foil membrane after exposure to 1,000 ppm H_2S at 723K detected the presence of sulfur in the membrane sample. Conversely, EDAX analysis of a $Pd_{60wt\%}Cu$ membrane showed no sulfur presence after a similar treatment in a gas mixture containing 500 ppm H_2S-in-H_2.

Bryden et al (Bryden et al. 2002) exposed nanocrystalline 10 μm-thick, $Pd_{97wt\%}Fe$ alloy membranes to a 51.9 ppm H_2S-in-H_2 mixture at 673K. Using polycrystalline and nanocrystalline samples, they observed a 95% and 75% reduction in H_2 flux, respectively, in the presence of the H_2S-H_2 mixture. Bryden et al., suggest better performance of the nanocrystalline Pd-Fe membrane as the nanocrystalline sample only lost 75% of its performance compared to the 95% decrease observed in the polycrystalline sample. Reverting back to a pure H_2 feed regenerated the nanocrystalline and polycrystalline samples in 30 mins and 400 mins, respectively.

Mundschau et al. (Mundschau et al. 2006) investigated a variety of Pd-alloy membranes in the presence of varying concentrations of H_2S. Exposure of a Pd foil to 20 ppm H_2S-in-60%H_2-He at 593K resulted in almost a 75% loss of H_2 permeability in less than 2 hours. XRD analysis of the membrane sample after the H_2S-H_2 exposure confirmed the formation of Pd_4S on the membrane surface. Similarly, exposure of a $Pd_{75wt\%}Ag$ membrane to 10 ppm H_2S-in-80%H_2-He at 593K resulted in a precipitous loss

of H_2 permeation accompanied by the formation of a ternary $Ag_5Pd_{10}S_5$ scale on the membrane surface.

A more recent study by Morreale (Morreale 2006) exposed various Pd-based membranes to a 1,000 ppm H_2S-in-H_2 feed mixture at 623, 723 and 908K for about 120 hours. The Pd membranes were observed to experience significant permeance reductions when exposed to the H_2S-H_2 feed stream, in addition to severe sulfidization at all three temperatures. SEM-EDS cross-sectional analysis of all three Pd membranes exposed to the H_2S-H_2 gas revealed sulfide thicknesses of ~15, 20 and 30 μm at experimental temperatures of 623, 723 and 908K, respectively. When the membranes were replaced with $Pd_{80wt\%}Cu$ membranes, similar permeance losses were observed at 623 and 723K. However, the permeance reduction was less severe at 908K, decreasing to about 85% of the predicted H_2 permeance for the H_2S-free gas. Although cross-sectional analysis of the membrane revealed a negligible sulfide scale, the SEM surface image showed a wrinkled membrane surface. Similar to the $Pd_{80wt\%}Cu$ membrane, the $Pd_{60wt\%}Cu$ experienced significant reductions in permeance at 623 and 723K accompanied by a significantly roughened membrane surface. The $Pd_{60wt\%}Cu$ membrane operated at 908K, however, experienced only a minute reduction in H_2 permeance and exhibited a negligible sulfide scale. Table 3 summarizes published literature results on the effect of varying concentrations of H_2S on Pd-based membrane materials.

Table 3. Summary of published literature results involving the effect of H_2S exposure to Pd-based membranes.

Reference	Membrane composition	Temp (K)	Feed composition	H_2S conc. in pure H_2 equivalent	Result
(Edlund et al. 1993)	Pd on vanadium	973	Pure H_2S	100% H_2S	Failure of Pd membrane by rupture and pitting within seconds.
(Kajiwara et al. 1999)	Pd on porous alumina	673	6,200 ppm in H_2	6,200 ppm	Cracked membrane surface.
(Hurlbert et al. 1961)	25 µm Pd	623	50 ppm H_2S in H_2	50 ppm	Grey surface scale.
(Kulprathipanja et al. 2005)	25 µm $Pd_{60wt\%}Cu$ foil	723	1,000 ppm H_2S in H_2	1,000	Formation of surface pores with sulfur detected.
(Kulprathipanja et al. 2005)	25 µm $Pd_{60wt\%}Cu$ foil	723	500 ppm H_2S in H_2	500	Formation of surface cracks and pores.
(Mundschau et al. April, 2005)	Pd	713	20 ppm H_2S in 40% H_2	50 ppm	Pitted surface. XRD showed Pd_4S.
(Mundschau et al. April, 2005)	$Pd_{75wt\%}Ag$	593	10 ppm H_2S - 80%H_2	12.5 ppm	Formed bulk sulfides.
(Mundschau et al. 2006)	Pd	593	20 ppm H_2S in 60% H_2	33.3 ppm	Formed Pd_4S.
(Mundschau et al. 2006)	$Pd_{80wt\%}Cu$	593	20 ppm H2S in 60% H2	33.3 ppm	Formed Pd_4S.

Table 3 (continued).

Reference	Membrane composition	Temp (K)	Feed composition	H_2S conc. in pure H_2 equivalent	Result
(Mundschau et al. 2006)	$Pd_{75wt\%}Ag$	593	10 ppm H_2S in 80% H_2	12.5 ppm	Formed $Ag_5Pd_{10}S_5$.
(Bryden et al. 2002)	10 µm $Pd_{97wt\%}Fe$	473	51.9ppm H2s in H_2	51.9 ppm	Membranes lost H_2 flux but regained after pure H_2 reintroduction.
(McKinley 1967)	23 µm Pd	623	4 ppm H_2S in H_2	4 ppm	Dull membrane surface.
(McKinley 1967)	23 µm $Pd_{73wt\%}Ag$	623	4 ppm H_2S in H_2	4 ppm	Dull & etched membrane surface.
(McKinley 1967)	26 µm $Pd_{60wt\%}Cu$	623	4 ppm H_2S in H_2	4 ppm	Retained original luster.
(McKinley 1967)	21 µm $Pd_{60wt\%}Au$	623	4 ppm H_2S in H_2	4 ppm	Retained original luster.
(McKinley 1967)	20 µm $Pd_{60wt\%}Au$	623	20.6 ppm H_2S in H_2	20.6 ppm	Retained original luster.
(McKinley 1967)	20 µm $Pd_{60wt\%}Au$	623	66,000 ppm H_2S in H_2	66,000 ppm	Retained original luster.

Table 3 (continued).

Reference	Membrane composition	Temp (K)	Feed composition	H_2S conc. in pure H_2 equivalent	Result
(Morreale et al. 2004)	100 um $Pd_{80wt\%}Cu$	600-1100K	1,000 ppm H_2S in 90%H_2	1,111 ppm	Minute reduction in H_2 permeance in presence of H_2-H_2S mix at 905K and below. Negligible reduction at 1000K.
(Morreale et al. 2004)	100 µm $Pd_{60wt\%}Cu$	600-1100K	1,000 ppm H_2S in 90%H_2	1,111 ppm	Significant loss of H_2 permeance at 605 & 714K. Negligible reductions at T>714K.
(Morreale et al. 2004)	100 µm $Pd_{53wt\%}Cu$	600-1100K	1,000 ppm H_2S in 90%H_2	1,111 ppm	Significant loss of H_2 permeance at T≤774K. Negligible reductions at T>774K.
(Morreale 2006)	100 µm Pd	623, 723 & 908	1,000 ppm H_2S in 90%H_2	1,111 ppm	Pd_4S formation over entire temperature range.
(Morreale 2006)	100 µm $Pd_{80wt\%}Cu$	623, 723 & 908	1,000 ppm H_2S in 90%H_2	1,111 ppm	Pd_4S and $Pd_{13}Cu_3S_7$ formation at 623 & 723K. Trace $Pd_{13}Cu_3S_7$ formation at 908K.
(Morreale 2006)	100 µm $Pd_{60wt\%}Cu$	623, 723 & 908	1,000 ppm H_2S in 90%H_2	1,111 ppm	Cu_2S, Pd_4S and $Pd_{16}Cu_3S_7$ formation at 623K. Trace amount of $Pd_{13}Cu_3S_7$ detected at 723K. No detectable sulfide at 908K.

Table 3 (continued).

Reference	Membrane composition	Temp (K)	Feed composition	H_2S conc. in pure H_2 equivalent	Result
(Edlund 1996)	50 µm $Pd_{60wt\%}Cu$	773	1,000 ppm H_2S in H_2	1,000 ppm	Stable H_2 flux for over 350 hours.

Some Pd-alloy membranes have, however, been reported to present resistance to permanent poisoning when exposed to varying concentrations of H_2S. Edlund (Edlund 1996) reported stable H_2 flux through a 50 µm $Pd_{60wt\%}Cu$ membrane reactor at 773K in the presence of 1,000 ppm H_2S for over 350 hours. Using a transient experimental approach, a previous study by Morreale et al (Morreale et al. 2004) also reported minute H_2 permeance decrease for face-centered-cubic (fcc) Pd-alloy membranes in the presence of 1,000 ppm H_2S-in-90%H_2-He, while B2 (CsCl-structure) alloys were observed to experience significant reductions to H_2 permeance when exposed to the same H_2-H_2S feed composition. They attributed the resistance of the fcc alloys to permeance reduction in the presence of H_2S to the crystal structure of the membrane, correlating the H_2S resistance to the crystal structure. However, it appears that each of their experiments utilized a single membrane sample over the entire temperature range of their study. Therefore, an initially poisoned membrane may have led to misleading results at subsequent test conditions. Furthermore, no post-H_2S exposure analyses were conducted on the membranes, therefore it was unclear if there was sulfide formation on any of the membranes following H_2S exposure. This led to a subsequent, more thorough study by Morreale (Morreale 2006).

McKinley (McKinley 1967) investigated various Pd-based membranes including Pd, $Pd_{60wt\%}Au$, $Pd_{73wt\%}Ag$ and $Pd_{60wt\%}Cu$ at 623K for potential sulfur tolerance. Most of the alloys in his study were observed to experience significant reductions in H_2 permeance when exposed to about a 4.5 ppm H_2S-in-H_2 feed stream, except the $Pd_{60wt\%}Au$ alloy which experienced negligible reduction in H_2 permeance until it was exposed to a 20 ppm H_2S-in-H_2 feed mixture. However, when the feed was reverted back to pure H_2, all the alloys completely regained their original H_2 permeance after about 10 days. Although, McKinley noted that the Pd and $Pd_{73wt\%}Ag$ alloys were physically observed to have been chemically attacked by the H_2S and exhibited dull surfaces after the H_2-H_2S exposure. The $Pd_{60wt\%}Au$ and $Pd_{60wt\%}Cu$ alloys retained their luster, however, suggesting negligible chemical interaction between the H_2S-feed and the alloy membranes.

The aforementioned results tabulated in **Table 3** suggest a slight discrepancy with regard to which conditions Pd-based membranes can be stably operated in the presence of a specified concentration of H_2S. For example, Morreale et al. (Morreale et al. 2004) show significant loss in H_2 permeance for a $Pd_{60wt\%}Cu$ membrane exposed to a 1,000 ppm H_2S-in-90%H_2-He feed at temperatures less than 833K, conflicting with Edlund's study (Edlund 1996) which shows stable H_2 permeation of a similar $Pd_{60wt\%}Cu$ alloy when exposed to a similar H_2S-H_2 mixture at 773K. Furthermore, inadequate attention has been given to examining the correlation between conditions where sulfides have been observed and the thermodynamic stability of sulfides at the same conditions. Previous reports have indicated that types of scales and scale morphologies (if any) formed on alloys are influenced by the alloy composition, the gaseous atmosphere (e.g. H_2S-to-H_2

ratio) and the exposure temperature (Lee 2002). In these gas-metal reaction systems, thermodynamics governs the reactions that can occur and can be used to predict the final products that are formed at the conditions of interest. Further, it has been shown that Pd sulfides are roughly two orders of magnitude less permeable than Pd (Morreale 2006) and therefore the flux of H_2 through the membrane would be limited by (i.e. poisoned by) the metal sulfide film on the surface of the membrane.

Thus, this study aimed to predict, and experimentally verify (at 1173K), the "sulfur tolerance" of the Pd and $Pd_{80wt\%}Cu$ system based on the sulfide scale thermodynamic stability (where the membrane is poisoned by sulfide scale formation) or the sulfide scale thermodynamic instability (where the membrane is sulfur-tolerant or sulfur-resistant) as a function of H_2S-to-H_2 partial pressure ratio and temperature. The high experimental temperature (1173K) was selected to be representative of a MR positioned just downstream of a coal gasifier to: a) enhance CO conversion by shifting the equilibrium of the WGSR toward more product formation, b) facilitate high-purity H_2 production, and c) permit complete, high-pressure CO_2 capture. Because of the mechanism of H_2S and H_2 interaction with metals, sulfidization of the metal is determined by the H_2S-to-H_2 ratio and not merely the inlet H_2S concentration. This prediction of membrane "poisoning" cannot, however, account for loss of permeance due to competitive adsorption of H_2S on the Pd or Pd-Cu membrane surface. H_2S need not necessarily form a metal sulfide on the metal surface to effectively block H_2 dissociation sites, as adsorbed sulfur can diminish the H_2 permeance of the membrane by inhibiting H_2 adsorption and dissociation (Castro et al. 2002). If successful, this could provide a useful

tool for facilitating the design of Pd- or Pd-Cu-based WGSMRs, given the level of difficulty associated with conducting high temperature, high pressure, long-term MR experiments with H_2S-contaminated gases.

4.2 EXPERIMENTAL

4.2.1 Effect of H_2S-to-H_2 Ratio on Sulfidization of Pd and Pd-Cu Membranes

The effect of H_2S-to-H_2 partial pressure ratio on the sulfidization of Pd and Pd-Cu membranes was studied at 1173K. The 3.175 mm OD, 125-µm thick Pd and Pd-Cu alloy tubes used to make the membranes in the present study were manufactured by Goodfellow using 99.9% purity (metals basis) Pd and Cu. The membranes were 3.81 cm in length with 0.3175 cm Swagelok nuts attached on either end to facilitate coupling of the membrane tube to quartz-lined, stainless-steel feed lines. **Figure 29** shows a schematic of the experimental apparatus. The gases used were research grade H_2, He, 1,000 ppm H_2S-10%He-balance H_2 (H_2S-to-H_2 ratio ≈ 0.0011) and 3%H_2S-10%He-balance H_2 (H_2S-to-H_2 ratio ≈ 0.034) purchased from Butler Gas Products. The H_2S-H_2 feed gas mixture was introduced in the tube-side, while the He sweep was introduced to the shell-side. The total sweep-side gas flow rate was maintained at 100 sccm. The feed-side gas flow was maintained at 300 sccm for all experiments, resulting in a residence time of about 0.013s in the MR zone. The low residence time was desired to minimize variation in H_2S/H_2 composition due to the loss of H_2 through the walls of the MR.

Variation in H_2S-to-H_2 composition was also mitigated by inserting a quartz tube in the tube-side of the MR assembly. The quartz tube served to minimize interaction between the H_2S feed and the stainless steel walls prior to reaching the Pd-based MR zone. Previous experiments had shown this to be an effective technique in reducing H_2S consumption by the stainless steel lines. The H_2S-to-H_2 feed ratio was controlled with calibrated rotameters. A thermocouple suspended on top the center of the membrane was used to monitor and control experimental temperature.

Prior to performing each experiment, the MRs were rinsed with acetone and blown dry with N_2. The reactor was then assembled and placed into the Lindberg tube furnace and purged for 10 minutes with He in the process and sweep streams. After purging the reactor, it was heated to the experimental temperature of 1173K at a rate of approximately 6K/min, still flowing He in both the process and permeate streams. At the experimental temperature of 1173K, the module was allowed to equilibrate for about 15 minutes. The desired H_2S-to-H_2 feed ratio was then introduced by regulating the H_2 and the 3%H_2S-10%He-H_2 gas flow rates to the desired amounts, or introducing the 1,000 ppm H_2S-10%He-H_2 gas. This condition was maintained for 30 minutes. The reactor was then purged with He for 10 minutes, after which the heater was switched off, rapidly cooling the membrane module (~3 hours) to room temperature in flowing He. Following the experiment, the samples were examined via SEM-EDS.

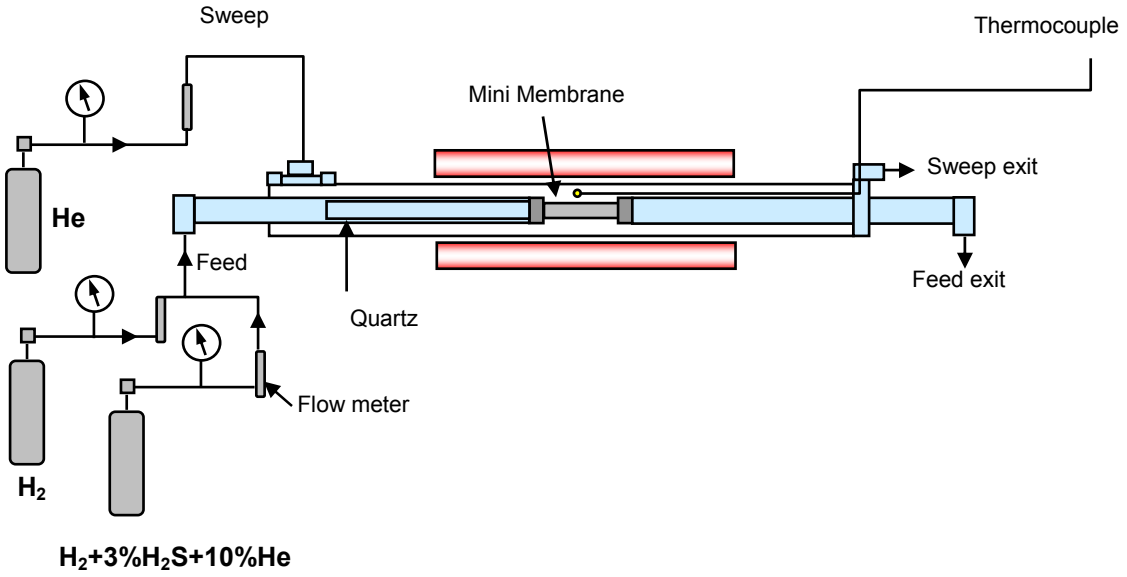

Figure 29. Schematic of mini tubular membrane assembly used for H_2S-H_2 experiments.

4.2.2 SEM-EDS Analysis

Membrane surface morphology and elemental composition were examined following exposure to the H_2-H_2S environment with a Philips XL30 FEG SEM equipped with EDS. Membranes were removed from the test assembly for characterization following testing by carefully cutting a small section of each tube using a jeweler's saw, taking care to limit surface contamination as much as possible. For inner surface analysis, the sample was carefully split in half with a surgical scissors, ensuring that the sample maintained its curvature, thereby preventing the introduction of superficial surface defects.

4.3 RESULTS AND DISCUSSION

4.3.1 Interaction of Pd and Cu With H_2S

When a Pd-Cu alloy is exposed to a H_2S containing environment at elevated temperature, the following reactions can occur on the surface of the metal:

$$Pd_4S + H_2 \leftrightarrow 4Pd + H_2S \quad (11)$$

$$PdS + H_2 \leftrightarrow Pd + H_2S \quad (12)$$

$$PdS_2 + 2H_2 \leftrightarrow Pd + 2H_2S \quad (13)$$

$$Cu_2S + H_2 \leftrightarrow 2Cu + H_2S \quad (14)$$

$$CuS + H_2 \leftrightarrow Cu + H_2S \quad (15)$$

The equilibrium constants for the reactions involving Pd and Cu were calculated from experimental values given by Taylor (Taylor 1985) and Barin (Barin 1993), respectively, are related to the gas composition by the equations below:

$$K_1 = \frac{a_{Pd}^4 P_{H2S}}{a_{Pd4S} P_{H2}} \quad (16)$$

$$K_2 = \frac{a_{Pd} P_{H2S}}{a_{PdS} P_{H2}} \tag{17}$$

$$K_3 = \frac{a_{Pd} P_{H2S}^2}{a_{PdS2} P_{H2}^2} \tag{18}$$

$$K_4 = \frac{a_{Cu}^2 P_{H2S}}{a_{Cu2S} P_{H2}} \tag{19}$$

$$K_5 = \frac{a_{Cu} P_{H2S}}{a_{CuS} P_{H2}} \tag{20}$$

where a_i is the activity of the solids, P_i is the partial pressure of the gases, and K_1, K_2, K_3, K_4 and K_5 are the equilibrium constants for Pd_4S-Pd, PdS-Pd, PdS_2-Pd, Cu_2S-Cu and CuS-Cu equilibrium, respectively. If Pd, Cu, Pd_xS_y and Cu_xS_y are assumed to be pure, immiscible metals, i.e., occur in their standard states, then their activities can be assumed to be unity (Gaskell 2003), and Equations (16) to (20) can be simplified to the ratio of H_2S-to-H_2, i.e., X_{H2S}:X_{H2}. However, in the case of Pd alloys, the activity of Pd would be less than unity and this decrease would have to be accounted for in Equations (16) to (20). Note that other reactions forming binary or tertiary compounds such as $Pd_xCu_yS_z$ are possible; however, these sulfides, such as $Pd_{13}Cu_3S_7$ were observed to be less

common at the conditions of interest (Table 3), while the other sulfides (i.e. PdS and PdS_2) require considerably higher sulfur concentrations, and hence will not be considered further in this analysis

4.3.2 Equilibrium H_2-to-H_2S Ratio for Sulfidization of Pd and Cu

Figure 30 and **Figure 31** represent the H_2S-to-H_2 partial pressure ratio predicted by Equations (16) and (19) for Pd-Pd_4S and Cu-Cu_2S equilibrium as a function of reaction temperature for pure Pd and Cu based on thermodynamic data from Taylor (Taylor 1985) and Barin (Barin 1993), respectively. In addition to H_2S-to-H_2 ratios required for sulfidization of the pure metals, the H_2S-to-H_2 ratios required for the sulfidization of alloyed Pd and Cu are also shown. Unlike the pure Pd and Cu which have unit activity, the activity of Pd and Cu in an alloy is less than unity. The H_2S-to-H_2 ratios required to form stable sulfides for the alloys were generated by assuming that the Pd-Cu alloy system forms Raoultian ideal solutions. The activity (a_i) of components of Raoultian ideal solutions equal the mole fractions (X_i) of the components in the alloy, i.e., $a_i = X_i$. This assumption results in the activity of Pd and Cu in the $Pd_{80}Cu$ (70mol%Pd-Cu) alloy equal to 0.7 and 0.3, respectively. Using these figures for the activity of Pd and Cu in Equations (16) and (19) results in an increased H_2S-to-H_2 ratio required to form a stable Pd and Cu sulfides relative to the unalloyed metals. Based on this assumption, **Figure 30** suggests that H_2S-to-H_2 ratio greater than about 0.0014 (~1.4 E-03, ~1400 ppm H_2S-in-H_2) should sulfidize pure Pd over the entire temperature range,

while the same concentration of H_2S-in-H_2 should only sulfidize the $Pd_{80wt\%}Cu$ alloy (assuming activity of Pd equal to 0.7) at temperatures up to about 923K.

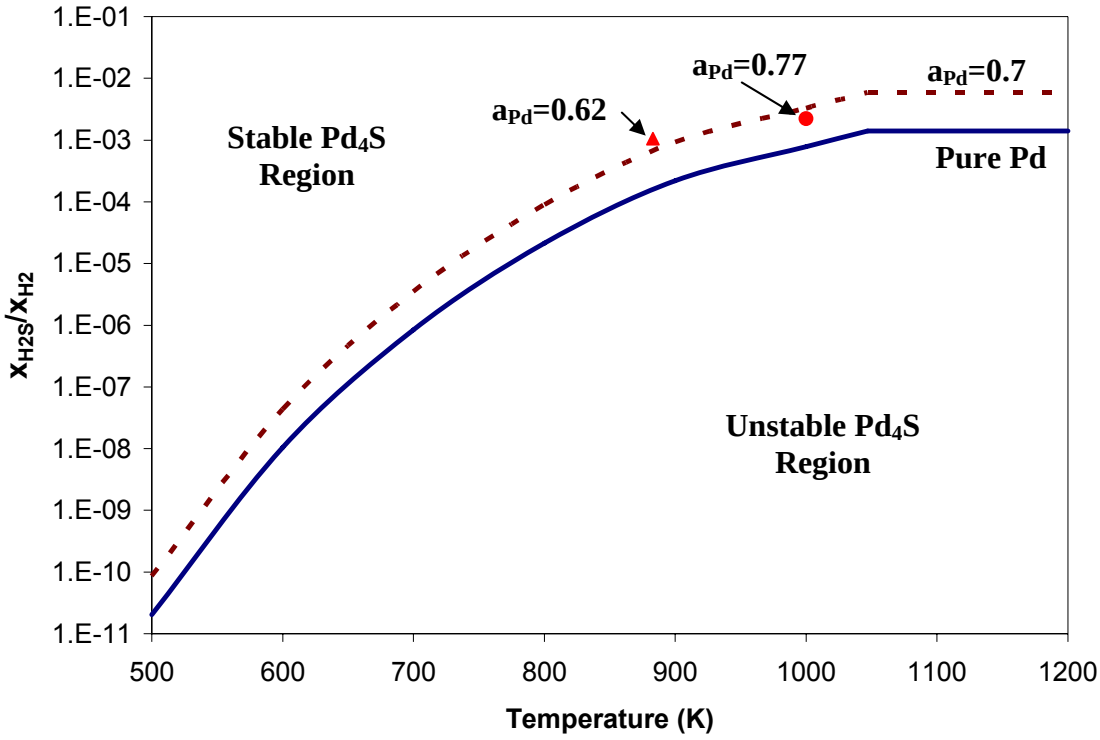

Figure 30. Ratio of H_2S-to-H_2 for Pd_4S (Taylor 1985) formation as a function of T (K) for pure Pd (solid line) and $Pd_{80}Cu$ (dashed line – generated by assuming $a_{Pd} = X_{Pd}$ (0.7)). Activity of Pd in $Pd_{80}Cu$ alloy at 883K (triangle) and 1000K (circle) obtained from experimental values from Myles et al. (Myles et al. 1968).

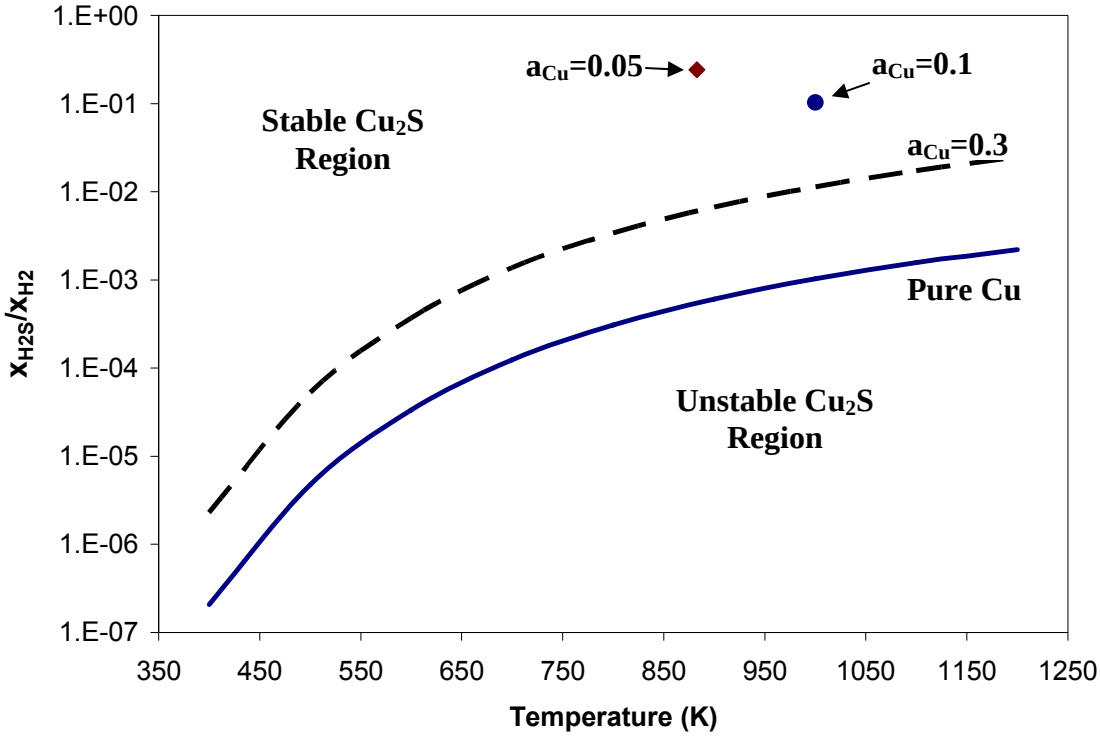

Figure 31. (a) Ratio of H_2S-to-H_2 for Cu_2S formation for pure Cu (solid line-thermodynamic values from Barin (Barin 1993)) and $Pd_{80}Cu$ (dashed line – generated by assuming $a_{Cu} = X_{Cu}$ (0.3)). Experimental values for the activity of Cu in Pd-Cu alloy of 0.05 and 0.1 at 883K (diamond) and 1000K (circle), respectively, were obtained from Myles et al. (Myles et al. 1968).

However, previous studies have shown that the Pd-Cu system forms non-ideal solutions (Myles et al. 1968), and therefore, the activities of Pd and Cu vary with alloy composition and temperature. Based on experimental values for the activity of Pd and Cu in Pd-Cu alloys obtained from Myles et al. (Myles et al. 1968), **Figure 30** and **Figure 31** also predict X_{H2S}-to-X_{H2} partial pressure ratios required for the sulfidization of Pd and Cu, respectively, in the $Pd_{80wt\%}Cu$ membrane at 883K and 1000K. As shown in **Figure 30**, the experimentally measured activity of Pd at 883K (a_{Pd}=0.62) in the $Pd_{80wt\%}Cu$ alloy is slightly lower than the assumed Raoultian activity of 0.7 for the 70mol%Pd-Cu. This lower activity results in a slightly higher H_2S-to-H_2 partial pressure ratio of 0.0011

(~1,055 ppm H_2S-in-H_2) required to form a stable sulfide scale, compared to approximately 0.00065 H_2S-to-H_2 ratio (~650 ppm H_2S-in-H_2) predicted assuming a Pd activity of 0.7. At 1000K, the activity of Pd was calculated from the experimentally measured values of the activity of Cu in Pd-Cu alloys (Myles et al. 1968) using the Gibbs-Duhem equation. The calculated value of the activity of Pd in the alloy, 0.77, is higher than the assumed activity of 0.7. This suggests that at 1000K, the Pd in the alloy experiences a slight positive deviation from Raoultian ideal behavior, resulting in the formation of a stable Pd_4S at a H_2S-to-H_2 ratio of 0.0022 (~2,200 ppm H_2S-in-H_2), appreciably lower than the predicted 0.0033 H_2S-to-H_2 ratio (~3,300 ppm H_2S-in-H_2) calculated assuming an activity of Pd of 0.7.

In the case of Cu, it is evident from **Figure 31** that compared to the experimentally observed values of 0.05 and 0.1 for the activity of Cu in $Pd_{80wt\%}Cu$ at 883K and 1000K, respectively, the assumption of 0.3 for the activity of Cu in the $Pd_{80wt\%}Cu$ alloy substantially underestimates the H_2S-to-H_2 concentration ratio required for stable Cu_2S formation. The measured activity of 0.05 and 0.1 for Cu at 883K and 1000K suggest that 24% and 10% H_2S-in-H_2 will be required to form a stable Cu_2S scale on the $Pd_{80wt\%}Cu$ membrane surface, respectively.

The above theoretical calculations, however, are only valid at the scale/metal interface as there is a Pd and Cu activity gradient across the scale/metal interface for sulfidized samples. According to the equations above, H_2S-to-H_2 ratios greater than or equal to values predicted for Pd_4S and Cu_2S equilibrium (i.e. above the corresponding trend lines in **Figure 30** and **Figure 31**) are required to form a stable sulfide scale on the membrane surface at the corresponding temperature of interest. Furthermore, the

composition of the sulfide formed depends on the magnitude of the sulfur partial pressure, i.e. the H_2S-to-H_2 partial pressure ratio.

4.3.3 Correlation of Literature Results

Table 4 compares the predicted minimum H_2S-to-H_2 ratios required to form stable Pd_4S based on the assumption of Raoultian behavior (i.e., $a_{Pd} = X_{Pd}$ in the alloy) for the various referenced Pd-alloys to the experimental H_2S-to-H_2 ratios utilized in the various references. Note that in the case of highly permeable membranes, depletion of the H_2 concentration at the membrane surface, accompanied by the corresponding increase in H_2S concentration may significantly increase the surface sulfur concentration, leading to membrane sulfidization in the presence of an original inlet H_2S-to-H_2 feed ratios which should otherwise prove innocuous to the membrane material (with respect to stable sulfide formation on the membrane surface).

Table 4. Comparison of predicted minimum H_2S-in-H_2 required for stable Pd_4S formation at various experimental temperatures with published experimental results.

Reference	Membrane composition (Mole %)	Temp (K)	Experiment H_2S-to-H_2 ratio ($*10^6$)	Predicted H_2S-to-H_2 ratio for stable Pd_4S formation ($*10^6$)	Experiment result
(Edlund et al. 1993)	Pd on vanadium	973	Pure H_2S	632	Failure of Pd membrane by rupture and pitting within seconds.
(Kajiwara et al. 1999)	Pd on porous alumina	673	6,200	0.7	Cracked membrane surface.
(Hurlbert et al. 1961)	25 μm Pd	623	50	0.2	Grey surface scale.
(Kulprathipanja et al. 2005)	25 μm, 47mol%Pd-Cu foil	723	1,000	72	Formation of surface pores with sulfur detected.
(Kulprathipanja et al. 2005)	25 μm, 47mol%Pd-Cu foil	723	500	72	Formation of surface cracks and pores.
(Mundschau et al. April, 2005)	Pd	713	50	3.5	Pitted surface. XRD showed Pd_4S.
(Mundschau et al. April, 2005)	75mol%Pd-Ag	593	12.5	0.03	Formed bulk sulfides.
(Mundschau et al. 2006)	Pd	593	33.3	0.0097	Formed Pd_4S.

Table 4 (continued).

Reference	Membrane composition (Mole %)	Temp (K)	Experiment H_2S-to-H_2 ratio ($*10^6$)	Predicted H_2S-to-H_2 ratio for stable Pd_4S formation ($*10^6$)	Experiment result
(Mundschau et al. 2006)	70mol%Pd-Cu	593	33.3	0.04	Formed Pd_4S.
(Mundschau et al. 2006)	75mol%Pd-Ag	593	12.5	0.03	Formed $Ag_5Pd_{10}S_5$
(Bryden et al. 2002)	10 µm 94mol%Pd-Fe	473	51.9	0.00003	Membranes lost H_2 flux but regained after pure H_2 reintroduction.
(McKinley 1967)	23 µm	623	4	0.32	Dull surface.
(McKinley 1967)	23 µm 73mol%Pd-Ag	623	4	0.71	Dull & etched surface.
(McKinley 1967)	26 µm 47mol%Pd-Cu	623	4	4.13	Retained original luster.
(McKinley 1967)	21 µm 74mol%Pd-Au	623	4	0.67	Retained original luster.
(McKinley 1967)	20 µm 74mol%Pd-Au	623	20.6	0.67	Retained original luster.
(McKinley 1967)	20 µm 74mol%Pd-Au	623	66,000	0.67	Retained original luster.

Table 4 (continued).

Reference	Membrane composition (Mole %)	Temp (K)	Experiment H_2S-to-H_2 ratio ($*10^6$)	Predicted H_2S-to-H_2 ratio for stable Pd_4S formation ($*10^6$)	Experiment result
(Morreale et al. 2004)	100 μm 70mol%Pd-Cu	600	1,111	0.044	Minute reduction in H_2 permeance in presence of H_2-H_2S mix at 905K and below. Negligible reduction at 1000K.
		700		3.5	
		800		89.3	
		905		1,040	
		1,000		3,260	
(Morreale et al. 2004)	100 μm 47mol%Pd-Cu	605	1,111	1.06	Significant loss of H_2 permeance at 605 & 714K. Negligible reductions at T>714K.
		714		72.1	
		917		6,480	
		1,005		17,400	
		1,040		27,000	

Table 4 (continued).

Reference	Membrane composition (Mole %)	Temp (K)	Experiment H_2S-to-H_2 ratio ($*10^6$)	Predicted H_2S-to-H_2 ratio for stable Pd_4S formation ($*10^6$)	Experiment result
(Morreale et al. 2004)	100 μm 40mol%Pd-Cu	670	1,111	24.7	Significant loss of H_2 permeance at T≤774K. Negligible reductions at T>774K.
		714		146	
		774		620	
		1,005		33,200	
		1,030		46,300	
(Morreale 2006)	100 μm Pd	623	1,111	0.2	Pd_4S formation over entire temperature range.
		723		5.6	
		908		266	
(Morreale 2006)	100 μm 70mol%Pd-Cu	623	1,111	0.8	Pd_4S and $Pd_{13}Cu_3S_7$ formation at 623 & 723K. Trace $Pd_{13}Cu_3S_7$ formation at 908K.
		723		23.2	
		908		1,110	

Table 4 (continued).

Reference	Membrane composition (Mole %)	Temp (K)	Experiment H_2S-to-H_2 ratio ($*10^6$)	Predicted H_2S-to-H_2 ratio for stable Pd_4S formation ($*10^6$)	Experiment result
(Morreale 2006)	100 μm 47mol%Pd-Cu	623	1,111	4.1	Cu_2S, Pd_4S and $Pd_{16}Cu_3S_7$ formation at 623K. Trace amount of $Pd_{13}Cu_3S_7$ detected at 723K. No detectable sulfide at 908K.
		723		114	
		908		5,450	
(Edlund 1996)	50 μm 47mol%Pd-Cu	773	1,000	325	Stable H_2 flux for over 350 hours.

Comparing the predicted minimum H_2S-to-H_2 ratios required to form stable Pd_4S to the H_2S-to-H_2 ratio utilized in the various experiments, it is evident from **Table 4** that most of the literature results (Hurlbert et al. 1961; Edlund et al. 1993; Kajiwara et al. 1999; Kulprathipanja et al. 2005; Morreale 2006; Mundschau et al. 2006; Mundschau et al. April, 2005) are consistent with our thermodynamic predictions, and indicate that many of the Pd-based membranes were operated in the presence of H_2S-to-H_2 concentration ratios greater than the equilibrium ratio required for stable Pd_4S formation. Therefore, it is no surprise that most membranes were observed to form stable sulfide scales on the membrane surface.

Although Bryden et al. (Bryden et al. 2002) did not report a sulfide scale on the 94mol%Pd-Fe membrane after exposure to the 62 ppm H_2S-in-H_2 mixture, the low H_2 flux when the H_2-H_2S mixed feed was initially reverted to pure H_2 (27% and 3% of the original H_2 flux before H_2S-H_2 exposure for the nanocrystalline and polycrystalline membranes, respectively), suggests that sulfide scales may have formed on the membrane samples. The membranes were regenerated because reverting back to a pure H_2 feed presents an environment with a H_2S-to-H_2 ratio below the equilibrium ratio required to sustain sulfidization. This environment, thus, favors the dissociation of the Pd sulfide back to pure Pd.

As noted earlier, McKinley's study (McKinley 1967) observed significant reductions in H_2 permeance when the Pd, Pd-Ag and Pd-Cu alloys were exposed to the H_2S-H_2 feed mixture. However, when the feed was reverted back to the pure H_2 feed, all the alloys completely regained their original H_2 permeance after a few days. Although, in agreement with our thermodynamic predictions, McKinley noted that the Pd and 73mol%Pd-Ag alloys were physically observed to have been chemically attacked by the H_2S and exhibited dull surfaces after the H_2-H_2S exposure. Also in agreement with our predictions, the 47mol%Pd-Cu membrane in McKinley's study was exposed to a H_2S-to-H_2 ratio ($4*10^{-6}$) slightly less than the predicted $4.13*10^{-6}$ H_2S-to-H_2 partial pressure ratio required to sulfidize the 47mol%Pd-Cu membrane. Hence, as expected, the membrane was not sulfidized. The recovery of initial H_2 permeance for the alloys involved in McKinley's study (which exhibited modified surfaces) when the feed was reverted to the pure H_2 feed suggests that at the low operating temperature (623K), the growth rate of the sulfide scale may have been extremely slow, thereby allowing the membranes to recover

their permeance after an extended period of time in the pure H_2 feed due to the decomposition of the thin sulfide scale.

Contrary to our predictions, however, the 74mol%Pd-Au membranes retained their luster after exposure to H_2S-in-H_2 concentrations of 4 ppm, 20 ppm and 6,600 ppm, suggesting negligible chemical interaction between the H_2S-feed and the alloy membranes. A plausible explanation for the lack of sulfidization of the Pd-Au alloys exposed to H_2S in McKinley's study is possible surface enrichment of the alloy with Au as a result of Au segregation at the membrane surface. Au has been reported to have a propensity to segregate to the surface of Pd-Au alloys due to the reduced surface energy of Au relative to Pd (Anton et al. 1993). For example a study by Swartzfager et al. (Swartzfager et al. 1981) using 80mol%Pd-20mol%Au alloy measured a surface Au composition of 52mol% after the alloy was annealed at 873K. Similar surface enrichment, attributed to surface segregation of Au, was observed by Piccolo et al. (Piccolo et al. 2005) using 70mol%Pd-Au single crystals at 523, 623 and 723K. Au is a more noble metal than Pd, Ag and Cu and requires an appreciably higher H_2S-to-H_2 partial pressure ratio to form a stable sulfide. Therefore, the reduced activity of Pd at the Au-enriched membrane surface as a result of possible Au segregation results in an appreciably greater H_2S-to-H_2 ratio required to form Pd_4S. Furthermore, the increased concentration of Au at the membrane surface (Au being a more noble metal), further enhances the sulfidization resistance of the alloy, preventing sulfidization as reported by McKinley.

Morreale's study (Morreale 2006) involving 100 μm Pd membranes at 623, 723 and 908K exposed to H_2S-to-H_2 partial pressure ratio of 0.0011 (1,000ppm H_2S-10%He-

H_2) resulted in the sulfidization of all three membrane samples. This is in agreement with our thermodynamic predictions (**Table 4**), which suggest that the 1,000 ppm H_2S-10%He-H_2 (H_2S-to-H_2 ratio ≈ 0.0011) feed mixture was greater than the H_2S-to-H_2 partial pressure ratios of $2*10^{-7}$, $5.6*10^{-6}$ and $2.66*10^{-4}$ (~0.2, 5.6 and 266 ppm H_2S-in-H_2, respectively) required for sulfidization of the membranes at 623, 723 and 908K, respectively. Interestingly, Morreale (Morreale 2006) observed significant loss of H_2 permeance accompanied by sulfidization at 623K and 723K when a 100 μm, 47mol%Pd-Cu membrane was exposed to the 1,000 ppm H_2S-10%He-H_2 feed, and observed neither permeance reduction nor membrane sulfidization at 908K. This is also in agreement with our thermodynamic calculations which suggest that the H_2S-to-H_2 ratio of 0.001 presented by the gas mixture was greater than the predicted equilibrium H_2S-to-H_2 ratio at 623K and 723K, but less than the 0.0055 (~5,450 ppm H_2S-in-H_2) H_2S-to-H_2 ratio required to form a stable Pd_4S scale at 908K, assuming the activity of Pd to be equal to the mole fraction of Pd in the alloy (0.47).

Although the earlier study by Morreale's group (Morreale et al. 2004) did not perform SEM-EDS analyses of the various membranes after exposure to the H_2S-H_2 environment to ascertain the presence or absence of a sulfide scale, their results present some interesting trends. For example, significant H_2 permeance losses were observed at conditions at which our calculations predict stable sulfide formation, while negligible permeance losses were observed at conditions at which the sulfide was not expected to be stable. Their results indicate dramatic reductions in H_2 permeance when a 47mol%Pd-Cu membrane was exposed to a 1,000 ppm H_2S-10%He-H_2 feed at 605 and 704K, while negligible reduction in H_2 permeance were observed when the 47mol%Pd-Cu membrane

was exposed to the same feed mixture at temperatures greater than 704K. According to our calculations, the H_2S-to-H_2 ratio of 0.0011 presented by the 1,000 ppmH_2S-10%He-H_2 feed mixture is greater that the predicted ratios of $1.1*10^{-6}$ and $72.1*10^{-6}$ (1.06 and 72 ppm H_2S-in-H_2, respectively) required to sulfidize the membrane at 605 and 704K, respectively. However, negligible H_2 permeance reductions were observed at conditions at which the feed H_2S-to-H_2 ratio was significantly less that that predicted for stable sulfide formation at noted in **Table 4**. Morreale et al. (Morreale et al. 2004) observed a similar trend for the 40mol%Pd-Cu membrane which experienced significant permeance reductions when exposed to the 1,000 ppmH_2S-10%He-H_2 feed at 670, 714 and 774K. This is also in agreement with our calculations which suggest that the 0.0011 H_2S-to-H_2 ratio was greater than the predicted H_2S-to-H_2 ratios of $2.47*10^{-5}$, $1.46*10^{-4}$ and $6.2*10^{-4}$ (~24.7, 146 and 620 ppm H_2S-in-H_2, respectively) required to sulfidize the 40mol%Pd-Cu membrane at 670, 714 and 774K, respectively. Conversely, at temperatures at which the 0.0011 H_2S-to-H_2 feed ratio provided by the feed mixture fell below the ratios predicted for stable sulfide formation, negligible H_2 permeance reductions were observed.

Surprisingly, Edlund et al., (Edlund 1996) claimed to have attained stable H_2 permeation through a 47mol%Pd-Cu membrane reactor for over 300 hours at 773K in the presence of 1,000 ppm H_2S-in-H_2 mixture (0.0011 H_2S-to-H_2 feed ratio). This is inconsistent with our calculations which suggest that H_2S-to-H_2 ratios above 0.00033 (~325 ppm H_2S-in-H_2) should sulfidize the 47mol% Pd at 773K.

Figure 32 summarizes the aforementioned literature results involving the pure Pd membranes in **Table 4** in comparison to the equilibrium H_2S-to-H_2 ratio predicted from thermodynamic values from Taylor (Taylor 1985). Current experimental results (squares)

at 1173K discussed in the subsequent section are also shown. The figure illustrates that all the tabulated reported experiments involving pure Pd membranes (**Table 4**) are in very good agreement with the Taylor data, and suggest that the experiments involving Pd membranes were conducted in the presence of H_2S-to-H_2 partial pressure ratios greater than the predicted equilibrium thermodynamic ratio required to form stable Pd_4S, and as a result were all sulfidized.

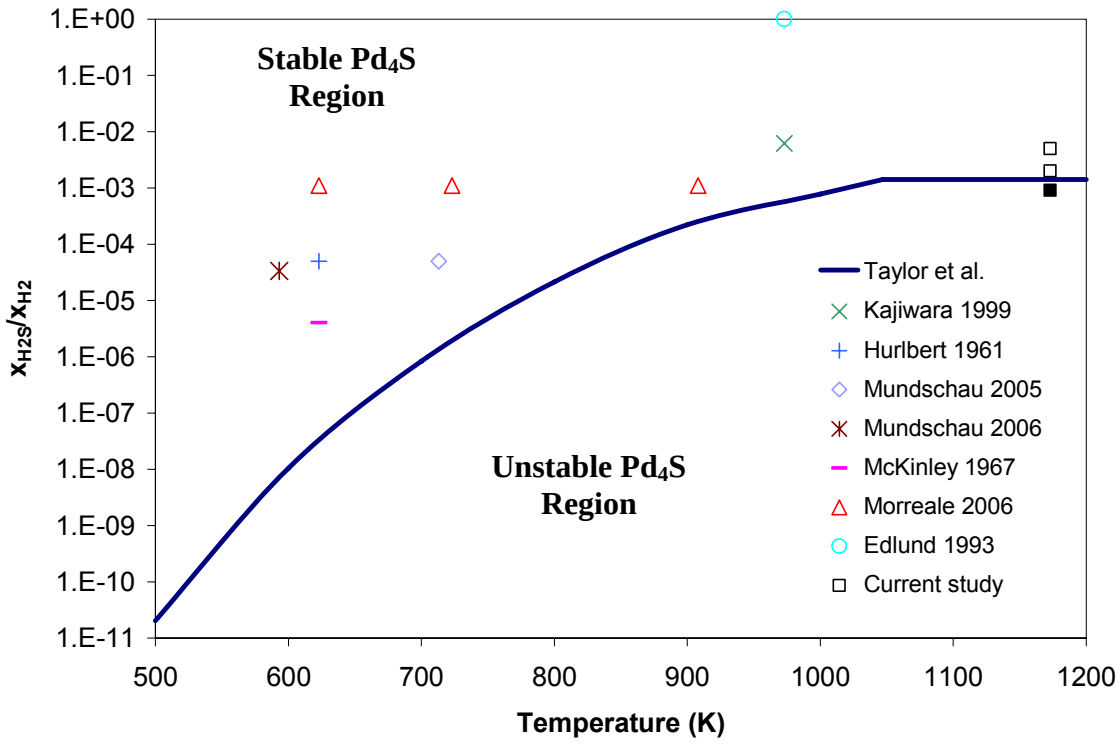

Figure 32. Comparison of H_2S-to-H_2 equilibrium ratio predicted from data from Taylor et al. (solid line) to literature results involving pure Pd membranes exposed to various H_2S-to-H_2 pressure ratios at various temperatures indicating sulfidization (hollow shapes). Squares indicate results form current experimental results discussed in the subsequent section involving Pd membranes at 1173K, showing conditions of sulfidization (hollow square) and condition of no sulfidization (filled square).

4.3.4 Current Experimental Results

Figure 33 to **Figure 49** illustrate SEM-EDS results from the current study in which Pd and $Pd_{80wt\%}Cu$ membrane samples were each exposed to H_2S-in-H_2 concentrations of 5,000 ppm (H_2S-to-H_2 ratio ≈ 0.005), 2,000 ppm (H_2S-to-H_2 ratio ≈ 0.002) and 1,000 ppm H_2S-10%He-H_2 (H_2S-to-H_2 ratio ≈ 0.0011) at 1173K for 30 minutes, using fresh membrane samples for each exposure. **Figure 33** shows an SEM image of the surface of the Pd membrane after exposure to the 0.005 H_2S-to-H_2 ratio at 1173K for 30 minutes. Thermodynamic calculations shown in **Figure 30** suggest that this ratio of H_2S-to-H_2 is greater than the equilibrium H_2S ratio required to sulfidize Pd and, therefore, was expected to form a stable sulfide scale on the Pd membrane. The SEM image depicts large grains on the membrane surface. As expected, EDS analysis of the area within the rectangle (**Figure 34**) revealed the presence of a uniform Pd-sulfide layer on the Pd membrane surface. XRD analysis of this sample (not shown) determined the sulfide scale to be Pd_4S.

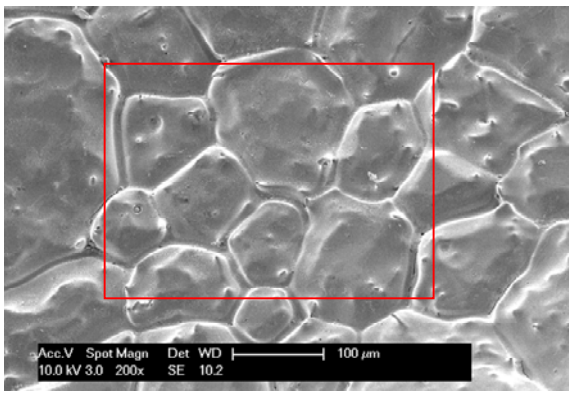

Figure 33. SEM image of inner surface of Pd membrane exposed to 0.005 H_2S-to-H_2 ratio (5,000 ppm H_2S-in-H_2) for 30 mins at 1173K.

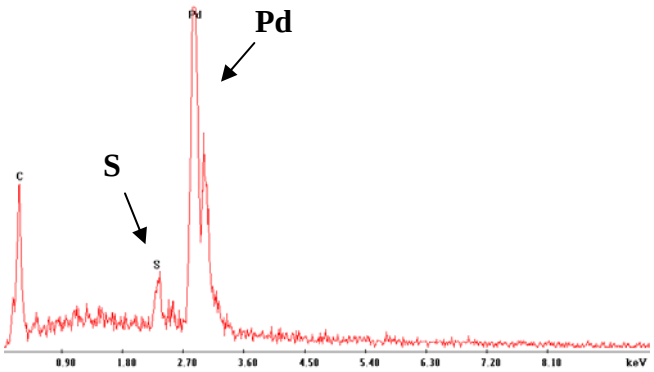

Figure 34. EDS spectrum of rectangular region pf Pd membrane above exposed to 0.005 H_2S-to-H_2 ratio (5,000 ppm H_2S-in-H_2) for 30 mins at 1173K indicating Pd sulfide formation.

Figure 35 to **Figure 37** show results of the $Pd_{80wt\%}Cu$ membrane exposed to the same 0.005 H_2S-to-H_2 feed mixture. The thermodynamic calculations illustrated in **Figure 30** and **Figure 31** suggest that the 0.005 H_2S-to-H_2 feed (5,000 ppm H_2S-to-H_2) at 1173K should prove innocuous to the $Pd_{80wt\%}Cu$ membrane because it exists below the equilibrium H_2S-to-H_2 line required for stable sulfide formation of alloyed Pd (assuming the activity of Pd = 0.7). Despite the increased H_2S concentration requirement predicted by our calculations, however, the alloy was observed to experience severe sulfidization. Contrary to the pure Pd membrane which exhibited a uniform Pd_4S scale after exposure to the 0.005 H_2S-to-H_2 feed for 30 minutes, SEM-EDS of the $Pd_{80wt\%}Cu$ membrane revealed regions of unsulfidized Pd-Cu surrounded by a sulfide scale. **Figure 35** shows the surface of the $Pd_{80wt\%}Cu$ membrane with a visible sulfide scale growing on the substrate Pd-Cu membrane. The non-homogeneous membrane surface after 30 minutes of H_2S-H_2 exposure suggests that alloying Pd with Cu slowed down the membrane sulfidization rate but did not completely prevent it. **Figure 36** and **Figure 37** are EDS

spectra of positions labeled 1 and 2 on surface SEM image showing regions without sulfide formation and sulfidized regions, respectively. The precise composition of the sulfide scale could not be ascertained, however, surface EDS (**Figure 37**) revealed the presence of Pd-Cu-S.

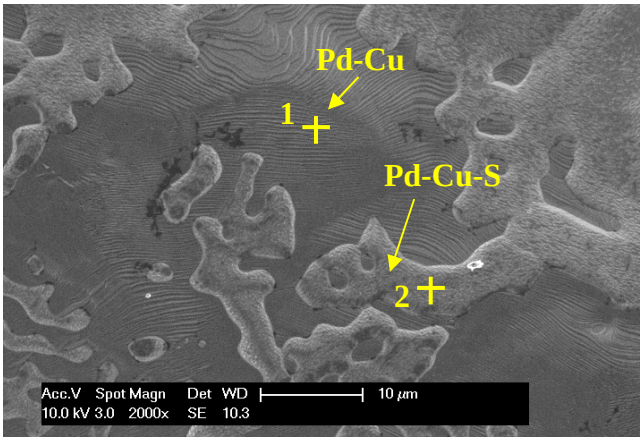

Figure 35. SEM image of inner surface of $Pd_{80wt\%}Cu$ membrane exposed to 0.005 H_2S-to-H_2 ratio (5,000 ppm H_2S-in-H_2)for 30 mins at 1173K.

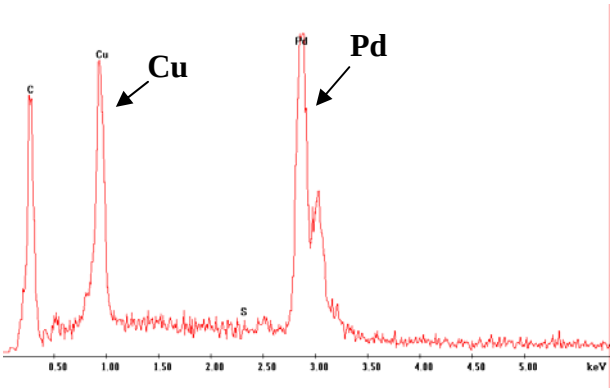

Figure 36. EDS spectrum of position 1 on surface of the $Pd_{80wt\%}Cu$ membrane exposed to 0.005 H_2S-to-H_2 ratio (5,000 ppm H_2S-in-H_2) for 30 minutes as 1173K indicating negligible sulfide formation on this region of the sample.

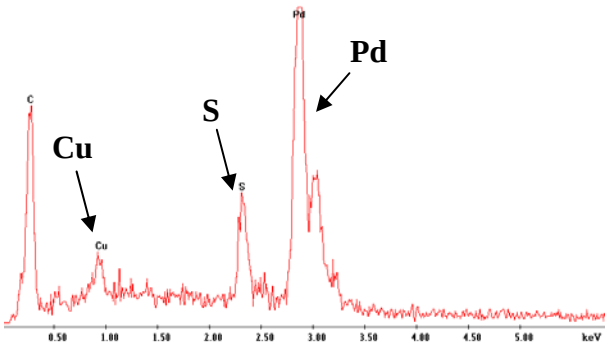

Figure 37**.** EDS spectrum of position 2 on the $Pd_{80wt\%}Cu$ membrane exposed to 0.005 H_2S-to-H_2 ratio (5,000 ppm H_2S-in-H_2) for 30 minutes as 1173K indicating sulfide growth on the sample.

As expected (**Figure 30**) suggests that stable Pd_4S formation for H_2S-to-H_2 ratio greater than ~0.0014), exposure of the Pd membrane to a 0.002 H_2S-to-H_2 mixture for 30 minutes resulted in sulfidization of the Pd membrane (Figure 38). **Figure 39** shows an EDS spectrum of the area within the rectangular region highlighted in Figure 38. Unlike the sample exposed to the 0.005 H_2S-to-H_2 mixture, however, this sample was not completely sulfidized within the 30 minute exposure period due to the lower H_2S concentration in the gas mixture. Higher magnification of a selected area of the membrane surface (**Figure 40**) revealed hillocks protruding from the membrane surface. EDS analyses determined the smooth regions of the membrane to be unsulfidized Pd (**Figure 41**), while the protrusions were shown to be a Pd-sulfide (**Figure 42**).

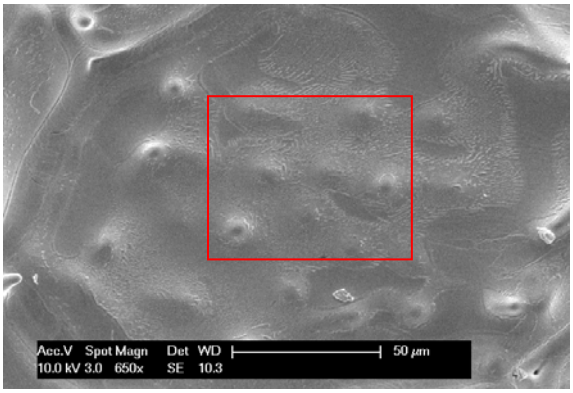

Figure 38. SEM image of inner surface of Pd membrane exposed to 0.002 H_2S-to-H_2 ratio (2,000 ppm H_2S-in-H_2) for 30 mins at 1173K.

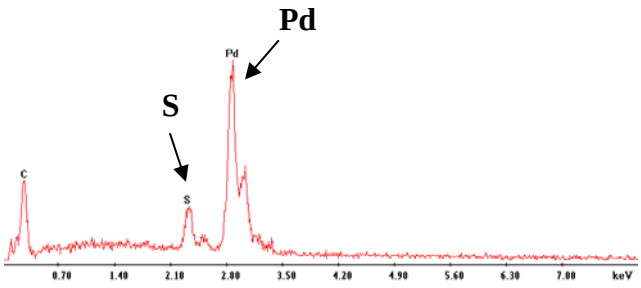

Figure 39. EDS spectrum of surface of Pd membrane exposed to 0.002 H_2S-to-H_2 ratio (2,000 ppm H_2S-in-H_2) for 30mins at 1173K depicting sulfide formation.

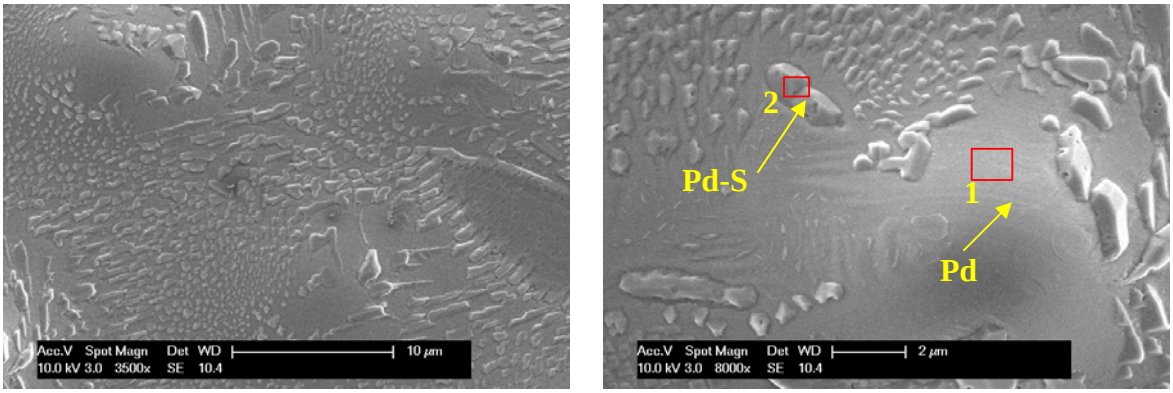

Figure 40. High magnification SEM image of inner surface of Pd membrane exposed to 0.002 H_2S-to-H_2 ratio (2,000 ppm H_2S-in-H_2) for 30 minutes at 1173K showing regions of sulfidized and unsulfidized Pd.

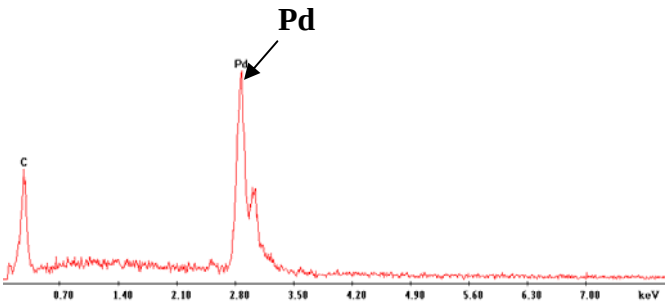

Figure 41. EDS spectrum of surface of Pd membrane (labeled 1) exposed to 0.002 H_2S-to-H_2 ratio (2,000 ppm H_2S-in-H_2) for 30mins at 1173K depicting negligible sulfide region.

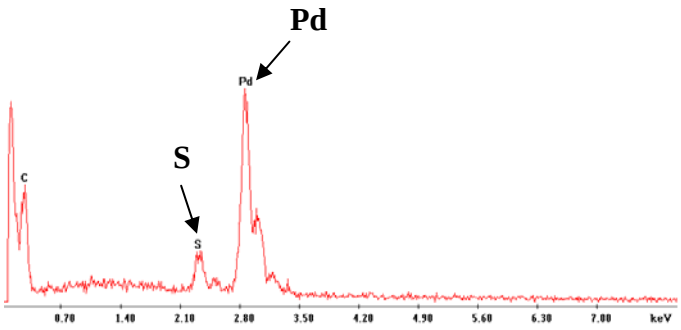

Figure 42. EDS spectrum of surface of Pd membrane (labeled 2) exposed to 0.002 H_2S-to-H_2 ratio (2,000 ppm H_2S-in-H_2) for 30mins at 1173K depicting sulfidized Pd.

Figure 43 shows SEM images of the of the $Pd_{80wt\%}Cu$ membrane exposed to the 0.002 H_2S-to-H_2 ratio environment, a ratio well below the 0.0034 H_2S-to-H_2 ratio predicted by thermodynamics (**Figure 30**) for the sulfidization of the alloyed Pd. Although the $Pd_{80wt\%}Cu$ alloy was expected to exhibit tolerance to a higher concentration of sulfur as a result of the decreased activity of Pd due to the alloying phenomena previously explained above, **Figure 43** reveals sulfidization of the $Pd_{80wt\%}Cu$ sample after exposure to 0.002 H_2S-to-H_2 ratio mixture. Unlike the sulfidization observed in the Pd membrane which resulted in the formation of a uniform Pd-sulfide scale, 2-phases were observed in this sample (**Figure 43**) in the form of Cu-S islands (**Figure 45**) formed within the substrate $Pd_{80wt\%}Cu$ (**Figure 44**) membrane. These images may be indicative of a Cu segregation mechanism which results in the formation of Cu islands at the surface the $Pd_{80wt\%}Cu$ substrate. Note that $Pd_{80wt\%}Cu$ u membrane samples exposed to pure H_2 at this temperature did not form Cu islands. Cu surface enrichment has been previously observed in Pd-Cu alloys exposed to H_2-H_2S mixtures where a $Pd_{80wt\%}Cu$ alloy membrane exhibited a surface Cu concentration of 90wt% after exposure to 1,000 ppm

H_2S-in-H_2 at 723K (Kulprathipanja et al. 2005). A similar occurrence in this case will result in these high Cu activity islands interacting with the available sulfur to form a stable Cu-sulfide as is evident in the SEM images. According to the thermodynamic calculation in **Figure 31**, Cu forms a stable sulfide at H_2S-to-H_2 ratio above about 0.002 (2,000 ppm H_2S-in-H_2) at 1173K.

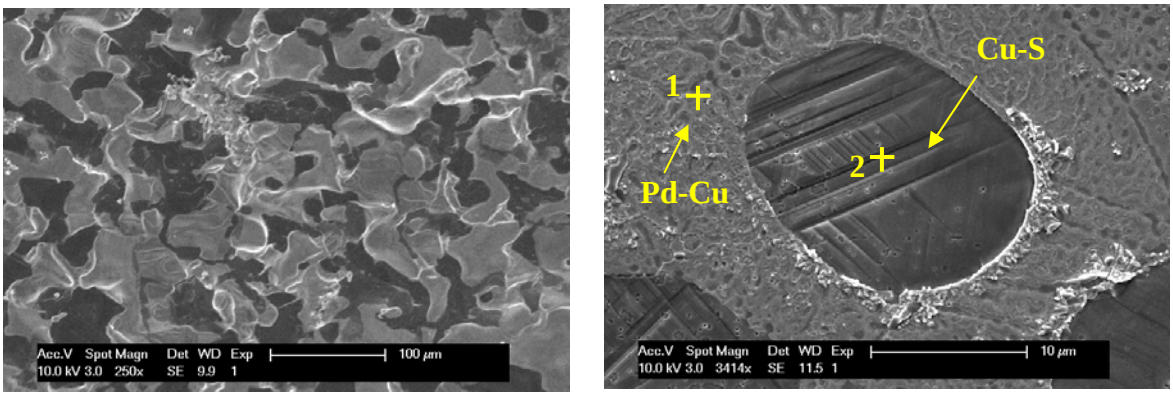

Figure 43. SEM image of inner surface of the $Pd_{80wt\%}Cu$ membrane exposed to 0.002 H_2S-to-H_2 ratio (2,000 ppm H_2S-in-H_2) for 30 mins at 1173K showing islands of Pd-Cu (grayish regions) and Cu-S (dark regions).

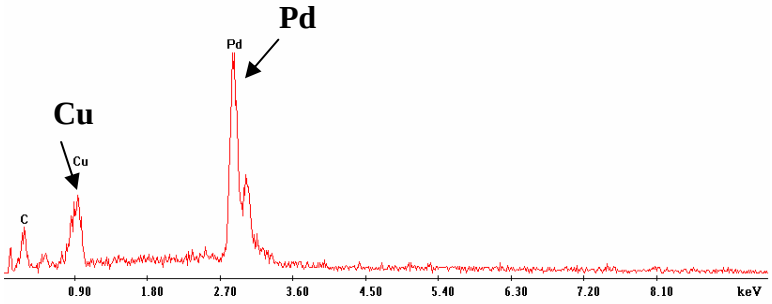

Figure 44. EDS spectrum of position 1 on surface of the $Pd_{80wt\%}Cu$ membrane exposed to 0.002 H_2S-to-H_2 ratio (2,000 ppm H_2S-in-H_2) for 30 mins at 1173K indicating negligible sulfide formation on this region of the sample.

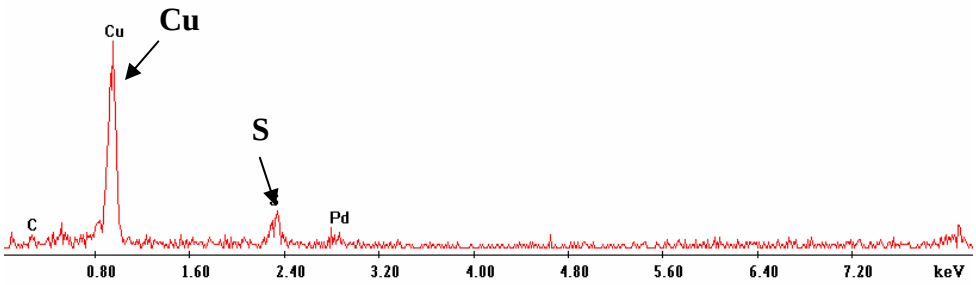

Figure 45.EDS spectrum of position 2 on surface of the $Pd_{80wt\%}Cu$ membrane exposed to 0.002 H_2S-to-H_2 ratio (2,000 ppm H_2S-in-H_2) for 30 mins at 1173K showing copper sulfide formation.

Figure 46 and **Figure 48** show the Pd and $Pd_{80wt\%}Cu$ membranes exposed to the 0.0011 H_2S-to-H_2 mixture for 30 minutes, respectively. The images depict grain boundary grooving with significantly smaller grains than samples exposed to the higher concentrations of H_2S-in-H_2. EDS analyses of the Pd (**Figure 47**) and $Pd_{80wt\%}Cu$ (**Figure 49**) membrane samples revealed negligible sulfide scales on either sample. Furthermore, a physical observation of the membrane samples indicated no deleterious effect (i.e. embrittlement) of the feed gas on the membranes. This is in agreement with the thermodynamic data plotted in **Figure 30** which suggests that H_2S-to-H_2 partial pressure ratio greater than ~0.0014 and 0.0034 are required to form a stable Pd_4S for pure Pd and the $Pd_{80wt\%}Cu$ at 1173K, respectively. These results suggest that both the Pd and $Pd_{80wt\%}Cu$ membrane reactors can be operated in the presence of H_2S-to-H_2 partial pressure ratios below 0.0011 (~ 1,100 ppm H_2S-in-H_2) at 1173K without being sulfidized. Performance of the membrane with respect to H_2 transport may, however, be

affected as a result of competitive adsorption between the H_2S and H_2 on the membrane surface.

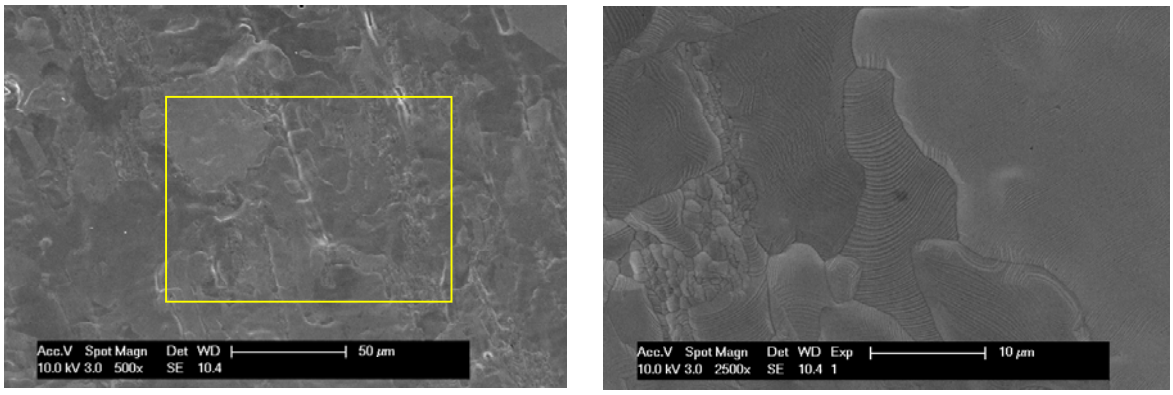

Figure 46. SEM image of inner surface of Pd membrane exposed to 0.0011 H_2S-to-H_2 ratio (1,100 ppm H_2S-in-H_2) for 30 mins at 1173K showing a smooth membrane surface.

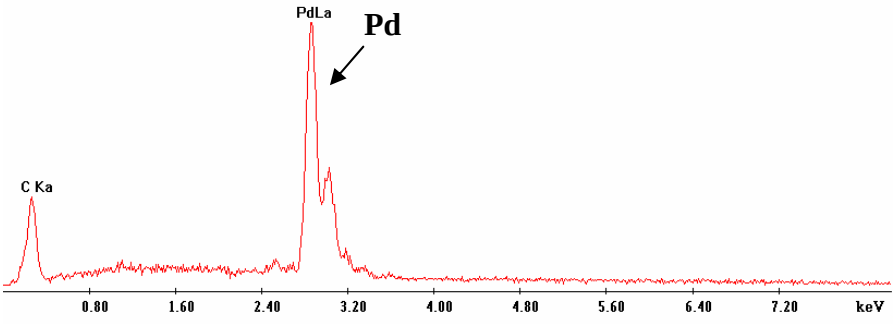

Figure 47. EDS spectrum of surface of the Pd membrane exposed to 0.0011 H_2S-to-H_2 ratio (1,100 ppm H_2S-in-H_2) for 30 mins at 1173K showing no detectable sulfide formation.

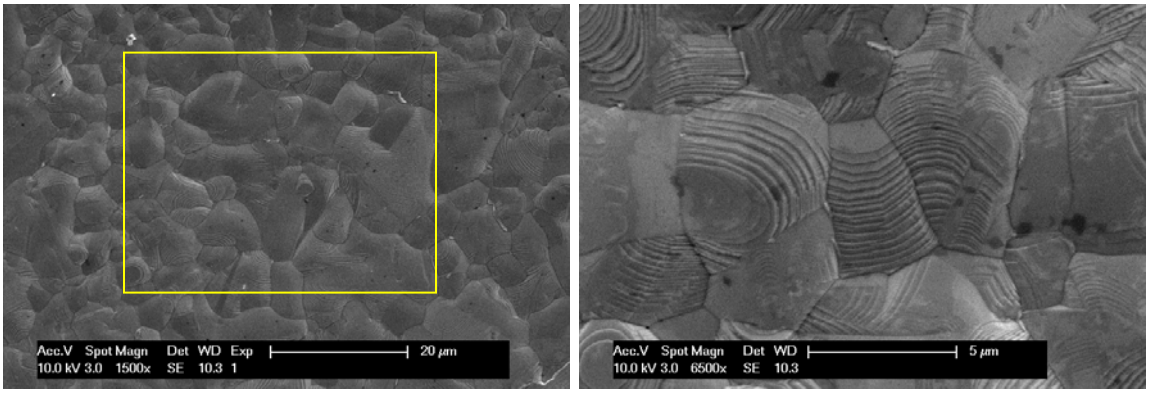

Figure 48.SEM image of inner surface of the $Pd_{80wt\%}Cu$ membrane exposed to 0.0011 H_2S-to-H_2 ratio (1,100 ppm H_2S-in-H_2) for 30 mins at 1173K showing a smooth membrane surface.

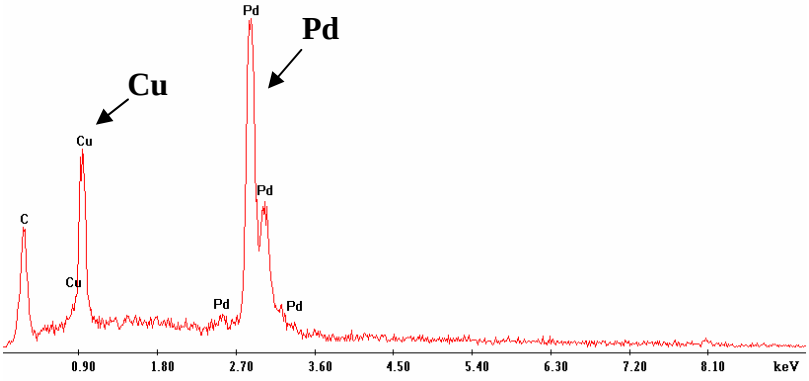

Figure 49. EDS spectrum of surface of the $Pd_{80wt\%}Cu$ u membrane exposed to 0.0011 H_2S-to-H_2 ratio (1,100 ppm H_2S-in-H_2) for 30 mins at 1173K showing no detectable sulfide formation.

Table 5 summarizes the current experimental results and compares experimental observations with the predicted outcomes for the Pd and $Pd_{80wt\%}Cu$ alloy at the respective H_2S-to-H_2 feed ratios. It is evident from **Table 5** that the Pd membranes exposed to the various H_2S-to-H_2 ratios were in good agreement with the predicted results, while the $Pd_{80wt\%}Cu$ membranes conflicted with our predictions at high H_2S-to-H_2 ratios.

Table 5. Summary of current investigation comparing experimental results to predicted outcome of the respective 125 μm Pd and $Pd_{80wt\%}Cu$ membranes exposed to various H_2S-to-H_2 ratios at 1173K for 30 minutes.

Membrane composition	Experimental H_2S-to-H_2 ratio	Minimum H_2S-to-H_2 ratio	Predicted outcome	Experimental outcome
Pd	0.005	0.0014	Sulfide formation	Formed uniform Pd_4S layer
$Pd_{80wt\%}Cu$	0.005	0.0058	Sulfur tolerant	Formed non-homogeneous sulfide layer
Pd	0.002	0.0014	Sulfide formation	Sulfide nodules on membrane surface
$Pd_{80wt\%}Cu$	0.002	0.0058	Sulfur tolerant	Cu-S islands on membrane surface
Pd	0.0011	0.0014	Sulfur tolerant	No detectable sulfide
$Pd_{80wt\%}Cu$	0.0011	0.0058	Sulfur tolerant	No detectable sulfide

4.4 CONCLUSION

The interaction of Pd and 80wt%Pd20wt%Cu membranes with H_2S was investigated experimentally and using thermodynamic calculations to predict the H_2S-to-H_2 partial pressure ratios below which Pd and Pd-Cu alloy membrane reactors can be safely operated. The prior thermodynamic study by Taylor was found to accurately correlate the results.

Our thermodynamic predictions were in good agreement with many of the reported studies in the literature involving Pd, Pd-Ag and Pd-Cu membranes exposed to varying H_2-H_2S mixtures at various temperatures. The Pd-Au membrane was an anomaly, exhibiting sulfidization resistance at conditions which stable sulfide formation was predicted. This may possibly be attributed to Au segregation at the membrane surface, decreasing the activity of Pd at the surface region.

In agreement with thermodynamic calculations, current experimental results revealed sulfidization of Pd membranes after exposure to H_2S-to-H_2 ratios of approximately 0.005 (5,000 ppm H_2S-in-H_2) and 0.002 (2,000 ppm H_2S-in-H_2) at 1173K. The Pd membrane resisted sulfidization by H_2S-to-H_2 ratio of 0.0011 (~1,100 ppm H_2S-in-H_2) at this temperature.

Similarly, the $Pd_{80wt\%}Cu$ membrane which was expected to exhibit tolerance to a higher concentration of H_2S due to the lower Pd activity in the alloy, was also observed to be sulfidized after exposure to H_2S-to-H_2 ratios of approximately 0.005 (5,000 ppm H_2S-in-H_2) and 0.002 (2,000 ppm H_2S-in-H_2) at 1173K. The unexpected sulfidization of

the $Pd_{80wt\%}Cu$ membrane was attributed to Cu segregation at the membrane surface, increasing the Cu activity at this region. This phenomenon was evidenced by islands of Cu-S surrounded by regions of unsulfidized Pd-Cu on the surface of the membrane after exposure to the 0.002 H_2S-to-H_2 ratio mixed gas.

Our results suggest that both the Pd or $Pd_{80wt\%}Cu$ MR systems can be safely operated at 1173K in the presence of H_2S-to-H_2 ratios as high as 0.0011 (~1,100 ppm H_2S-in-H_2) without experiencing sulfidization. Alternatively, other Pd-alloy compositions may be utilized, however, the Pd-based MRs will have to be engineered such that the H_2S-to-H_2 ratio remains below the ratio required for sulfidization, as this ratio increases down the length of the tubular reactor due to extraction of H_2 from the reaction zone. This phenomenon increases the likelihood of sulfidization as greater proportions of H_2 are removed from the retentate. Further, one would also have to assess whether the migration of a metal to the surface could lead to sulfidization at these sites of enrichment that would be unexpected based on the bulk composition of the membrane.

5.0 CHAPTER FIVE: COMSOL MULTIPHYSICS MODELING OF A Pd MEMBRANE REACTOR FOR THE WATER-GAS SHIFT REACTION IN THE PRESENCE OF H_2S

Abstract

A COMSOL Multiphysics® model was developed to analyze and predict the performance of a high-temperature catalytic palladium membrane reactor (MR) for H_2 production via the water-gas shift reaction (WGSR) in the absence and presence of H_2S. The catalytic effect of the palladium MR walls toward the WGSR was accounted for using a modified version of the gas-phase WGSR rate expression in which the pre-exponential factor was 50 times greater than the pre-exponential constant of the homogeneous gas-phase WGS reaction rate expression. Our results show that the H_2 permeance of the membrane was significantly reduced due to a H_2-depleted concentration boundary layer, and competitive adsorption of the water-gas shift components present in high concentrations. This phenomenon was dependent on the reactant composition and was compensated for by using apparent membrane permeance values of $1.5*10^{-5}$ and $4.4*10^{-5}$ mols/($m^2 \cdot s \cdot Pa^{0.5}$) for the cases where the mixtures consisted of 40%CO-60%H_2O, and 29.5%CO-19.5%H_2-6.7%CO_2-44.3%H_2O, respectively. The COMSOL model was also used to calculate H_2S-to-H_2 ratios, a critical parameter influencing the sulfidization of Pd-based membranes, along the length of the MR. Our results show that portions of the MR may be particularly susceptible to sulfidization, such as the MR outlet

due to an increasing H_2S concentration, accompanied by a depletion of H_2 along the length of the MR. Deactivation of the catalytic Pd surface was also shown to result in elevated H_2S-to-H_2 ratios, which may result in sulfidization of the MR when these values exceed minimum ratio expected to sulfidize Pd at 1173K.

5.1 INTRODUCTION

The water-gas shift reaction is one of the most important reactions for the generation of H_2. The increasing demand for H_2 and the desire to minimize greenhouse gas generation has led to increasing interest in conducting the WGSR in H_2 selective membrane reactors (MR) which a) enhance CO conversions above the equilibrium value, b) generate a high-purity H_2 stream and c) capture the produced CO_2 at high pressure. This concept has been widely investigated in the literature as a method of circumventing low conversions for equilibrium limited reactions by shifting the reaction equilibrium toward more product formation due to the extraction of H_2 from the reaction zone (Assabumrungrat et al. 2002). This unique property allows the coupling of chemical reaction and product separation into a single unit operation.

Pd-based MRs have been extensively investigated for MR applications as a means of enhancing equilibrium limited reactions, and generating high-purity H_2. This is because in addition to being completely selective to H_2 and exhibiting mechanical stability at high-temperature, Pd and its alloy exhibit very high rate of H_2 permeation. Furthermore, studies have shown that Pd-based membranes exhibit moderate catalytic

activity toward the WGSR (Bustamante et al. 2005). Chapter 3 showed that by taking advantage of the inherent catalytic activity of Pd toward the WGSR, and its high H_2 permeance, Pd MRs resulted in CO conversions significantly higher than the equilibrium value at 1173K, in the absence of additional heterogeneous catalyst particles.

Various operating conditions influence the performance of the MR for H_2 generation and separation. Reports in the literature have suggested that the rate of H_2 transport through membranes is influence by three main mechanisms: competitive adsorption, membrane poisoning and the formation of a concentration boundary layer.

Adsorption of components like CO (Hara et al. 1999), steam (Li et al. 2000) and H_2S (McKinley 1967; Burke et al. 1990) on the surface of Pd-based membranes has been observed to decrease H_2 permeation. For example, Hara et al. observed a decrease in H_2 permeation at temperatures below 573K when a pure H_2 feed was replaced with a H_2-CO binary mixture. A H_2-Ar mixture was also observed to reduce H_2 permeation, but not as much as the H_2-CO feed. The higher decrease in the presence of CO was attributed to CO adsorption on the surface of the membrane. Li et al., (Li et al. 2000) conducted a similar experiment using a fixed flow rate of N_2, CO and steam and a variable feed of H_2 at 653K. Li et al. observed a more significant decrease in H_2 permeation when steam was introduced along with the H_2 feed. Although Hara et al. suggest that this phenomenon is significantly reduced at higher temperatures (>573K), other researchers have reported similar H_2-permeation reduction at elevated temperatures when H_2 is present in a mixed gas. For example, Dorris et al. (Dorris et al. 2006) showed about a 17% reduction in H_2 flux through a Pd membrane at 1173K when the feed was changed from pure H_2 to a 80%H_2-balance He mixture.

Poisoning of Pd-based membranes by impurities such as carbon and sulfur has been a significant technological hurdle for the commercialization of Pd-based membranes and has been the subject of a few investigations (Antoniazzi et al. 1989; Morreale 2006). Carbon (Jung et al. 2000; Hou et al. 2002) and sulfur (Burke et al. 1990) have been shown to adsorb strongly on the surface of Pd membranes, blocking active sites for H_2 dissociation and transport. Furthermore, in the case of sulfur, studies have shown that at certain conditions the sulfur can form a stable compound with the Pd (i.e. Pd_4S), decreasing the membrane permeance by as much as two orders of magnitude (Morreale 2006).

Concentration boundary layer phenomenon arises when a high rate of H_2 extraction through a membrane results in the accumulation of a non-diffusing species at the surface of the membrane (Zhang et al. 2006). Previous reports have suggested that the boundary layer thickness depends on the membrane permeability and operating conditions of the MR (Lüdtke et al. 1998; He et al. 1999). Because the driving force for H_2 transport through the membrane is the trans-membrane H_2 partial pressure difference, the resulting H_2-depleted boundary layer results in a loss of membrane performance due to the reduced H_2 concentration at the membrane surface. This phenomenon causes the permeance of the membrane system to be appreciably smaller that the permeance of the membrane, and could significantly decrease the H_2 diffusion rate in this study due to the high reactant concentrations and the high membrane permeance.

This work presents a COMSOL Multiphysics model of a Pd MR for the WGSR at steady state. In light of the ability of the aforementioned mechanisms to influence the H_2

permeance of the membrane when H_2 is present in a gas mixture, the present work evaluates the performance of a Pd membrane by identifying an apparent permeance value equivalent to a fraction of the H_2-permeance of a Pd membrane measured in a pure H_2 feed at 1173K. This model was developed for three cases. To determine the validity of our MR model, Case 1 and Case 2 consider a mixture of steam and CO in a 1.5 steam-to-CO molar ratio (i.e. 60% H_2O and 40% CO), and a simulated syngas mixture composed of 29.5%CO, 19.5%H_2, 6.7%CO_2 and 44.3%H_2O, respectively, and compares the simulation results to previous experimental results. Case 3 then uses the modified rate expression and apparent permeance values identified in cases 1 and 2 to predict H_2S-in-syngas concentrations below which the Pd MR can be safely operated.

Chapter 4 suggested that the critical parameter for sulfidization of Pd-based membranes is not merely the bulk H_2S concentration, but rather the H_2S-to-H_2 ratio in the reactor. For example, Chapter 4 showed that Pd and $Pd_{80wt\%}Cu$ MRs can be successfully operated when the H_2S-to-H_2 ratio was maintained below 0.0011 and showed that when this ratio exceeds 0.0014, the Pd MR experiences sulfidization which may lead to catastrophic rupture of the MR. Therefore, knowledge of the H_2S-to-H_2 ratio along the length of the reactor is critical to the successful operation of Pd-based MRs. Thus, in addition to evaluating the performance of the Pd MR for the WGSR with respect to CO conversion, this model aims to generate H_2S-to-H_2 ratios along the length of the reactor as a function of residence time and inlet H_2S concentration.

5.2 MEMBRANE REACTOR AND COMSOL MODEL

The WGSR, the reaction between CO and steam to produce CO_2 and H_2, is a slightly exothermic reaction with equilibrium conversion decreasing with increasing temperature:

$$CO + H_2O \leftrightarrow CO_2 + H_2 \qquad \Delta H_{298K} = -41 \text{ kJ/mol}$$

Experiments were conducted at 1173K in multi-tubular, 125-μm thick Pd MR and has been described previously (Chapter 3). Briefly, the 3.175 mm OD, 125-μm thick Pd tubes used each had an active membrane length of about 13 cm and internal radius of 0.146 cm. A three-zone ceramic fiber heater with independent temperature control was used to maintain an isothermal reaction environment of 1173K.

The WGSR occurs inside the tube and is described by the gas phase WGS rate expression given by the Bradford mechanism (Bustamante et al. 2005). Further, previous experiments by Bustamante et al. (Bustamante et al. 2005) reported that the Pd membrane is inherently catalytic to the WGSR. To describe this enhancing effect of the Pd reactor walls, a modified version of the gas-phase reaction was developed by introducing a correction factor (F) to increase the value of the pre-exponential constant of the gas-phase WGSR. The inaccuracies of such a simplification would be of most concern near the reactor entrance which is the rate-limited portion of the reactor, but not as great a concern in the downstream transport-limited portion of the MR.

5.2.1 COMSOL Membrane Reactor Model Development

Because of the symmetry of the tubular membrane reactor, the 3-D problem can be modeled as a 2-D axis-symmetric problem. This allows us to describe the MR tube by only modeling half of the tube cross section as shown in **Figure 50**. The reactants flow in from the bottom of the reactor and the products flow out of the top. The membrane is selectively permeable to H_2, allowing H_2 to diffuse out of the reaction zone through the membrane walls, while being impermeable to the other components. An argon sweep gas was used in the experiments to sweep the permeated H_2, limiting the H_2 concentration in the sweep-side to less than 3%. To simplify our computation, the model assumes zero H_2 concentration in the sweep. In order to determine the effect of residence time on CO conversion experiments, the residence times of the reactor systems were varied by changing the operating pressure, while keeping the inlet feed flow rate and reaction temperature constant. Note that previous work conducted by Bustamante et al. (Bustamante et al. 2005) provides a rate expression for the forward WGSR based on high pressure data obtained at NETL. Increasing the reaction pressure in our experiments therefore increased the residence time, increased the H_2 partial pressure driving force for H_2 flux, and also increased the rate of reaction.

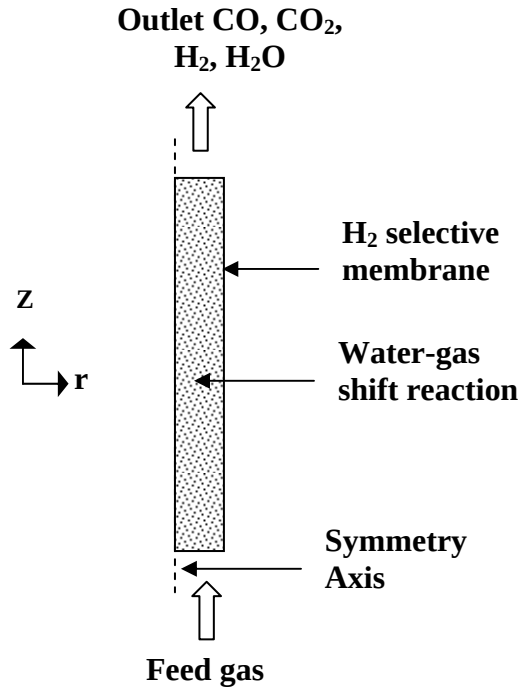

Figure 50. Geometry of membrane reactor depicting modeled domain.

5.2.1.1 Model Assumptions

The MR was assumed to operate at steady state. As a result of isothermal environment maintained by the 3-zone heater, the WGSR equilibrium constant was assumed to be the same throughout the reactor. H_2 permeation across the membrane was based on the trans-membrane H_2 partial pressure difference. The gases were assumed to obey the ideal gas law. The enhancement of the WGSR by the Pd walls was described by modified gas-phase reaction by including a correction factor which enhanced the gas-phase WGSR rate within the feed-side of the membrane reactor. The model also assumed

negligible pressure drop along the length of the membrane unit, and complete selectivity of the Pd MR to H_2.

5.2.1.2 Governing Equations

The model was formulated by coupling the Maxwell-Stefan Diffusion and Convection application mode to the Navier-Stokes equation to account for the gas mixture flow. The non-isothermal flow application mode of the Navier-Stokes equation was used to account for the variation in gas density which results from the extraction of H_2 from the reaction zone at constant pressure. The flow was coupled to the mass balance through the density and velocity field. The dependent variables are the total pressure, P (Pa), and the inlet mass fraction of species, ω_i (kg_i/kg).

The Maxwell-Stefan formulation (Equation (21)) solves for the fluxes in terms of mass fraction for N-1 components specified. The mass fraction of the last component is determined by subtracting the sum of the mass fractions of all the other components from unity according to Equation (22).

$$\nabla \cdot \left[-\rho_{mix}\omega_i \sum_k \left[D_{ik}\left(\nabla x_k + \left(x_k - \omega_k\right)\left(\left(\nabla P\right)/P\right)\right)\right] + D^T\left(\left(\nabla T\right)/T\right)\right] = R_i - \left(\rho_{mix} u . \cdot \nabla \omega_i\right) \quad (21)$$

$$\sum \omega_i = 1 \quad (22)$$

where D_{ik} is the inter-diffusion coefficient (m^2/s) of species i in species k, P is the pressure (Pa), T is the reaction temperature (K), u is the velocity vector (m/s), x is the

mole fraction and ω the mass fraction. The mixture density, ρ_{mix} (kg/m^3), is defined by Equations (23) and (24).

$$\rho_{mix} = \sum c_i \cdot M_i \tag{23}$$

$$c_i = x_i \cdot P / R / T \tag{24}$$

where R is the universal gas constant. The Maxwell-Stefan Convection and Diffusion application forces the mass fluxes of the species to equal the velocity field, and therefore always requires a consistent input of the velocity field.

The mass-balance equation for each species is:

$$\nabla \cdot \mathrm{n_i} = \upsilon_i \, \mathrm{R_i} \tag{25}$$

where n_i is the mass flux vector for species i (kg/m^2/s), R_i is the source term given in Equation (26), and υ_i is the stoichiometric coefficient for the various species given in Table 6. The source term is given by modified version of the gas-phase reaction kinetics of the WGSR according to the Equation (26) (Moe 1962) and Equation (27).

$$R_i = \upsilon_i \cdot F \cdot k_f \cdot cCO^{0.5} \cdot cH_2O \cdot (1 - \beta) \tag{26}$$

$$k_f = k_0 \exp\left(-\frac{E_A}{RT}\right) \tag{27}$$

where

$$\beta = \frac{cCO_2 \; cH_2}{cCO \; cH_2O \; K_{eq}} \tag{28}$$

$$K_{eq} = \exp\left(\frac{4577.8}{T} - 4.33\right) \tag{29}$$

where F is a correction factor used to reproduce experimental results obtained by trial-and-error, k_f is the forward reaction rate constant ($(m^3/mol)^{0.5}s^{-1}$) given by the Bradford mechanism (Bustamante et al. 2005), c_i is the component concentration (mol/m^3), β is the approach to equilibrium factor which goes to unity at equilibrium, and K_{eq} is the temperature dependent WGS reaction equilibrium constant given by Moe (Moe 1962). The conversion of CO was calculated from the concentration of CO_2 and CO in the retentate effluent stream according to Equation (30).

$$X = \frac{\left(xCO_{in} \cdot v_0 - xCO_{out} \cdot u\right)}{\left(xCO_{in} \cdot v_0\right)} * 100 \tag{30}$$

Where v_0 is the reactant inlet superficial velocity (m/s), and xCO_{in} and xCO_{out} are the inlet feed and the outlet CO mole fractions, respectively.

Table 6. Stoichiometric coefficient for components in WGSR

i	CO	H_2O	H_2	CO_2
υ_i	-1	-1	1	1

The mechanism of H_2 permeation through Pd-based membranes has been extensively studied. It has been found that H_2 permeates through the membrane via a solution-diffusion mechanism, and the rate of H_2 permeation per unit area of the membrane, J_{H2} ($mols/m^2/s$), is proportional to the partial pressure difference according to the equation:

$$J_{H2} = k*(P_{H2,r}^{0.5} - P_{H2,p}^{0.5}) \tag{31}$$

In this study, the rate of H_2 extraction through the membrane was approximated by assuming that the partial pressure of H_2 in the permeate stream ($P_{H2,p}$) was equal to

zero and an apparent permeance, k′, was computed. This equation was expressed in terms of H_2 concentration and is described by the expression:

$$N_{H2} = M_{H2}\, k' * R^{0.5} * T^{0.5} * c_{H2}{}^{0.5} \tag{32}$$

where N_{H2} is the H_2 flux (kg/(m^2·s)), M_{H2} is the molecular weight of H_2 (kg/mol) and k′ is the apparent H_2 permeance (mol/(m^2·s·Pa$^{0.5}$)) used to reproduce experimental results.

As the reactants proceed along the length of the reactor, there is a decrease in average velocity of the bulk as a result of the mass loss due to H_2 extraction from the reaction zone. This is accompanied by a corresponding increase in gas mixture density due to H_2 depletion and heavier CO_2 production. The gas flow is modeled by solving the steady state momentum balance (Equation (33)) and continuity equation (Equation (34)) based on the non-isothermal flow functionality which accounts for the change in mixture density.

$$\rho_{mix}(u \cdot \nabla)u = \nabla \cdot \left[-P \cdot I + \eta\left(\nabla u + (\nabla u)^T\right) - (2\eta/3 - \kappa)(\nabla \cdot u)I\right] \tag{33}$$

$$\nabla \cdot (\rho_{mix} u) = 0 \tag{34}$$

Where η is the mixture viscosity (kg/m/s), κ is the gas mixture dilatational viscosity (kg/m/s), and I is the identity matrix.

As noted earlier, the residence time was varied by changing the reaction pressure, while maintaining the inlet volumetric flow rate (sccm) constant. This process results in a reduced reactant volumetric flow rate (therefore increased residence time) at the elevated

pressure conditions inside the reaction zone which is calculated by Equation (35), assuming ideal gas behavior. The reactor parameters and input component used in the simulation are tabulated in Table 7 and Table 8, respectively. The retentate pressures used in the simulation corresponding to the various residence times are listed in Table 9.

$$v_0 = \left(\frac{v_1 * T * P\_atm}{4 * T_{std} * P * A} \right) \tag{35}$$

Where v_1 is the total reactant feed flow rate at STP (m^3/s), T is the reaction temperature (K), T_{std} is the standard temperature (300K), P_atm is atmospheric pressure (Pa), P is the reaction pressure (Pa), A is the reactor cross-sectional area (m^2), and the number 4 is used to express the flow going into one of the four-tube bundle.

Table 7: Parameters used in the simulation

Parameters	values
T (K)	1173
Reactor length (m)	$1.3*10^{-1}$
Tube internal radius (m)	$1.46*10^{-3}$
A (m^2)	$6.72*10^{-6}$
v_1 (m^3/s)	$3.33*10^{-6}$
K_f ($(m^3/mol)^{0.5}s^{-1}$)	0.002093
K_{eq}	0.65

Table 8: Inlet mass fraction composition used in the simulations

Case	k´ ($mol/m^2/s/Pa^{0.5}$)	ωCO	ωH_2O	ωCO_2	ωH_2	ωH_2S
Case 1 (CO+steam)	$1.5*10^{-5}$	0.491	0.519	-	-	-
Case 2 (syngas+steam)	$4.4*10^{-5}$	0.4278	0.4125	0.1395	0.0202	-
Case 3 (syngas+steam+H_2S)	$4.4*10^{-5}$	0.4278	0.4125	0.1394823	0.0202	$1.77*10^{-5}$

Table 9: Retentate pressures used in the simulations

Pressure (*10^5Pa)	τ (s)
2.70355	0.7
3.1509	0.82
4.45737	1.16
7.01197	1.81
7.74802	2.0
11.5625	3.0
19.1467	4.96

5.3 SIMULATION RESULTS

The results of the developed COMSOL Multiphysics model for simulating the performance of the Pd MR for the WGSR are presented in terms of CO conversion and molar fraction profiles for all reaction species (CO, CO_2, H_2O, and H_2).

5.3.1 Model Validation Results

5.3.1.1 WGSR in Pd Membrane Reactor Using CO and Steam

To validate the COMSOL Multiphysics model, we simulated previously reported experimental results of the WGSR in a Pd MR (Chapter 3). **Figure 51** shows the results of the COMSOL modeling of the Pd wall-catalyzed WGSR (steam-to-CO ratio: 1.5) for various residence times (Case 1), compared to the experimental results reported in Chapter 3. Using an apparent permeance value and correction factor of $1.5*10^{-5}$ mols/(m^2·s·$Pa^{0.5}$) and 50 attained by trial-and-error, respectively. The simulation results of CO conversion calculated from Equation (30) accurately reproduced the experimental

results and depict increasing CO conversion (**Figure 51**) with increasing residence time. These results validate the formulation of the COMSOL model.

The low apparent H_2 permeance value ($1.5*10^{-5}$ mols/($m^2 \cdot s \cdot Pa^{0.5}$)) used to replicate the experimental results, relative to the measured permeance of ~$3.1*10^{-4}$ mols/($m^2 \cdot s \cdot Pa^{0.5}$ in a pure H_2 atmosphere (Chapter 6), was attributed to competitive adsorption between H_2 and the high concentration of CO, CO_2 and steam in the MR, in addition to the significant H_2-depleted concentration boundary layer that arises in the MR especially because of the large H_2 permeance (Hara et al. 1999) at the high operating temperature. The correction factor of 50 used to correlate experimental results suggests that the Pd MR enhanced the gas phase WGSR about 50-fold. Figure 52a to d show the axial concentration profiles of the WGSR components obtained along the center of the reactor for residence times of 0.82, 1.81, 3.01 and 4.96s (based on inlet gas flows), respectively. The figures show increasing CO_2 concentration with increasing residence time, while the H_2, CO and H_2O concentrations are observed to decrease with increasing residence time.

Figure 53 shows the normalized superficial velocity profile along the length of the Pd MR for the four residence times in this study (0.82, 1.81, 3.01 and 4.96). The decreasing superficial velocity along the length of the MR is the result of the loss of H_2 through the H_2 selective membrane walls which reduces the gas flow rate. It is evident in the data presented in Figure 53 that the superficial velocity decreases more with increasing residence time. This is as a result of increasing H_2 permeation through the MR due to the increased H_2 production, leading to a higher H_2 concentration in the retentate, which results in a higher H_2 driving force.

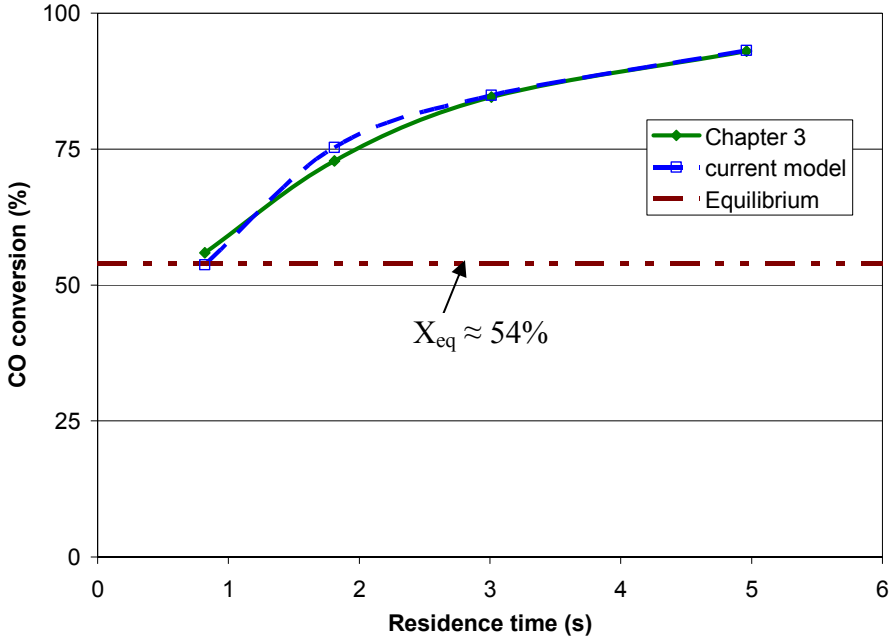

Figure 51. Comparison of experimental (Chapter 3) and current simulation results for CO conversion in the Pd MR at 1173K as a function of residence time (Case 1). Equilibrium CO conversion at these conditions ≈ 54%.

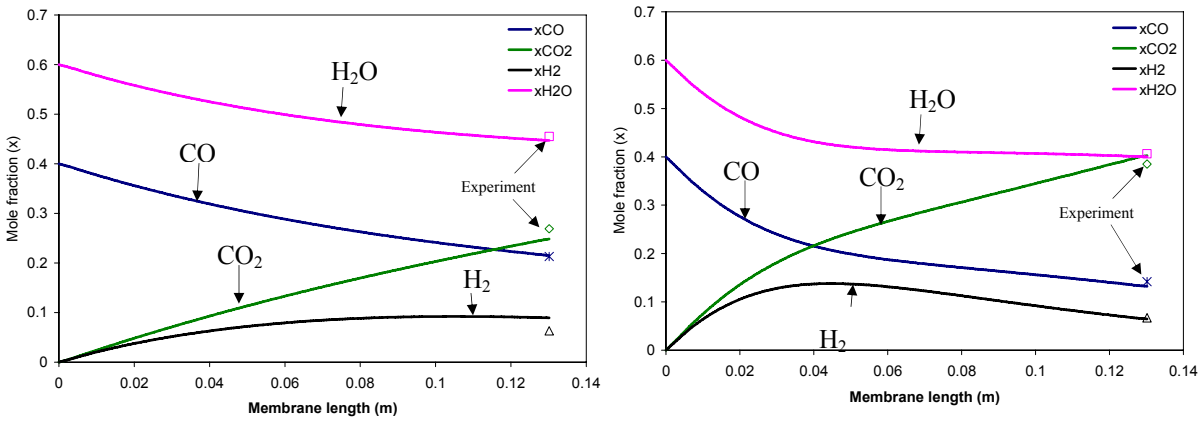

(a) (b)

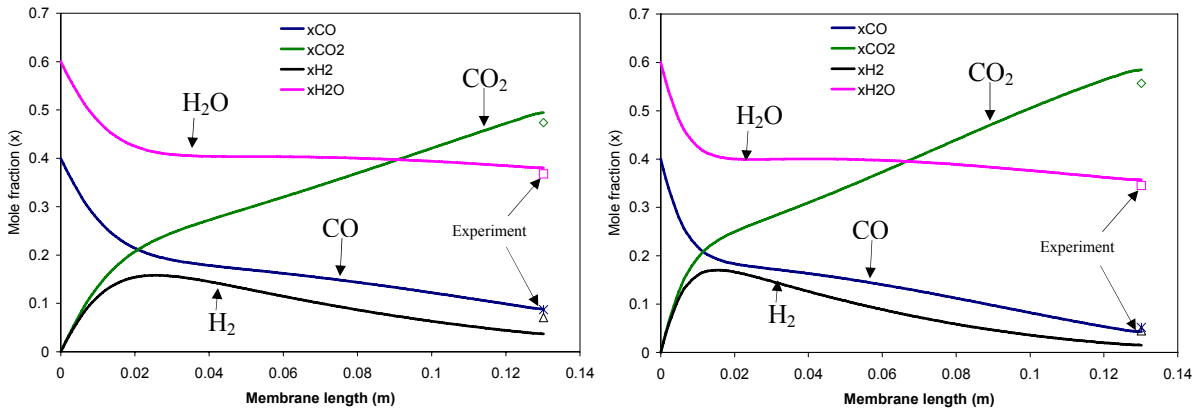

Figure 52. CO, H_2O, CO_2 and H_2 axial concentration profiles in the Pd MR for residence times (based on inlet gas flow rate) of 0.82 (a), 1.81 (b), 3.01 (c) and 4.96s (d) corresponding to CO conversions of 53.7, 75.3, 84.9 and 93.2%, respectively (Case 1). The experimental measurements of the effluent concentrations of the various components at the exit of the reactor are also plotted for comparison.

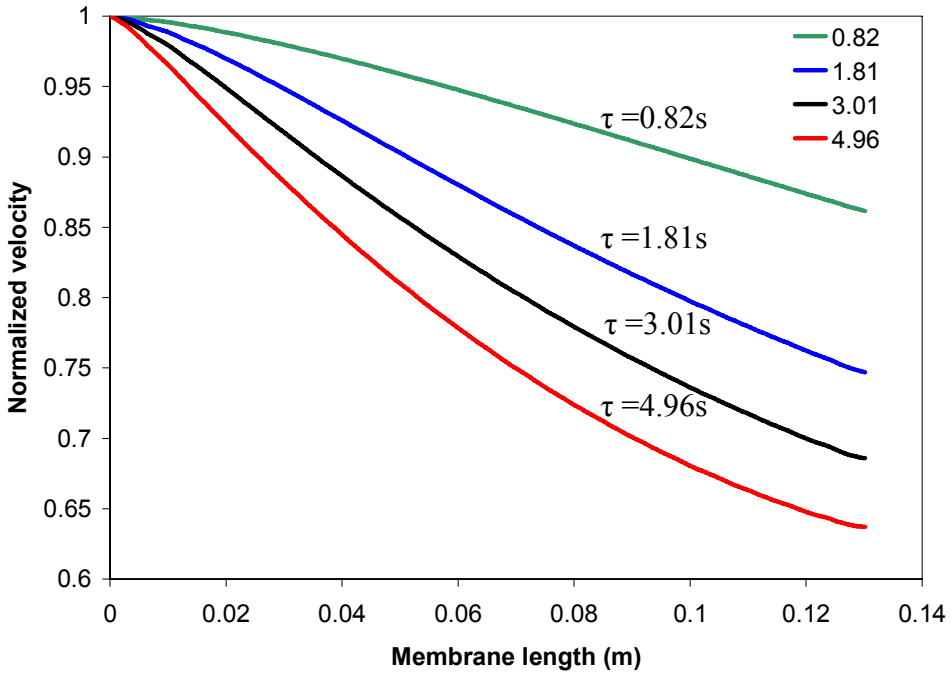

Figure 53. Normalized gas superficial velocity profile as a function of reactor length for residence times (based on inlet gas flow rate) of 0.82, 1.81, 3.01 and 4.96s (Case 1).

5.3.1.2 WGSR in Pd Membrane Reactor Using Syngas and Steam

Subsequently, the COMSOL model was used to simulate a MR system which utilized a simulated syngas feed composed of 53%CO, 35%H_2 and 12%CO_2 (dry basis) at 1173K (Case 2). Steam was introduced at a flow rate to result in a steam-to-CO ratio of 1.5, resulting in a reactant feed composition of 29.5%CO, 19.5%H_2, 6.7%CO_2 and 44.3%H_2O. Using the same correction factor (F=50) determined to accurately replicate the experimental results in the simulation involving the pure CO with steam reactants (Case 1), the apparent permeance of the Pd MR required to reproduce experimental results was determined to be $4.4*10^{-5}$ mols/($m^2 \cdot s \cdot Pa^{0.5}$). A plausible explanation for the higher apparent H_2 permeance value for this system which utilized syngas, compared to the previous system which used a pure CO feed, is the higher inlet H_2 concentration in the syngas feed resulting in a less H_2-depleted boundary layer in the MR.

Figure 54 illustrates the results of the COMSOL simulations compared to experimental values attained in Chapter 6 involving the syngas feed. Once again the simulation results are in very good agreement with experimental data, and show an increasing trend of CO conversion with increasing residence time. **Figure 55**a to c show the component axial concentration profiles as a function of reactor length for CO conversions of 56.1, 82.3 and 99.1%, respectively. It is worth pointing out that the CO and H_2 concentrations decrease along the length of the membrane reactor due to increasing CO conversion and H_2 extraction. Further, the CO_2 effluent concentration of observed to reach a maximum of about 70% at the 2s residence time. Thus, in agreement to the experimental results, the Pd MR may be effectively used to attain near complete CO conversion, while producing a high-pressure CO_2-rich effluent stream which is

amenable to sequestration strategies. Similar to the previous simulation involving pure CO and steam, the normalized velocity (**Figure 56**) was observed to decrease with increasing residence time, due to the increasing H_2 production, and extraction from the reaction zone. Note that at 2s residence time (**Figure 56**), almost 50% of the inlet gas volume is extracted through the MR as H_2.

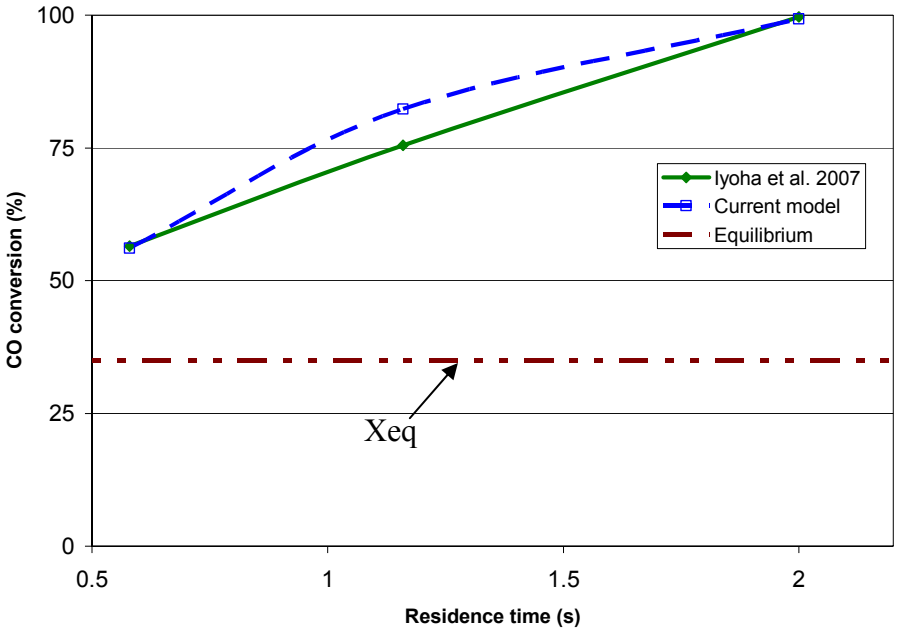

Figure 54. Comparison of experimental and current simulation results for CO conversion in the Pd MR at 1173K for 0.7, 1.2 and 2s residence time (based on inlet gas flow rate) using simulated syngas feed (29.5%CO, 19.5%H_2, 6.7%CO_2 and 44.3%H_2O). Membrane apparent permeance value = $4.4*10^{-5}$ mols/(m^2·s·$Pa^{0.5}$) (Case 2). Equilibrium CO conversion at these conditions ≈ 32%.

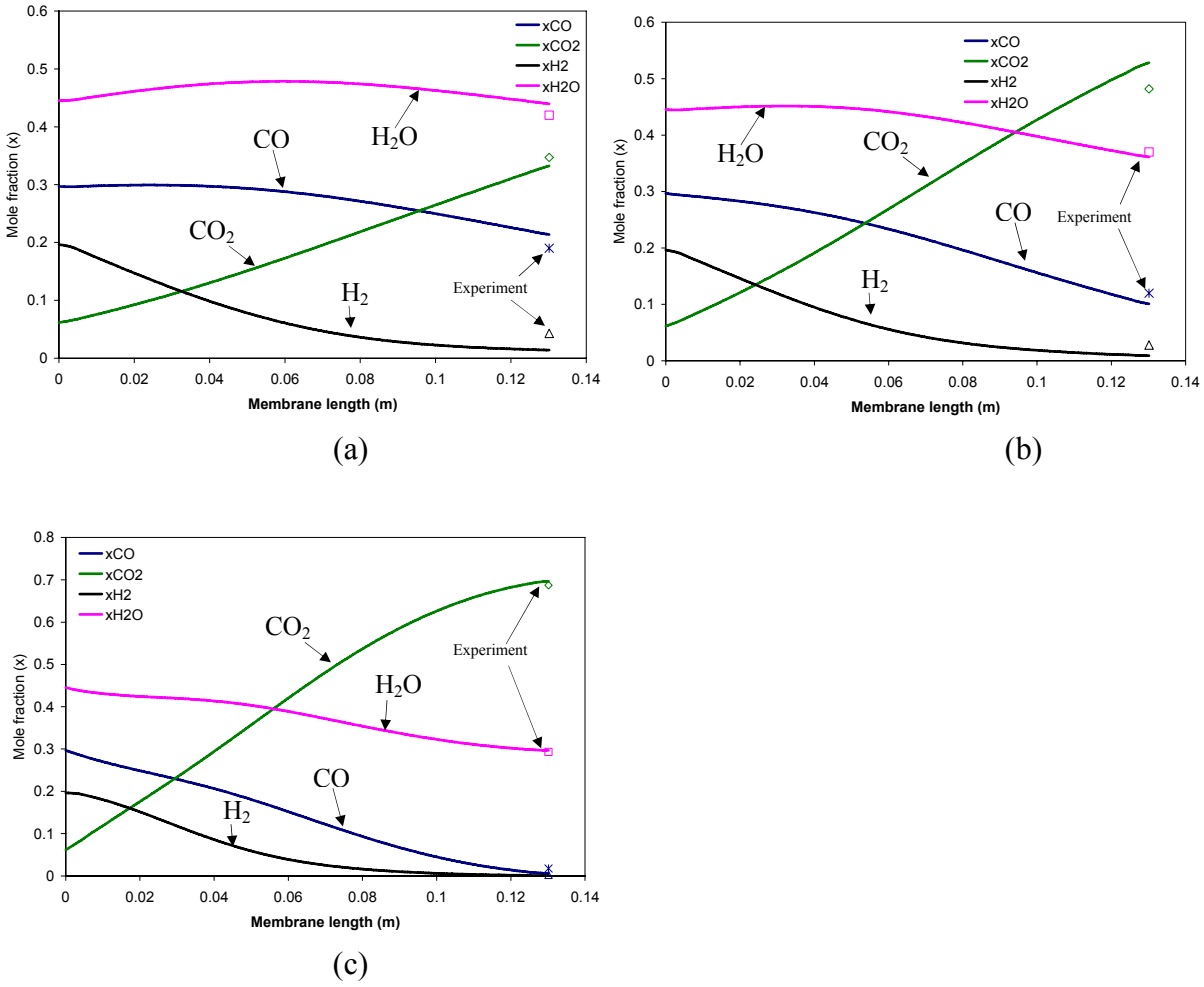

Figure 55. CO, H_2O, CO_2 and H_2 concentration profiles in the Pd MR for residence times (based on inlet gas flow rate) of 0.7 (a), 1.2 (b), and 2s (c) corresponding to CO conversions of 56.1, 82.3 and 99.1%, respectively (Case 2). The experimental measurements of the effluent concentrations of the various components at the exit of the reactor are also plotted for comparison.

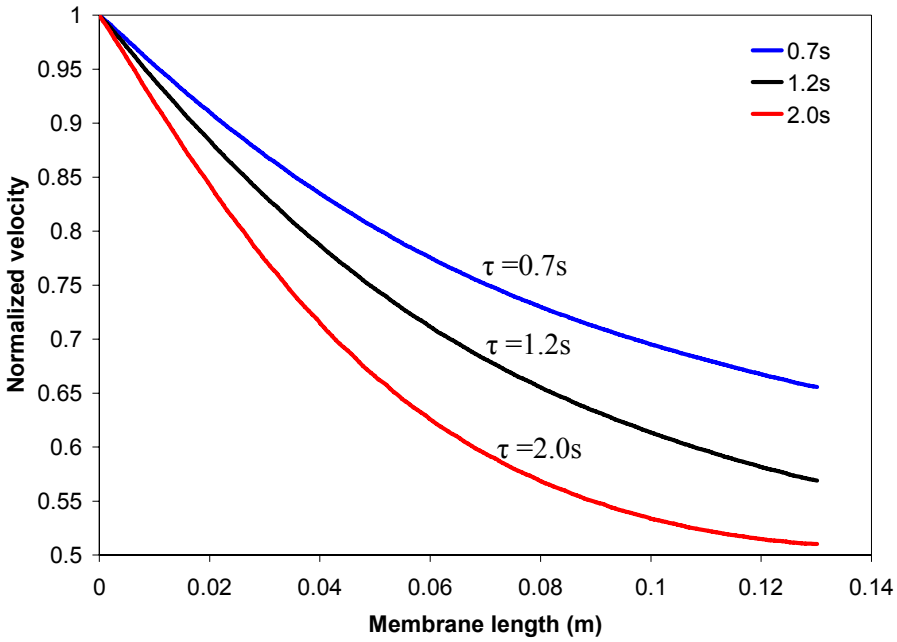

Figure 56. Normalized superficial velocity as a function of MR length for residence times (based on inlet gas flow rate) of 0.7, 1.2 and 2.0s corresponding to CO conversions of 56.1, 82.3 and 99.1%, respectively (Case 2).

5.3.2 Effect of Increased Catalytic Activity and H_2 Permeance on Membrane Reactor Performance

The effect of higher apparent H_2 permeance and catalytic activity (i.e. loading the MR with a bona fide WGS catalyst) of the membrane walls on reactor performance was investigated by varying the apparent permeance and correction factor values of the Pd membrane. **Figure 57** illustrates the effect of increasing the apparent membrane permeance by factors of 1.5 and 2, on CO conversion as a function of residence time for the pure CO and steam reactants in section 5.3.1.1. (Case 1). The figure illustrates the enhancing effect of increased H_2 extraction from the reaction zone, and suggests that by increasing the apparent permeance of the MR by a factor of 2, the residence time required

to attain a similar CO conversion may be significantly reduced. For example, **Figure 57** shows that the maximum CO conversion of 93% attained at 5s residence time using an apparent permeance value of $1.5*10^{-5}$ mols/(m^2·s·$Pa^{0.5}$), was reached in less than 2s when the apparent permeance value was increased to $3.0*10^{-5}$ mols/(m^2·s·$Pa^{0.5}$).

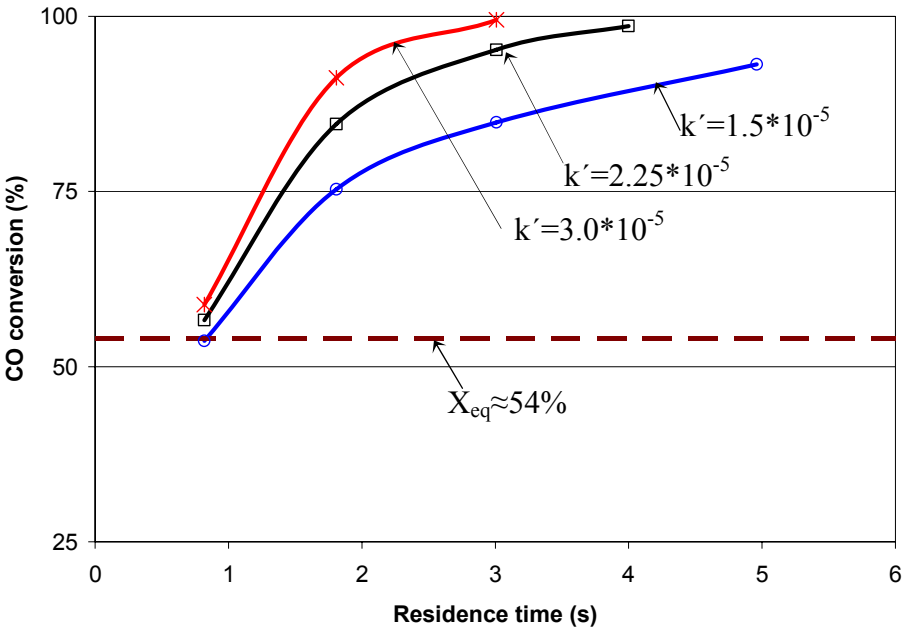

Figure 57. Effect of increasing apparent H_2 permeance on CO conversion via the WGSR in Pd MR at 1173K using a correction factor of 50. Equilibrium CO conversion at these conditions ≈ 54%.

Figure 58 indicates the effect of increasing the catalytic activity of the membrane walls (or using bona fide WGSR catalysts) on CO conversion as a function of residence time for the pure CO and steam reactants in section 5.3.1.1. (Case 1), while maintaining the H_2 permeance value of $1.5*10^{-5}$ mols/(m^2·s·$Pa^{0.5}$) constant. The figure indicates an enhancing effect of increasing catalytic activity on CO conversion at the short residence time of 1s. However, this enhancement was observed to diminish with increasing

residence time. This suggests that the MR was kinetic limited at the short residence time, while at longer residence times the MR became membrane limited.

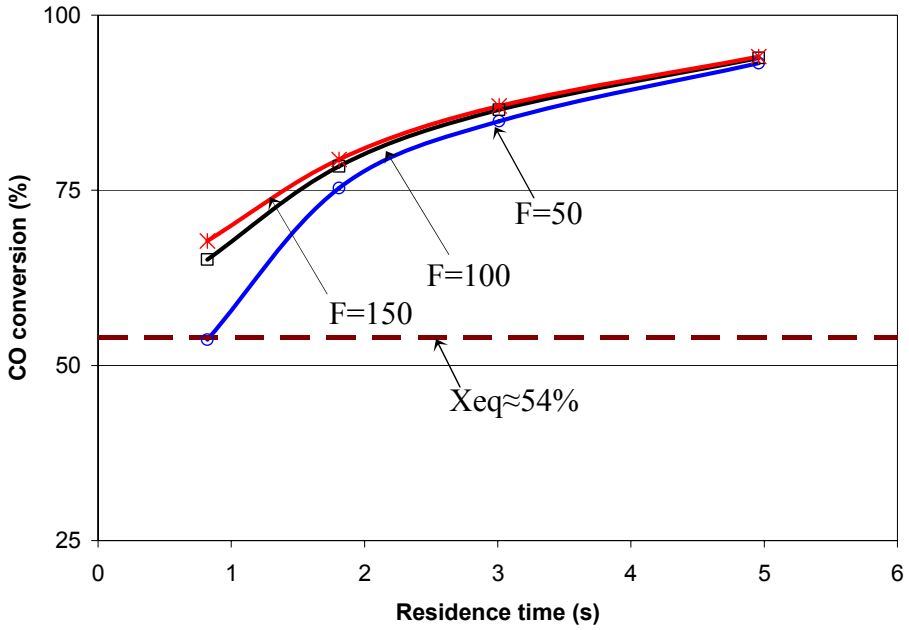

Figure 58. Effect of increasing membrane catalytic activity on CO conversion via the WGSR in Pd MR at 1173K, maintaining the membrane apparent H_2 permeance of $1.5*10^{-5}$ mols/(m^2·s·$Pa^{0.5}$) constant. Equilibrium CO conversion at these conditions ≈ 54%.

5.3.3 Predicting the Sulfidization of Pd MR for WGSR Using Syngas Containing H_2S

The COMSOL model was also used to generate component concentration profiles and H_2S-to-H_2 ratios for the WGSR which employed a syngas feed containing 10 ppm H_2S. As noted earlier, the study in Chapter 4 showed that the sulfidization of Pd-membranes is dependent on the H_2S-to-H_2 ratio in the feed gas, and showed that Pd was sulfidized by H_2S-to-H_2 ratios greater than about 0.0014. The 10 ppm H_2S feed

concentration was selected because the feed H_2S-to-H_2 ratio of approximately $5.13*10^{-5}$ (equivalent to a 51 ppm H_2S-in-pure H_2 feed), was below the 0.0014 value required to sulfidize the Pd at low residence times. Further, simulations involving H_2S concentrations higher than 20 ppm resulted in H_2S-to-H_2 ratios above the equilibrium value required to sulfidize the Pd membrane over the entire conditions simulated, indicating that at similar operating conditions (H_2 effluent concentrations), the Pd MR would be expected to sulfidize if exposed to syngas mixtures with H_2S concentrations greater than about 20 ppm.

5.3.3.1 Effect of CO Conversion and H_2 Recovery in Pd MR on H_2S-to-H_2 Ratio

Assuming no influence of the H_2S on CO conversion (i.e. catalytic deactivation) and H_2 permeance of the membrane (experimentally verified), **Figure 59** shows axial H_2S concentration profile along the length of the Pd MR for a simulation involving a 10 ppm H_2S introduced with the syngas feed at the operating conditions shown in **Figure 55**a, b and c, corresponding to CO conversions of 56.1, 82.3 and 99.1%, respectively. The increasing trend of H_2S concentration (Figure 59) along the length of the reactor stems from the fact that H_2 is extracted from the reaction zone of the MR as the reaction progresses, resulting in a loss of gas volume. **Figure 59** illustrates about a 1.5, 1.8 and 2-fold increase (15.5, 18 and 20 ppm H_2S, respectively) in H_2S concentration at the exit of the reactor with increasing residence times of 0.7, 1.2 and 2.0s, respectively. The H_2S-to-H_2 ratio in the MR was calculated as a function of MR length, and is depicted in **Figure 60**, along with the equilibrium H_2S-to-H_2 ratio (~0.0014) expected to sulfidize the Pd

membrane at 1173K. The intersection of the equilibrium line and the H_2S-to-H_2 ratios for the various conditions simulated, indicate the location at which sulfidization of the MR is expected to initiate. Therefore, the results suggest that in the absence of H_2S deactivation of the catalytic Pd walls, the MR should maintain its structural integrity in the presence of 10 ppm H_2S in the syngas feed at 0.7s residence time. Figure 60 also indicates that for higher residence times (1 and 2s), the H_2S-to-H_2 ratio increases above the equilibrium H_2S-to-H_2 ratio, suggesting that at these conditions, MR sulfidization can be expected beyond about 0.115 and 0.085 m from the MR inlet at 1.2 and 2s residence times, respectively. In is worth pointing out that the location at which sulfidization of the membrane is expected to begin (0.115 and 0.085 m from the MR inlet at 1.2 and 2s residence times), draws closer to the MR inlet with increasing CO conversion and H_2 recovery.

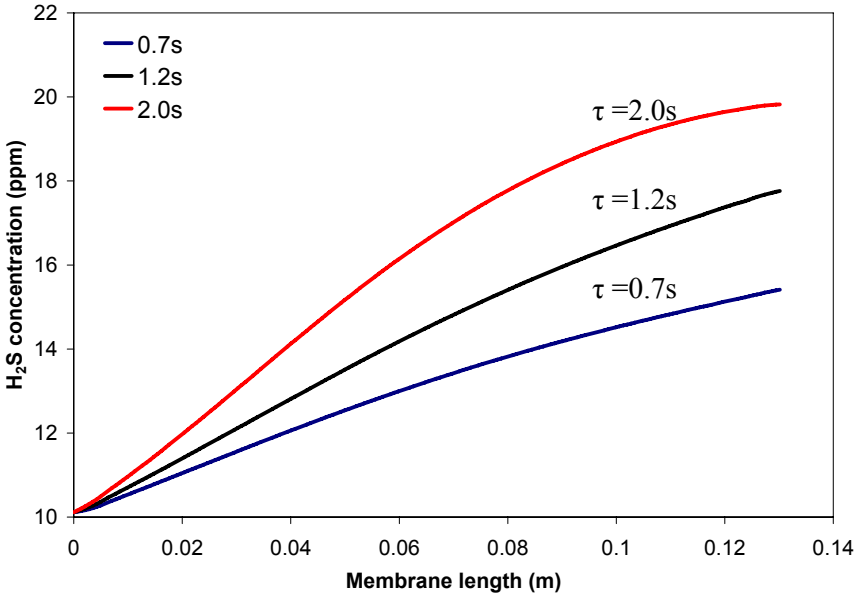

Figure 59. H_2S concentration profile in Pd MR as a function of reactor length for residence times of 0.7, 1.2 and 2.0s, corresponding to CO conversions of 56.1, 82.3 and 99.1% using syngas containing 10 ppm H_2S.

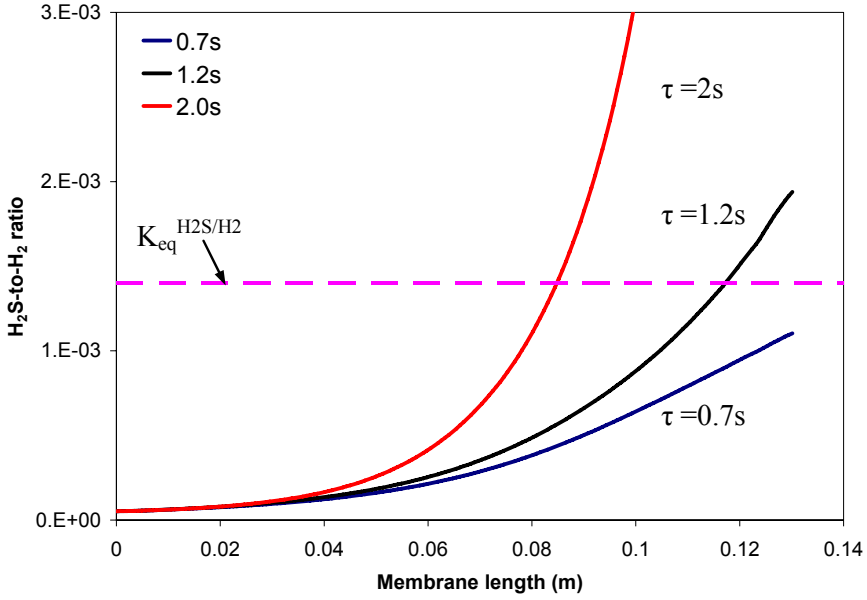

Figure 60. H_2S-to-H_2 ratio in Pd MR as a function of reactor length for residence times of 0.7, 1.2 and 2.0s, corresponding to CO conversions of 56.1, 82.3 and 99.1% using syngas containing 10 ppm H_2S. Dashed line represents equilibrium H_2S-to-H_2 ratio required for sulfidization of Pd at 1173K.

5.3.3.2 Effect of Deactivation of Catalytic Pd walls on CO Conversion and H_2S-to-H_2 Ratio

Catalyst deactivation by H_2S is one of the most serious deactivation problems with the use of metal catalysts, where a few ppm of H_2S is sufficient to completely deactivate the catalyst (Rodriguez et al. 1997). Therefore, the ability of H_2S to poison the catalytic activity of the Pd walls towards the WGSR was simulated by assuming that the presence of H_2S in the feed gas reduced the WGSR rate by a fraction of the correction factor initially used to accurately correlate experimental results in section 3.1. **Figure 61**a-d show the effect of catalytic deactivation of the Pd walls on MR performance with respect to CO conversion and H_2S-to-H_2 ratio at 0.7s residence time, assuming the H_2S does not adversely impact H_2 permeance at this temperature.

The data presented in **Figure 61**a suggests that a 50% (F=25) and 80% (F=10) reduction in catalytic activity reduces CO conversion from 56.1% to 35% and 18%, respectively. Note that in the absence of catalyst deactivation, the syngas containing 10 ppm H_2S should not result in the sulfidization of the Pd MR at 0.7s residence time (**Figure 60**) as a result of the H_2S-to-H_2 ratio being lower than the equilibrium ratio expected to result in sulfide formation. However, **Figure 61**d suggests that deactivation of the catalytic Pd membrane results in an increasing H_2S-to-H_2 ratio along the length of the MR which may eventually lead to catastrophic Pd sulfidization. **Figure 61**b indicates a modest decrease in H_2S concentration as a result of deactivation of the catalytic walls. The increasing H_2S-to-H_2 ratio observed in **Figure 61**d is the result of the appreciably lower H_2 production rate due to the reduced catalytic activity of the Pd walls. Since the H_2 permeance of the membrane is not appreciably impacted by the H_2S at this

temperature, the H_2 concentration profile is observed to decrease along the length of the MR (**Figure 61**c) for decreasing catalytic activity. Thus the potential deactivation of the catalytic Pd membrane may result in an appreciably higher H_2S-to-H_2 ratio which may result in catastrophic MR failure due to sulfidization at conditions at which sulfidization would otherwise not be expected. In this case, MR sulfidization can be expected beyond about 0.095 and 0.07 m from the MR inlet at 50% and 80% reduction in catalytic activity, respectively.

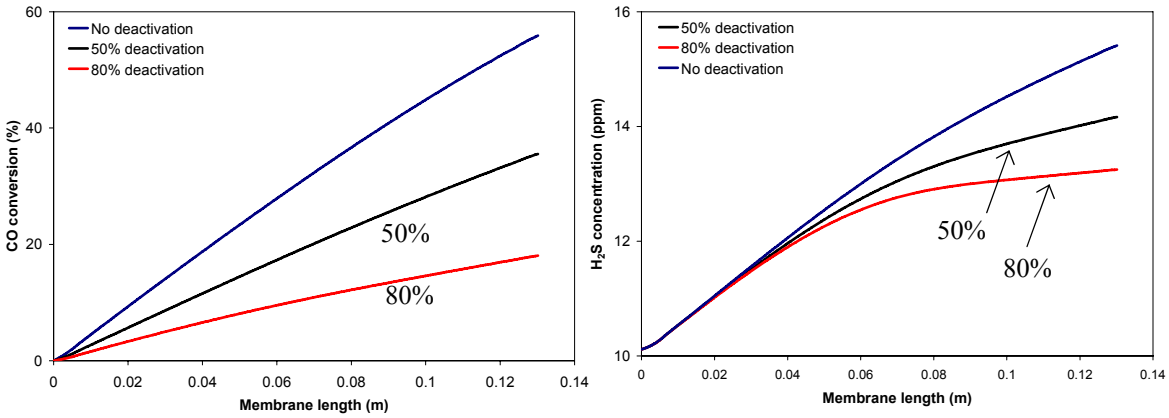

(a) (b)

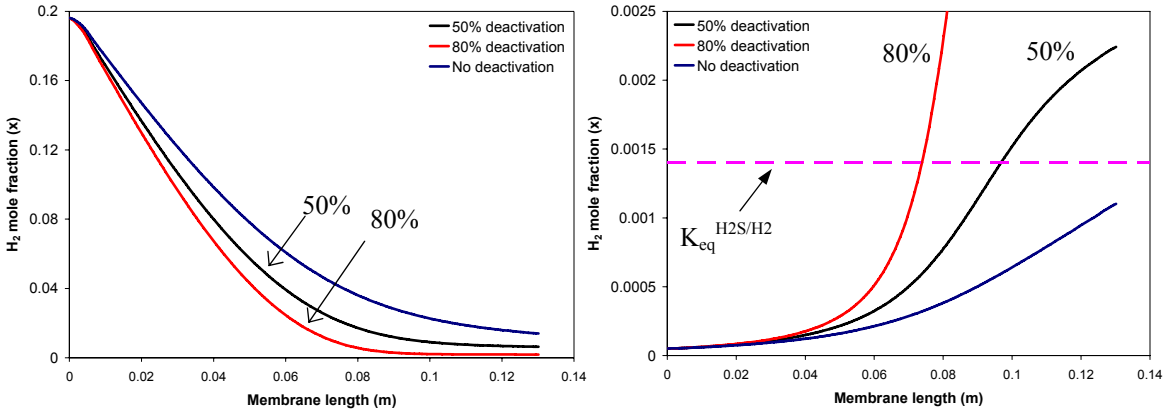

(c) (d)

Figure 61. Effect of H_2S catalytic surface deactivation of Pd MR on CO conversion (a), H_2S concentration profile (b), H_2 concentration profile (c) and H_2S-to-H_2 ratio (d) for syngas containing 10 ppm H_2S at 1173K and 0.7s residence time. Correction factor reduced from 50 to 25 and then to 10 to simulate 50% and 80% reduction in catalytic activity of Pd, respectively. Dashed line (d) represents H_2S-to-H_2 ratio for sulfidization of Pd at 1173K.

5.4 CONCLUSION

A COMSOL Multiphysics model was developed to analyze the WGSR in a Pd membrane reactor at 1173K. The reduction in H_2 permeation through the Pd MR in the presence of high concentration of reactant species was accounted for by using an apparent permeance value which accurately predicted experimental results.

The model reproduced experimental results when a modified version of the gas-phase water-gas shift reaction, which included a correction factor of 50, and apparent H_2 permeance values $1.5*10^{-5}$ and $4.4*10^{-5}$ were used for the WGSR involving pure CO and

CO present in a syngas mixture, respectively. The model also showed that the CO conversion could be further increased by increasing the apparent permeance and catalytic activity of the membrane.

In addition to being capable of accurately generating the concentration profile of the various components in the gas mixture, this model was capable of generating H_2S-to-H_2 concentration profiles -- a critical parameter for predicting the sulfidization of MRs -- along the length of the MR for various CO conversions, and H_2 retentate concentrations. This has the potential to be a very useful tool in the design of Pd-based MR for H_2 production from H_2S-containing feed gases.

The results show that at low conversions, the Pd MR may be successfully operated in the presence of 10 ppm H_2S in a syngas mixture. However, increasing H_2 production at higher residence times resulted in lower H_2 retentate concentrations, which increased the H_2S-to-H_2 ratios along the length of the MR to values above the equilibrium H_2S-to-H_2 ratio expected to sulfidize Pd at 1173K. This phenomenon may result in catastrophic failure of the membrane reactor module due to sulfidization of the MR. Simulation results indicated that H_2S concentrations above 20 ppm could result in deleterious membrane sulfidization over the conditions of interest.

The results also show that in the absence of H_2 permeance reduction by the presence of H_2S, deactivation of the catalytic Pd walls may appreciably increase the H_2S-to-H_2 ratio due to the decreased production of H_2, resulting in membrane failure in the presence of H_2S-to-H_2 ratios which would otherwise have been tolerated by the MR.

Although this model was fairly accurate in reproducing experimental results, it was developed by assuming a pseudo-homogeneous reaction mechanism which occurred

uniformly throughout the reactor domain. This simplification does not accurately describe the experimental MR which involved the surface catalyzed WGSR occurring at the membrane surface only. A more accurate formulation would have to consider this phenomenon, using precise rate expressions for the WGSR over Pd catalysts.

6.0 CHAPTER SIX: H_2 PRODUCTION FROM SIMULATED COAL SYNGAS CONTAINING H_2S IN MULTI-TUBULAR, Pd AND 80WT%Pd-20WT%Cu MEMBRANE REACTORS AT 1173K

Abstract

99.7% conversion of CO in a simulated syngas feed containing 53%CO, 35%H_2 and 12%CO_2 was achieved via the water-gas shift (WGS) reaction in a countercurrent Pd multi-tube membrane reactor (MR) at 1173K and 2s residence time. This conversion is significantly greater than the 32% equilibrium conversion associated with a conventional (non-membrane) reactor primarily due to the high rate of H_2 extraction from the reaction zone through the Pd membranes at elevated temperatures. Furthermore, nearly complete H_2 recovery was attained in the permeate, resulting in the simultaneous production of a high-pressure CO_2 (>99%) retentate stream after condensation of the steam. When $Pd_{80wt\%}Cu$ tubes were used in the reactor, a significantly lower CO conversion of 68% was attained at comparable residence times, probably due primarily to the lower H_2 permeance of the alloy.

When H_2S was added to the syngas feed and the H_2S-to-H_2 ratio was maintained below the threshold required for thermodynamically stable sulfides to form, the Pd and $Pd_{80wt\%}Cu$ MRs retained their mechanical integrity and H_2 selectivity, but a precipitous drop in CO conversion was observed due to deactivation of the catalytic surface. The Pd and $Pd_{80wt\%}Cu$ MRs were observed to fail within minutes after increasing the H_2S-to-H_2 ratio to levels above that expected for thermodynamically stable sulfides to form, as

evidenced by rupturing of the membrane tubes. SEM-EDS analyses of the membranes suggested that at high H_2S-to-H_2 ratios, the H_2S compromised the mechanical integrity of the MRs by preferentially attacking the grain boundary region.

6.1 INTRODUCTION

H_2 generation from coal, natural gas and biomass is expected to remain a major source of H_2 in the foreseeable future. For example, H_2 production from coal gasification has gained renewed interest in recent years as a result of the vast amount of available coal which can be gasified to produce a syngas stream with relatively high concentrations of H_2 (~35vol%) and CO (~51vol%). The CO can be further reacted with steam via the water-gas shift reaction (WGSR) to increase the H_2 concentration in the syngas. At the same time, this reaction produces CO_2 that, once separated from the H_2, can be geologically sequestered to mitigate the greenhouse effect.

Conventionally, coal gasification occurs at high temperatures (above 1173K) and high pressures (above 2000 kPa) in the presence of O_2 and steam. The produced CO/H_2-rich (about 86vol%) syngas is scrubbed of impurities, cooled to low temperature, and then directed to a two-stage shift reactor where high temperature (593–723K) and subsequent low temperature (473-523K) water-gas shift reactors are used to increase the H_2 concentration by reacting CO in the syngas with steam. The low temperature WGSR allows high levels of CO conversion to be attained because CO conversion of this exothermic reaction is thermodynamically favored at low temperature. Alternatively,

high CO conversions can be realized at elevated temperatures (>~ 973K) if MRs that are selective to one of the products, CO_2 or H_2, are used.

Pd-based membranes have gained a great deal of attention for MR application because these membranes are highly permeable to H_2, are virtually impermeable to other gases and are stable at relatively high temperatures. Such Pd-based MRs have been successfully demonstrated to enhance CO conversions via the WGSR (Equation (36)) to values above the thermodynamic equilibrium at various temperatures (Uemiya et al. 1991; Basile et al. 1996; Basile et al. 2001; Chapter 3) as a result of the selective and rapid extraction of H_2 from the reaction zone.

$$CO + H_2O \leftrightarrow CO_2 + H_2, \ \Delta H^o_{298} = -41\text{kJ/mol} \qquad (36)$$

However, most of these experiments have been conducted using pure reactant feeds (i.e. CO and H_2O) and have been limited to temperatures below 600K. Only a few studies have explored conducting the WGSR in a MR when the CO is present in a mixture with components other than steam. Basile et al. (Basile et al. 1996) carried out the WGSR in a Pd composite membrane (~0.2 μm Pd coated on the inner surface of a tubular ceramic membrane) at 595K using a mixed feed composed of 7%H_2, 25%CO, 15%CO_2 and 53%N_2 (dry basis). Using a 3.86 steam-to-CO molar ratio, they reported CO conversions always below the corresponding equilibrium value of 97.64%, with the highest attained conversion being 95.97% when the pressure in the reaction zone was increased to 120 kPa. They attributed the lower-than-equilibrium CO conversions to a) the low selectivity of the composite MR used, b) the reduced reaction rate as a result of the presence of other components reducing the partial pressures of the reactants (CO +

H_2O), and c) the reduced partial pressure of H_2 which reduced the H_2 flux through the membrane. A more recent study by Criscuoli et al. (Criscuoli et al. 2000), however, surpassed equilibrium CO conversions for three different feed mixtures containing various concentrations of CO, CO_2, H_2 and N_2 in a 75-μm thick Pd MR at 595K, with a steam-to-CO ratio of 1.1. Furthermore, for the mixture containing 32%CO, 12%CO_2, 4%H_2 and 52%N_2, essentially complete CO conversion was demonstrated. A subsequent study by Tosti et al. (Tosti et al. 2003) explored conducting the WGSR in 70-μm Pd-Ag MRs. Tosti et al. achieved CO conversions greater than the equilibrium value for experiments involving pure reactants (40%CO and 60%H_2O), and mixed reactants (20%CO, 30%H_2O and 50%CO_2) at 600K. However, Tosti et al. noted that when CO_2 was present in the mixture, a slightly reduced CO conversion of 96.5%, compared to the 99% CO conversion for the CO_2-free mixture was attained. They attributed this reduction in CO conversion to a reduced H_2 flux through the MR as a result of the reduced H_2 partial pressure in the feed mixture, and the presence of excess CO_2 favoring the reverse WGSR.

Although the latter two MR studies attained CO conversions greater than their corresponding equilibrium values, these studies were conducted at low temperatures where the thermodynamic equilibrium favors high CO conversions. Furthermore, the issue of contaminants, such as H_2S, present in the feed mixture was not explored.

H_2S is a common contaminant present in coal-derived syngas and is a known poison of Pd-based membranes, resulting in reduced H_2 permeance (McKinley 1967; Morreale 2006), sulfidization (Morreale 2006), pitting (Kulprathipanja et al. 2005), and catastrophic rupture of the membrane within seconds of contact (Edlund et al. 1994). To

successfully integrate a MR immediately downstream of the coal gasifier for high-purity H_2 production, robust MRs capable of tolerating poisoning by contaminants such as H_2S, would have to be developed. The $Pd_{80wt\%}Cu$ membrane used in the present work was selected because it was expected to exhibit tolerance to higher concentrations of H_2S relative to the pure Pd membrane. Although studies by Morreale (Morreale 2006) showed that both Pd and $Pd_{80wt\%}Cu$ were sulfidized after exposure to 1,000 ppm H_2S-in-10%He-H_2 feed mixtures at temperatures lower than 1037K, Chapter 4 suggested that the sulfidization of Pd-based membranes is dependent on the H_2S-to-H_2 ratio associated with the thermodynamic stability of the sulfide. Further, chapter 4 showed that it is possible to operate Pd and $Pd_{80wt\%}Cu$ MRs at 1173K in the presence of H_2S-to-H_2 molar ratios below 0.0011.

Thus, the objective of this work was to investigate enhanced CO conversion via the WGSR, and high-purity H_2 recovery in Pd and $Pd_{80wt\%}Cu$ MRs using simulated, coal-derived syngas composed of 53%CO, 35%H_2 and 12% CO_2 at 1173K, in the absence and presence of varying concentrations of H_2S. This temperature was selected to be representative of a MR positioned immediately downstream of the coal gasifier. No heterogeneous catalyst particles were incorporated in the MR because it was expected that the Pd and $Pd_{80wt\%}Cu$ membrane surfaces would sufficiently catalyze the WGSR at this temperature condition. Thick-walled tubes (125 μm) were selected to facilitate the construction of robust MRs that could yield reproducible results. However, the wall thickness used in this study would not be considered viable for commercial application. Rather, this investigation was designed to be a proof-of-concept assessment of the

prospects of using Pd and $Pd_{80wt\%}Cu$ MRs at elevated temperatures to enhance CO conversions via the WGSR and produce high-purity H_2 in the presence of H_2S.

6.2 EXPERIMENTAL

6.2.1 WGS reaction in Multi-tube Pd and Pd-Cu Membrane Reactors

The four-tube MR (Figure 18) and experimental apparatus used in this study has been described previously (Chapter 3). Briefly, the 3.175 mm OD, 125-μm thick Pd and $Pd_{80wt\%}Cu$ alloy tubes used in the present study were each 15.25 cm in length. The effective surface area of the four tubes for H_2 transport was about 51.9 cm^2 and the total reactor volume was 3.5 cm^3.

The gases used were He, Ar, 1,000 ppm H_2S-10%He-balance H_2 and a simulated syngas containing 53%CO, 35%H_2 and 12%CO_2 purchased from Butler Gas Products. All gases were 99.999% certified calibration gases. He and Ar were used during heat-up of the various reactor systems to the reaction temperature of 1173K. The reactor module was heated using the three-zone heater also previously described (Chapter 3). The incorporation of three independently controlled heaters, rather than one, facilitated the establishment of a uniform temperature profile along the length of the MR (±5K). At the desired operating temperature, syngas and steam were introduced into the four-tube reactor at a flow rate of 90 sccm and 72 sccm, respectively. These flow rates resulted in a feed composition of about 29.5%CO, 19.5%H_2, 6.7%CO_2 and 44.3%H_2O. For

experiments involving H_2S, the 1,000 ppm H_2S-10%He-balance H_2 gas was introduced after steady-state CO conversion was attained at the specified condition, at a flow rate selected to result in the desired H_2S-to-H_2 ratio. As noted earlier, Chapter 4 showed that the sulfidization of Pd-based membranes is dependent on the H_2S-to-H_2 ratio. Therefore, the amounts of H_2S introduced into the Pd and $Pd_{80wt\%}Cu$ MRs were judiciously specified to be either below or above the threshold H_2S-to-H_2 ratios expected to result in membrane sulfidization, based on the H_2 concentration of the effluent retentate stream of the respective MR systems measured by GC. This addition amounted to an increase in the total flow rate of less than 6%, and was compensated for by raising the feed-side pressure accordingly.

The desired amount of steam was introduced by injecting distilled water into the flowing gas stream using a calibrated ISCO 500D syringe pump. The water was vaporized in the heated feed line before entering the reactor. Excess steam was used to prevent carbon formation in the membrane tubes. Prior control studies suggested that the 1.5 steam-to-CO ratio was adequate to suppress carbon formation in the reactor systems. A trap was placed on the exit line to collect the unreacted steam before the effluent gases were directed to a Hewlett-Packard 5890 Series II GC equipped with a 3 m long by 3.2 mm OD zeolite-packed column and thermal conductivity detector for quantification. The water trap was used to mitigate inaccurate quantification of the components in the effluent gas stream which could result from a water saturated column or films of liquid water in the flow lines. The Ar sweep gas, which was introduced in a counter current flow mode, was typically about 1,650 sccm, ensuring H_2 concentrations of less than 3% in the permeate stream. The flow rate of each gas was controlled by Brooks mass flow

controllers. The feed and permeate pressures were regulated by pneumatically-actuated stainless steel control valves. The volumetric flow-rate of the effluent stream was measured with a wet gas meter. The mass balance closure was within ±3%.

Equations (37) to (40) were used to calculate the CO conversion and the H_2 recovery from the reaction zone, while Equation (41) was used to determine the H_2 permeance of the membranes. These expressions are based on the syngas feed to the reactor which contained CO, CO_2 and H_2. The amounts/concentrations of H_2, CO and CO_2 in the reactor effluent were determined by gas chromatography. The CO conversion, X_{CO}, calculated by Equation (37) was assumed to have taken place only within the reactor. Negligible conversion occurred in the tubing leading to and from the reactor because of the steep temperature changes before and after the reaction zone. Further, the feed lines were lined with quartz inserts to minimize interaction of the reactant gases with the stainless-steel walls.

To determine the effect of residence time on CO conversion, the residence times of the reactor systems were varied by changing the operating pressure, while keeping the inlet feed flow rate and reaction temperature constant. Note that previous work conducted by Bustamante et al. (Bustamante et al. 2005) provides a rate expression for the forward WGSR based on high pressure data obtained at NETL. Increasing the reaction pressure in our experiments therefore increased the residence time, increased the H_2 partial pressure driving force for H_2 flux, and also increased the rate of reaction.

$$X_{CO} = \left(\frac{x_{CO,in} \cdot Q_{feed,in} - x_{CO,out} \cdot Q_{effluent}}{x_{CO,in} \cdot Q_{feed,in}} \right) * 100 \qquad (37)$$

$$H_{2\,\text{total}}\,(\text{sccm}) = x_{H2,in} \cdot Q_{feed,in} + 0.01 \cdot X_{CO} \cdot x_{CO,in} \cdot Q_{feed,in} \tag{38}$$

$$H_2\,\text{extracted}\,(\text{sccm}) = \frac{x_{H2,sweep}}{1 - x_{H2,sweep}} * Q_{Ar,sweep} \tag{39}$$

$$H_2\,\text{recovery}\,(\%) = \frac{H_{2\ extracted}}{H_{2\ total}} * 100 \tag{40}$$

$$J_{H2}\,(\text{mol}/(\text{m}^2 \cdot \text{s})) = k' \left(P_{ret}^{0.5} - P_{perm}^{0.5} \right) \tag{41}$$

where X_{CO} is the molar CO conversion; x_{CO} and x_{H2} are the mole fractions of CO and H_2, respectively; J_{H2} is the H_2 flux through the membrane; k' is the H_2 permeance ($\text{mol}/(\text{m}^2 \cdot \text{s} \cdot \text{Pa}^{0.5})$); P_{ret} and P_{per} are the H_2 partial pressures (Pa) in the retentate and permeate streams, respectively; Q_{feed} is the inlet syngas flow rate (sccm); $Q_{effluent}$ is the effluent retentate flow rate measured by the wet gas meter (sccm); and Q_{Ar} is the argon sweep gas flow rate (sccm).

Note that all results presented in this paper were collected during periods of complete H_2 selectivity of the MR.

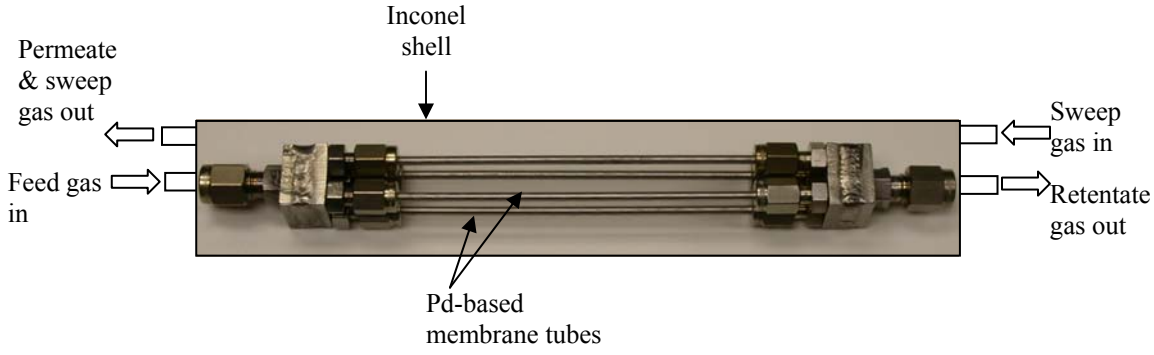

Figure 62. Detail of the NETL four-tube Pd-based membrane reactor.

6.2.2 SEM-EDS Analysis

Membrane surface morphology and compositional information following exposure to the experimental environment were obtained using a Philips XL30 FEG SEM equipped with EDS. Membranes were removed from the test assembly for characterization following testing by carefully cutting a small section of each tube using a jeweler's saw, taking care to limit surface contamination as much as possible. For inner (retentate-side) surface analysis, the sample was carefully split in half with a surgical scissors, ensuring that the sample maintained its curvature, thereby preventing the introduction of superficial surface defects resulting from tube deformation.

6.3 RESULTS AND DISCUSSION

6.3.1 H_2 Permeance

Figure **63**a and b show control experiments in which the H_2 permeance of the Pd and $Pd_{80wt\%}Cu$ MRs were calculated (Equation (41)) using single membrane tubes (3.175 cm in length) at 1173K in 90%H_2-He and 90%H_2-1,000 ppm H_2S-He environments. The figures show that steady state H_2 permeance values were attained in both MR systems within about 2 hours of the introduction of the 90%H_2-He mixture. The results indicate that the permeance of the $Pd_{80wt\%}Cu$ membrane, $1.42*10^{-4}$ mol/($m^2 \cdot s \cdot Pa^{0.5}$), was about 46% that of the pure Pd membrane ($3.10*10^{-4}$ mol/($m^2 \cdot s \cdot Pa^{0.5}$)) at 1173K. These values are in very good agreement with permeance values of $1.61*10^{-4}$ and $3.73*10^{-4}$

mol/(m^2·s·$Pa^{0.5}$) for $Pd_{80wt\%}Cu$ (Howard et al. 2004) and Pd (Morreale et al. 2003) membranes, respectively, calculated from published correlations for H_2 permeance in the open literature. **Figure 63**a and b also show that introducing H_2S to the system by switching the feed mixture to 90%H_2-1,000 ppm H_2S-He resulted in no discernable change in H_2 permeance for both membrane systems. Furthermore, **Figure 63**b shows that when the 90%H_2-1000 ppm H_2S-He mixture was reverted to the 90%H_2-He mixture (~24hrs), and subsequently reintroduced (28hrs), there was no change in H_2 permeance of the $Pd_{80wt\%}Cu$ membrane. Therefore, it was concluded that the presence of H_2S (H_2S-to-H_2 ratio ~ 0.0011) does not affect the H_2 permeance of the Pd and $Pd_{80wt\%}Cu$ membranes at 1173K.

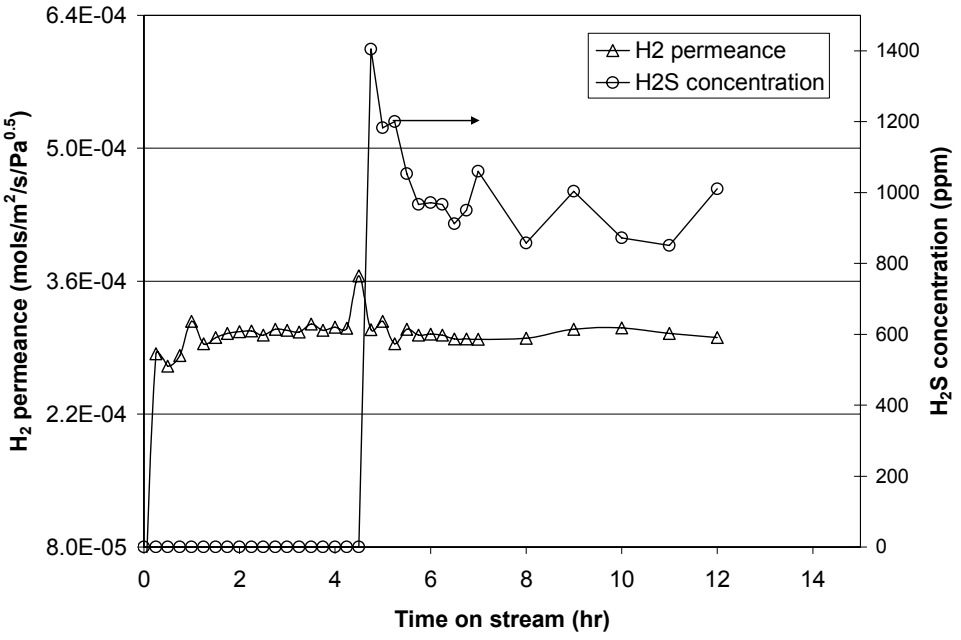

(a)

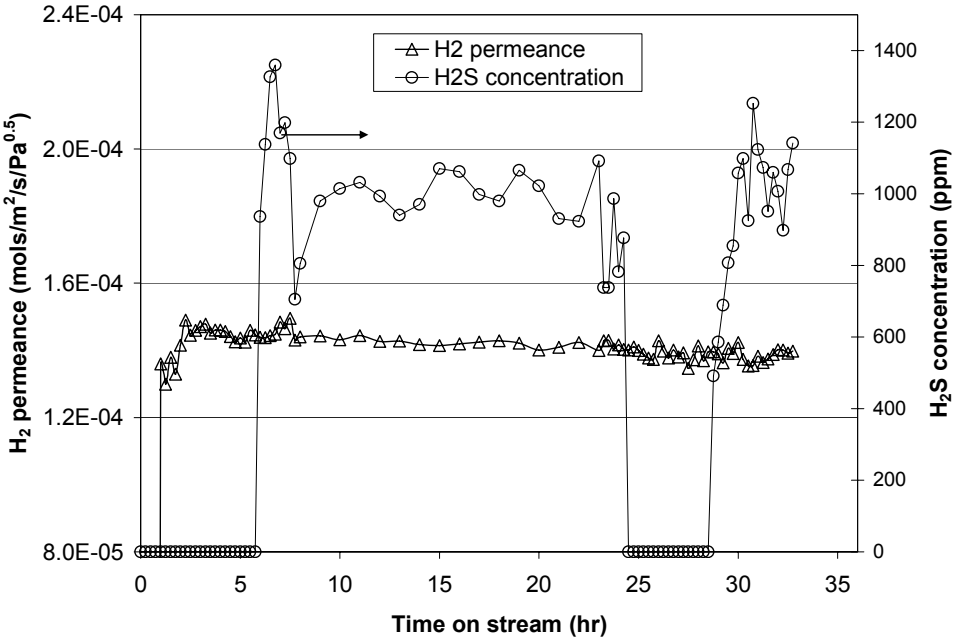

(b)

Figure 63. H_2 permeance of Pd (a) and $Pd_{80wt\%}Cu$ (b) MRs in 90%H_2-He and 90%H_2-1,000 ppm H_2S-He atmospheres at 1173K.

6.3.2 Four-tube Pd and Pd-Cu MR Testing Using Simulated, H_2S-free, Syngas Feed

Following H_2 permeance testing of the Pd and $Pd_{80wt\%}Cu$ membranes, the efficacy of the MR for enhancing the conversion of CO contained in the simulated coal-derived syngas was determined at 1173K. The WGSR was conducted using a H_2S-free, simulated syngas feed in both Pd and $Pd_{80wt\%}Cu$ four-tube MRs operated in countercurrent mode, i.e. with the reactant gases and the sweep gas flowing in opposite directions. Experiments involving H_2S are discussed in section 6.3.3. The effect of feed-side residence time on

CO conversion was investigated by varying the feed-side pressure while keeping the inlet feed flow rate and permeate side pressure of 159 kPa constant.

6.3.3.1 WGSMR in Pd MR Using Simulated, H_2S-free, Syngas Feed

Figure 64 depicts the real-time CO, CO_2 and H_2 effluent concentration trend (after condensation of steam) in the Pd MR for feed-side pressures of 143, 239 and 412 kPa which correspond to MR residence times of 0.7, 1.2 and 2s (based on inlet flow rates), respectively. The specified operating condition was maintained until steady state effluent concentrations were attained, after which the pressure was increased in order to increase the residence time. **Figure 64** illustrates increasing CO_2 concentration with increasing residence time, while CO and H_2 concentrations were observed to decrease. The decrease in CO concentration with increasing residence time was the result of increasing CO conversion via the WGSR. The decreasing H_2 concentration from approximately 9% H_2 to 5% H_2 to <0.5% H_2 was attributed to the combination of the longer residence time of reactants in the MR, the higher rate of reaction, and the higher transmembrane H_2 partial pressure differential (as a result of the higher operating pressure) resulting in higher H_2 flux through the Pd membrane. This is further substantiated by the increasing H_2 recovery observed in **Figure 65**.

Figure 65 shows the CO conversion and H_2 recovery for the four-tube Pd MR as a function of time-on-stream for residence times of 0.7, 1.2 and 2s, which correspond to feed-side pressures of 143, 239 and 412 kPa, respectively. These results demonstrate the efficacy of the MR to significantly enhance CO conversion of the equilibrium limited WGSR to nearly complete conversion (**Figure 65**), while simultaneously producing a

high-purity H_2 stream. Compared to the equilibrium CO conversion of 32% for the syngas feed mixture at these conditions, the results show about a 2, 2.4 and 3-fold enhancement of CO conversion (56.4, 75.2 & 99.7%, respectively) for increasing residence times of 0.7 to 1.2 to 2s, respectively. The shift in the CO conversion above the equilibrium value was attributed primarily to the high rate of H_2 extraction from the reaction zone through the Pd membranes. Also note that all of the CO_2 was removed in the high pressure retentate effluent stream, which also contained steam. **Figure 64** and **Figure 65** also show that the Pd MR operated in counter-current configuration is capable of nearly complete H_2 recovery if a sweep gas is used to remove the permeate.

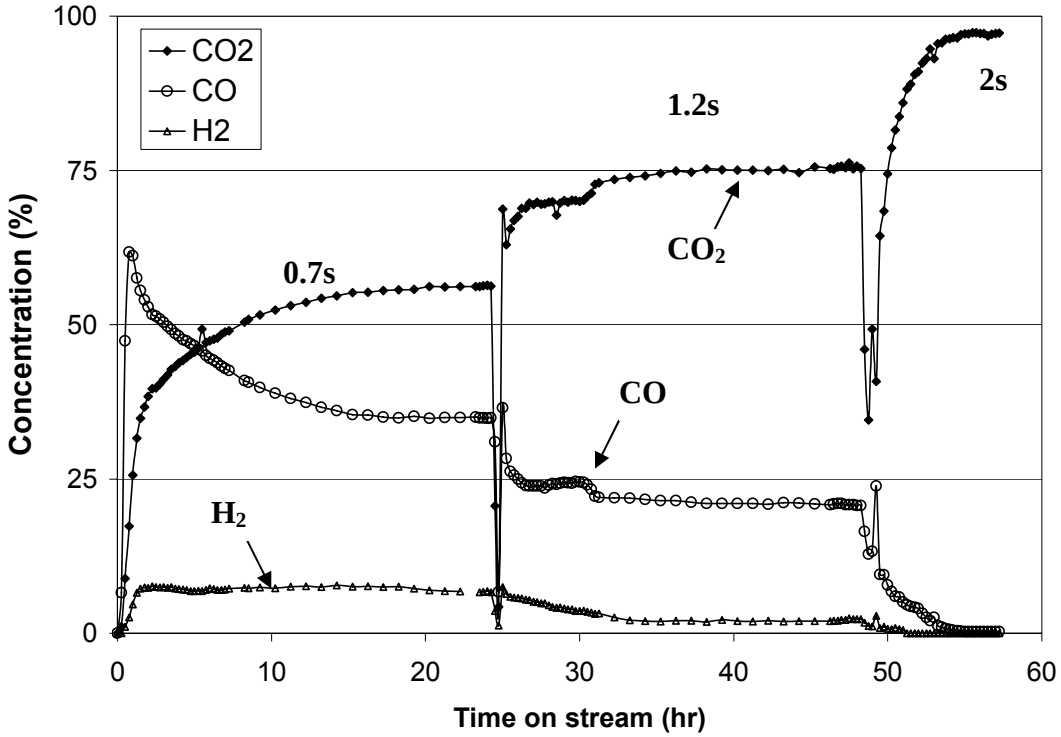

Figure 64. Real-time concentration (CO, CO_2 and H_2) trend in the four-tube Pd MR at 1173K for 0.7s, 1.2s and 2s residence times using simulated syngas feed (53%CO, 35%H_2 and 12%CO_2) and steam-to-CO ratio of 1.5**.** MR exposed to syngas environment for ~60 hours.

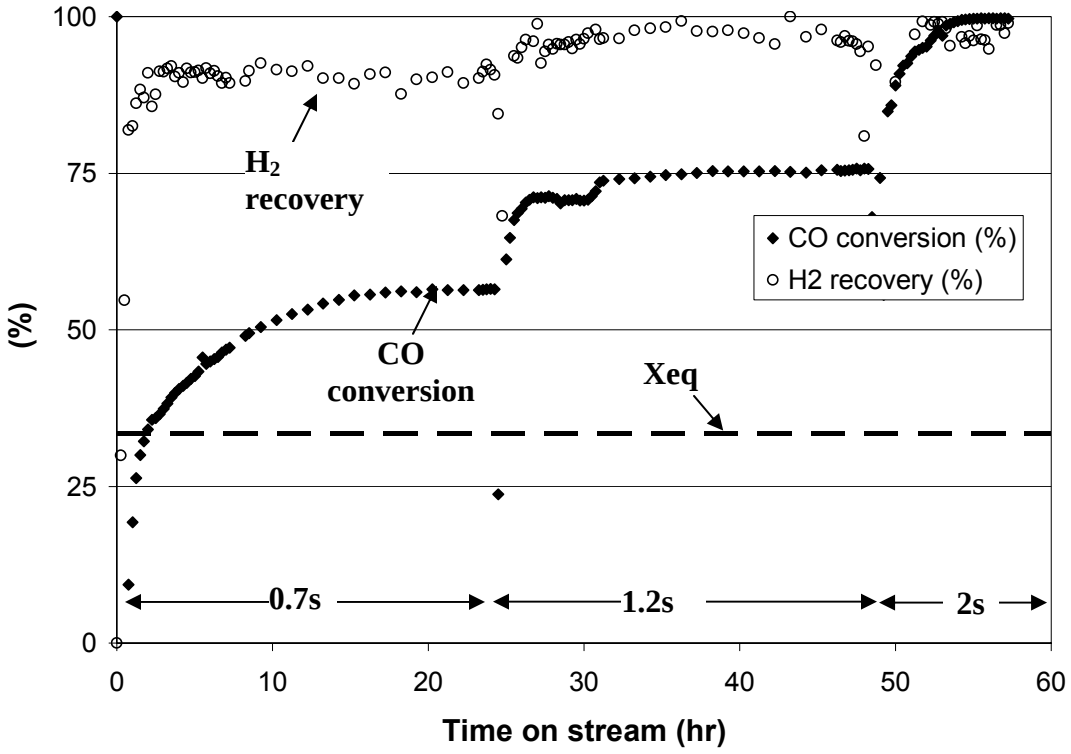

Figure 65. Real-time CO conversion and H_2 recovery trend in the four-tube Pd MR at 1173K for residence times of 0.7s, 1.2s and 2s using simulated syngas (53%CO, 35%H_2 and 12%CO_2) feed and steam-to-CO ratio of 1.5. Equilibrium CO conversion at this condition ≈ 32%. MR exposed to syngas environment for ~60 hours, and developed pinholes after about 3 days at 1173K.

6.3.3.2 WGSMR in $Pd_{80wt\%}Cu$ MRs Using Simulated, H_2S-free, Syngas Feed

Figure 66 depicts the real-time component effluent concentration trend in the $Pd_{80wt\%}Cu$ MR at 1173K for residence times of 0.96, 2 and 2.8s, corresponding to feed-side pressures of 198, 412 and 483 kPa. The figure suggests a similar trend of effluent concentrations (decreasing CO and H_2, and increasing CO_2 concentrations) and CO conversion (**Figure 65**) observed in the Pd MR system. The results also show that the

$Pd_{80wt\%}Cu$ MR effectively enhanced CO conversions above the equilibrium value of 32% over the conditions of the study. It is evident that when the Pd MR was replaced with a $Pd_{80wt\%}Cu$ MR, however, the CO_2 concentration in the retentate stream (**Figure 66**), and the level of CO conversions attained (**Figure 67**) were always lower than that of the Pd MR. Specifically, the maximum CO conversions attained in the $Pd_{80wt\%}Cu$ MR were 62% and 78% at 2 and 2.8s residence times, respectively, compared to the 99.7% CO conversion attained in the Pd MR at 2s residence time. This phenomenon had been previously observed for WGSMR involving pure CO and steam reactant gases at a similar temperature (Chapter 3), and was primarily attributed to the lower H_2 permeance of the $Pd_{80wt\%}Cu$ membrane relative to Pd at this temperature. Further, **Figure 67** also shows that the H_2 recovery of the $Pd_{80wt\%}Cu$ MR, 75%, was lower than the H_2 recovery in the Pd MR, nearly 100%, at a feed-side pressure of 412 kPa corresponding to a residence time of 2s.

With regards to the longevity of the membrane, the $Pd_{80wt\%}Cu$ MR was successfully operated for about 6 days in the WGSR environment without experiencing failure. The Pd MR lasted 3 days under comparable conditions before pinhole defects formed. This suggests that alloying Pd with Cu may result in a more robust MR that can better withstand the harsh, high-temperature operating conditions of the post-gasifier environment (H_2S-free).

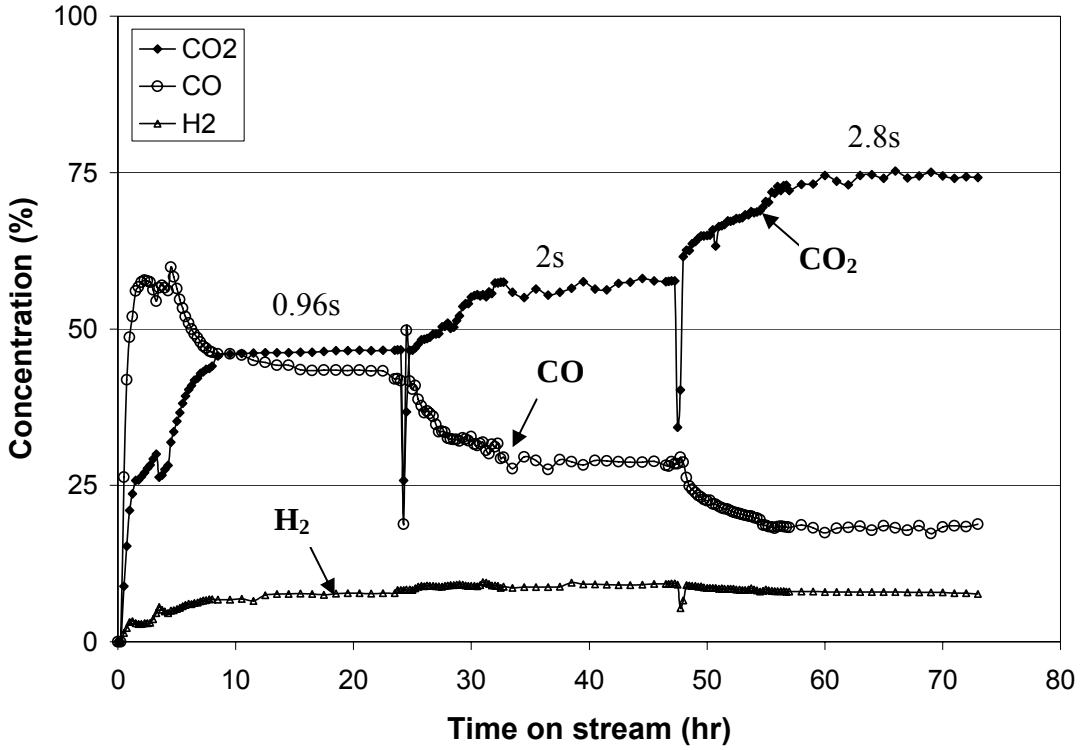

Figure 66. Real-time concentration (CO, CO_2 and H_2) trend in the four-tube $Pd_{80wt\%}Cu$ MR at 1173K for 0.96, 2 and 2.8s residence times using simulated syngas feed (53%CO, 35%H_2 and 12%CO_2) and steam-to-CO ratio of 1.5. MR operated for about 6 days without failure.

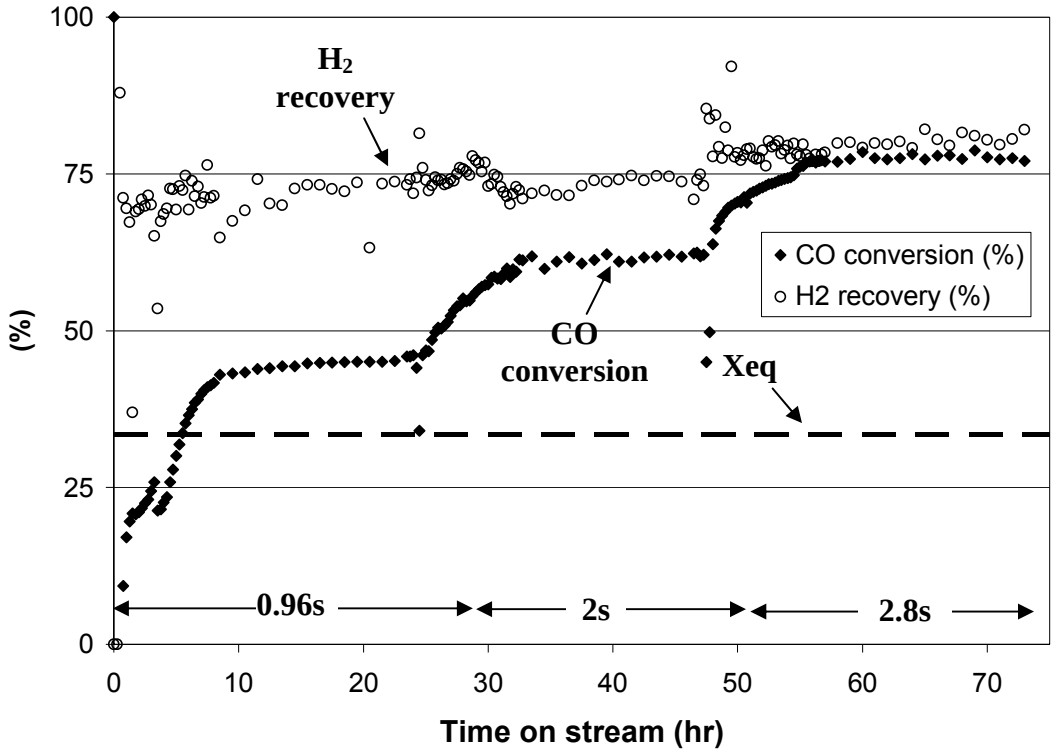

Figure 67. Real-time CO conversion and H_2 recovery trend in the four-tube $Pd_{80wt\%}Cu$ MR at 1173K for residence times of 0.96, 2 and 2.8s using simulated syngas (53%CO, 35%H_2 and 12%CO_2) feed and steam-to-CO ratio of 1.5. Equilibrium CO conversion at this condition ≈ 32%. The $Pd_{80wt\%}Cu$ MR was successfully operated for about 6 days without failure.

6.3.3.3 SEM-EDS Analysis of Pd MR

Figure 68a and b show SEM-EDS analysis results for the Pd MR after exposure to the syngas environment at 1173K for about 60hrs. The SEM image (**Figure 68**a) revealed 100 - 200 μm Pd grains on the membrane surface. Moderate pinhole formation was also apparent along the grain boundaries. (These pinholes apparently penetrated the membrane and compromised its selectivity after about 3 days of operation, as evidenced

by the appearance of CO and CO_2 in the permeate at that time). Control experiments (images not shown) suggest that the formation of pinholes is caused and/or accelerated by the WGSR environment, as exposure of Pd and $Pd_{80wt\%}Cu$ MRs to 90%H_2-He environments for about 6 days resulted in relatively smooth membrane surfaces, with no apparent surface pits. EDS analysis (**Figure 68**b) of this Pd membrane after the WGSR experiments did not indicate that oxides or surface impurities were present. Carbon peaks observed in all EDS images are the result of exposing the samples to the atmosphere.

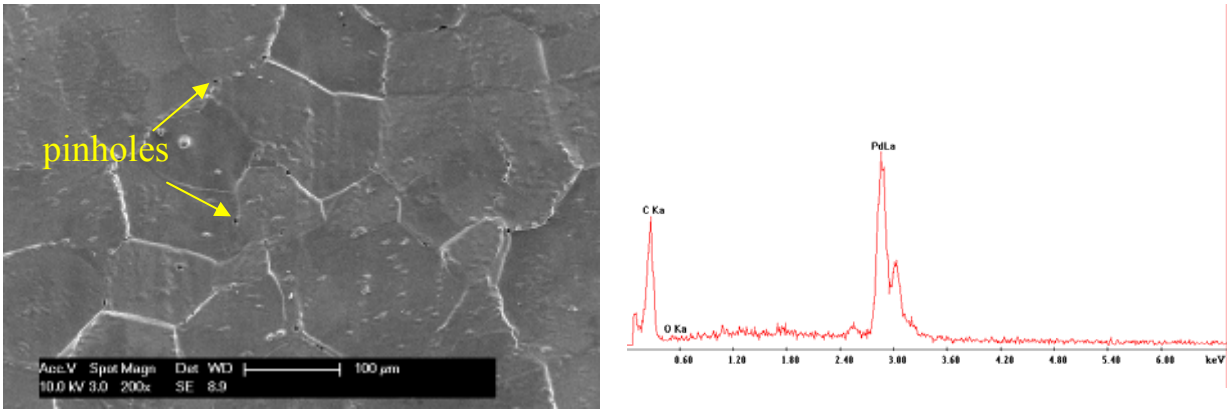

(a) (b)

Figure 68. SEM (a) and EDS (b) images of inner (retentate) surface of Pd MR after 3 days of WGSR with H_2S-free syngas feed at 1173K depicting large grains and moderate pitting on membrane surface.

6.3.3.4 SEM-EDS Analysis of $Pd_{80wt\%}Cu$ MR

Figure 69a and b show SEM-EDS analysis results for the $Pd_{80wt\%}Cu$ MR after exposure to the syngas environment at 1173K for about 6 days. The SEM image (**Figure 69**a) revealed a relatively smooth membrane surface with generally smaller grains, about

50 µm wide, compared to the Pd MR. EDS analysis of the surface (**Figure 69**b) detected no impurity or oxide presence. Unlike the Pd MR which was observed to exhibit pinhole formation along the grain boundaries, negligible pinhole formation was detected on the membrane surface. Furthermore, in contrast to the Pd MR tubes which became quite malleable after testing at 1173K and typically collapsed with the application of minimal pressure, the $Pd_{80wt\%}Cu$ MR remained rigid after similar reaction testing. The ability of the $Pd_{80wt\%}Cu$ MR to retain its structural integrity for relatively longer periods of time compared to the pure Pd membrane further supports the conjecture that even though alloying Pd with Cu may reduce H_2 permeance, the alloy may be a more mechanically resilient membrane material for high temperature MR construction and use.

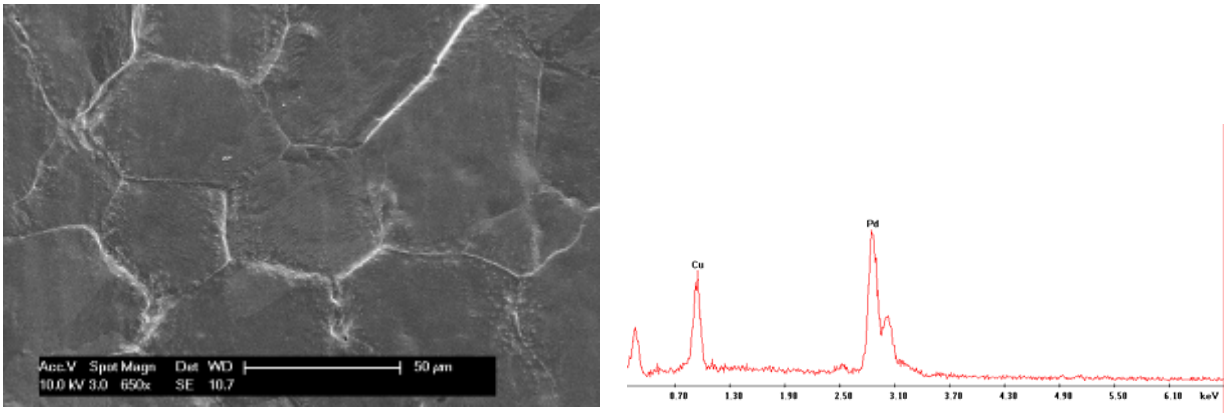

(a) (b)

Figure 69. SEM (a) and EDS (b) images of inner (retentate) surface of $Pd_{80wt\%}Cu$ MR after 6 days of WGSR with H_2S-free syngas feed at 1173K depicting relatively smooth membrane surface.

6.3.3 Four-tube Pd and $Pd_{80wt\%}Cu$ MR Using Simulated Syngas Feed Containing H_2S

The WGSR was also conducted in Pd and $Pd_{80wt\%}Cu$ MRs in the presence of varying concentrations of H_2S. The amounts of H_2S introduced to the Pd and $Pd_{80wt\%}Cu$ MRs were specified to either be below or above the threshold H_2S-to-H_2 ratios expected to result in membrane sulfidization, based on the H_2 concentration in the effluent retentate stream of the respective MR systems.

6.3.3.1 WGSR in Pd MR Using Simulated Syngas Feed Containing H_2S

For experiments involving H_2S, the desired amount of H_2S was introduced by co-feeding the 1,000 ppm H_2S-He-H_2 with the syngas. The slight increase in total feed flow rate (less-than 6%) was compensated for by increasing the retentate pressure to achieve the same residence time. When the H_2S flow rate was controlled such that the H_2S-to-H_2 ratio remained below the equilibrium ratio expected for stable Pd_4S formation (i.e. 0.0014 at 1173K for Pd (Taylor 1985; Chapter 4), a precipitous drop in CO conversion was observed. **Figure 70** illustrates the real-time CO conversion and H_2 recovery trend for the Pd MR in the absence and presence of 30 ppm H_2S at a residence time of 0.4s. With a H_2 effluent concentration of 10 mol% before the H_2S introduction (**Figure 71** (18hrs)), the introduced H_2S concentrations of 30 ppm to the Pd MR resulted in H_2S-to-H_2 ratios of about 0.0003 (equivalent to about 300 ppm H_2S-in-pure H_2) at the reactor exit. It is evident in **Figure 70** that after a steady state conversion of about 49% CO conversion was attained, introducing 30 ppm H_2S resulted in the immediate decrease in CO

conversion, reaching a new steady-state value of about 12% after approximately 3 hours. This reduction in CO conversion is also observed in the data depicted in **Figure 71** which shows the real-time component concentration trend for the Pd MR exposed to the syngas mixture.

When the H_2S was introduced along with the syngas (~19hrs), a rapid reduction in CO_2 concentration, accompanied by the increase in CO concentration was observed, probably due to the deactivation of the catalytic activity of the Pd membrane towards the WGSR. H_2 concentration in the retentate stream was also observed to decrease from about 10% to 3.5%. As expected (control experiments shown in **Figure 63**a and b resulted in no discernable influence of H_2S on H_2 permeance), this catalyst deactivation phenomenon did not appear to impact H_2 transport through the MR, and no decrease in H_2 recovery was observed. Furthermore, when the H_2S was switched off (39hr, **Figure 70**), the CO conversion was observed to recover to about 83% of its original conversion. This corroborates the assertion that the decrease in CO conversion observed was not the result of sulfidization of the MR, but deactivation of the catalytic Pd walls towards the WGSR. In addition, the MR was observed to maintain its mechanical integrity and H_2 selectivity for the duration of the 30 ppm H_2S-syngas testing period.

When the H_2S concentration was increased to 50 ppm (68hrs), the MR failed within minutes, as evidenced by a rupture in one of the four membrane tubes. The failure of the MR was probably the result of the sulfidization of the MR due to the presence of a H_2S-to-H_2 ratio of greater than 0.0014. At the time of the 50 ppm H_2S introduction to the MR, the effluent H_2 concentration of about 3.5% (**Figure 71** (68hrs)) resulted in a H_2S-to-H_2 ratio of approximately 0.00145 at the exit of the MR. This value is slightly above

the minimum H_2S-to-H_2 ratio that is expected to result in sulfidization of Pd at 1173K (Chapter 4). It was therefore not surprising that the MR failed.

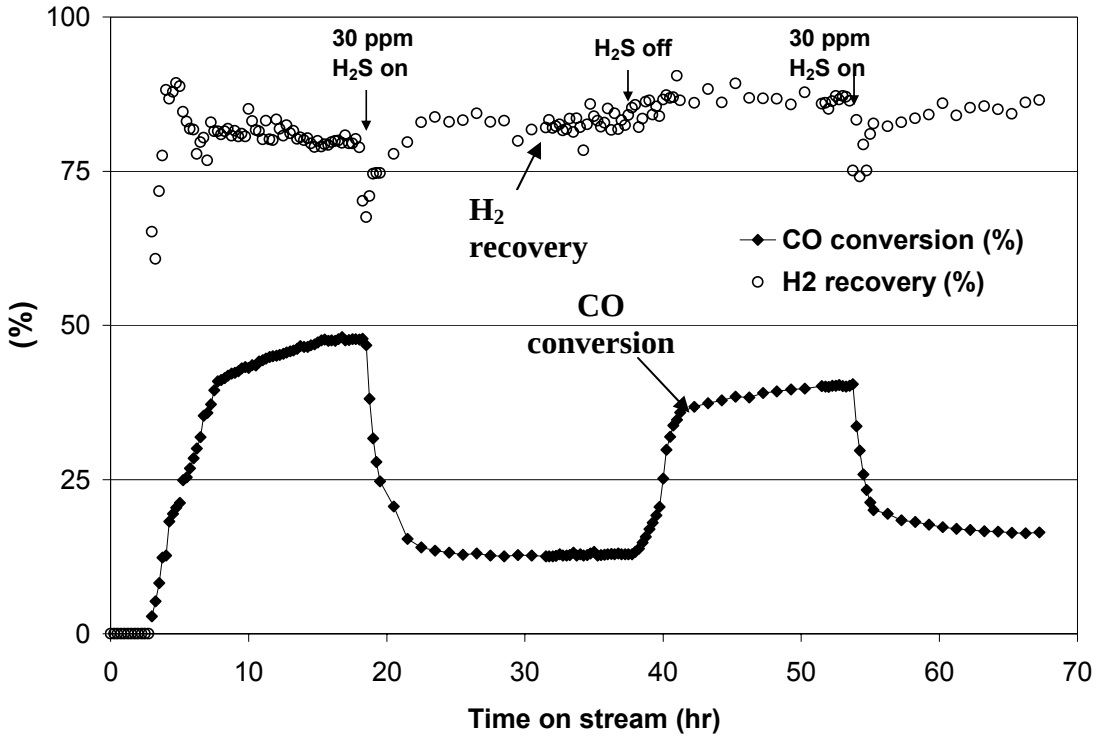

Figure 70. Real-time CO conversion and H_2 recovery trend in the four-tube Pd MR at 1173K for residence times of 0.4s before and after reaction testing with 30 ppm H_2S-syngas. Membrane failed within minutes of exposure to 50 ppm H_2S that began at 68hrs.

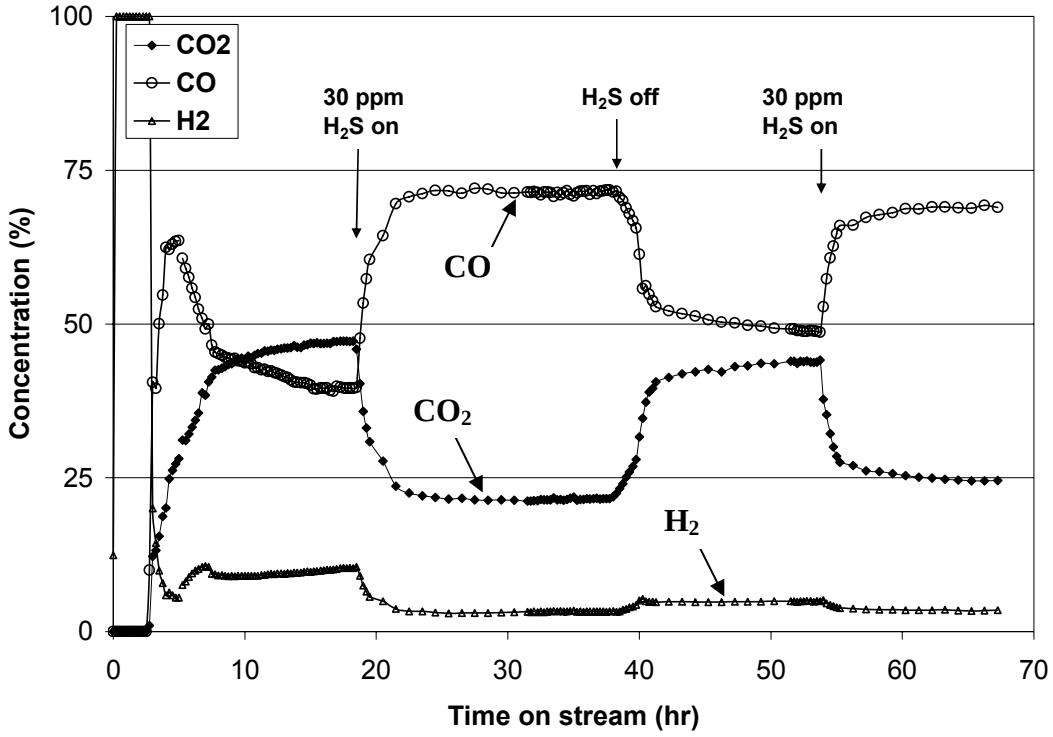

Figure 71. Real-time concentration (CO, CO_2 and H_2) trend for the four-tube Pd MR at 1173K and 0.4s residence time before and after reaction testing with 30 ppm H_2S-syngas. Membrane failed within minutes of exposure to 50 ppm H_2S that began at 68hrs.

6.3.3.2 WGS in $Pd_{80wt\%}Cu$ MR Using Simulated Syngas Feed Containing H_2S

Figure 72 depicts CO conversion and H_2 recovery for the $Pd_{80wt\%}Cu$ at 2s residence time in the presence and absence of H_2S, after flowing a 90%H_2-He mixture in the MR for the first 27 hours. In the absence of H_2S (27 to ~51hrs), the CO conversion and H_2 recovery were both observed to reach steady state values of about 67%. Similar to the Pd MR, when 40 ppm H_2S was introduced to the MR, a rapid reduction in CO

conversion was observed, decreasing from 67% to a steady state value of ~16%, within 3 hours of introduction. However, in contrast to the Pd MR which experienced no change in H_2 recovery when H_2S was introduced, the H_2 recovery in the $Pd_{80wt\%}Cu$ MR was observed to decrease slightly from about 68% to a new steady-state value of approximately 56% (**Figure 72**). **Figure 72** also shows that when the H_2S was switched off, CO conversion did not recover to its original level within the 10-hour period. In fact, only a modest increase to about 30% conversion was observed. Increasing the H_2S concentration to 60 ppm (77hrs) decreased the CO conversion from 30% back to about 16%.

Figure 73 shows the real-time effluent concentration data for the $Pd_{80wt\%}Cu$ MRs exposed to the syngas mixture containing 40 and 60 ppm H_2S. Similar to the Pd MR system, when the H_2S was introduced (~49hrs), a rapid reduction of CO_2 concentration, accompanied by the increase in CO concentration was observed. Assuming no change in H_2 concentration measured in the effluent retentate stream (~12% H_2 between 40 & 50 hr (Figure 73)), the introduced 40 ppm H_2S resulted in a H_2S-to-H_2 ratio of approximately 0.0004 (equivalent to ~400 ppm H_2S-in-H_2). When the 60 ppm H_2 was introduced after about 77 hours, the H_2 concentration was observed to decrease to about 10% (Figure 73 (85 hr)), resulting in a H_2S-to-H_2 ratio of approximately 0.0006 (equivalent to ~600 ppm H_2S-in-H_2). These ratios were below the H_2S-to-H_2 ratios expected to sulfidize the $Pd_{80wt\%}Cu$ membrane (Chapter 4), therefore it is no surprise that the membrane maintained its H_2 selectivity and mechanical integrity.

Control experiments shown in **Figure 63**a and b suggest no influence of the H_2S on H_2 permeance of both MRs. This observation, coupled with the fact that the H_2

recovery was observed to only be slightly reduced in the presence of H_2S, support the supposition that the observed reduction of CO conversion experienced by the MR when H_2S was introduced with the syngas mixture likely resulted from the blocking of catalytic surface sites for the WGSR by sulfur. The presence of adsorbed sulfur on the membrane surface may impede the transfer of WGS reactants from the bulk to the membrane catalytic surface, appreciably reducing the catalytic activity of the MR for the WGSR. It is uncertain, however, why the CO conversion did not increase more appreciably in the $Pd_{80wt\%}Cu$ system after the H_2S was turned off.

When the inlet H_2S concentration was increased to 90 ppm H_2S for the $Pd_{80wt\%}Cu$ MR system, the MR module failed within minutes, resulting in the complete loss of membrane selectivity and the depressurization of the reactor. With a steady-state H_2 effluent concentration of about 8% before the H_2S introduction (100 hrs, figure not shown), introducing 90 ppm H_2S to the syngas feed resulted in a H_2S-to-H_2 ratio of about 0.0012 (~1,200 ppm H_2S-in-H_2), a value just below the H_2S-to-H_2 ratio expected to sulfidize the membrane. However, note that further reduction of CO conversion, due to increased deactivation of the catalytic membrane by the higher H_2S concentration, would have resulted in a lower H_2 concentration as less H_2 is produced. This process may have resulted in a much higher H_2S-to-H_2 ratio (i.e. >0.002), which would explain the observed failure of the MR.

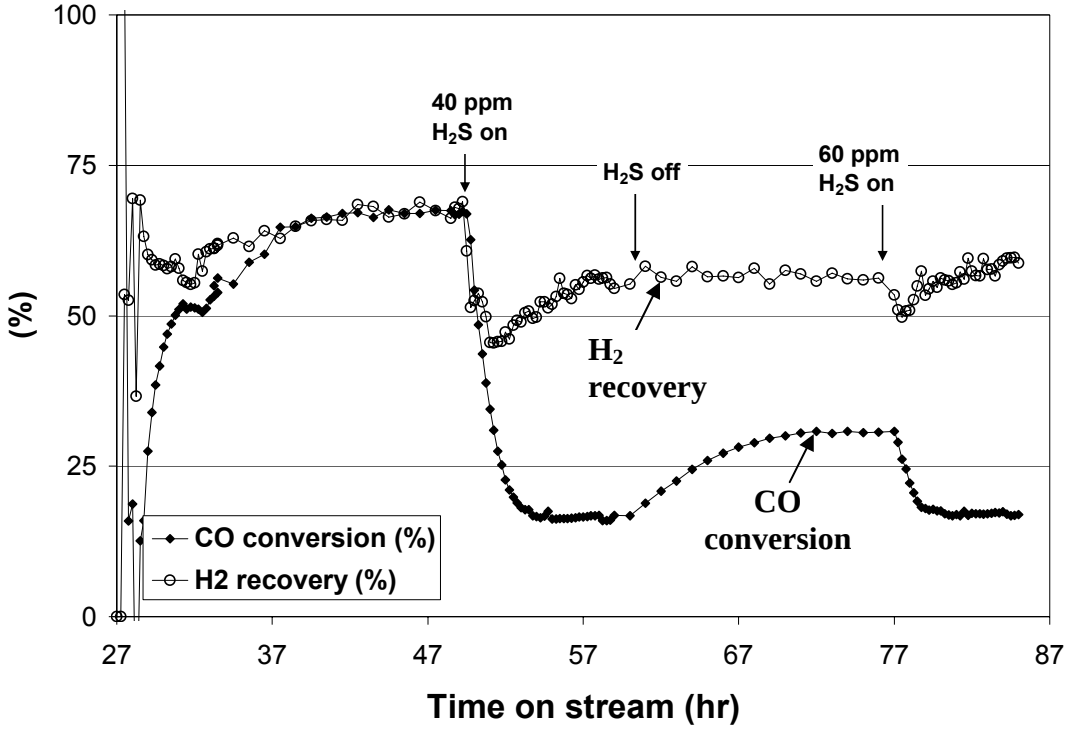

Figure 72. Real-time CO conversion trend and H_2 recovery in the four-tube $Pd_{80wt\%}Cu$ MR at 1173K and residence time of 2s before and after 40 and 60 ppm H_2S-syngas reaction testing. Membrane failed after exposure to 90 ppm H_2S.

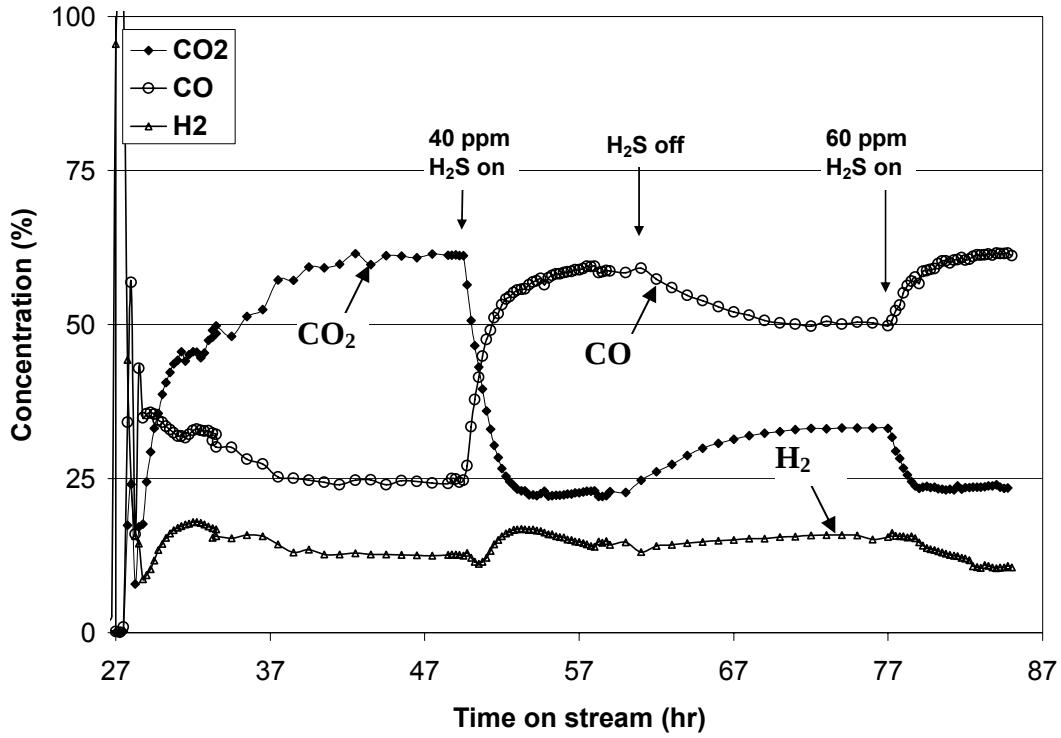

Figure 73. Real-time concentration (CO, CO_2 and H_2) trend for the four-tube $Pd_{80wt\%}Cu$ MR at 1173K and 2s residence time before and after 40 and 60 ppm H_2S-syngas reaction testing. Membrane failed after exposure to 90 ppm H_2S.

6.3.3.3 SEM-EDS Analyses of Pd MRs After H_2S-containing Syngas Exposure

SEM and EDS analyses of the Pd MR after exposure to H_2S-containing syngas are shown in **Figure 74** to **Figure 77**. **Figure 74**a to c show SEM-EDS images of the failed Pd MR tube after introduction of 50 ppm H_2S with the syngas feed. As noted earlier, the MR was observed to fail within minutes of increasing the inlet H_2S concentration to 50 ppm. **Figure 74**a and b show the inner and outer surface of the failed region of the Pd MR, respectively. No apparent surface modifications (i.e. pits or

crevices) that are attributable to reactant gas exposure are evident. Furthermore, EDS analysis of this region (**Figure 74**c) showed no detectable sulfur.

The fracture appears to follow the grain boundaries (**Figure 74**a and b), suggesting that the sulfur preferentially attacks and weakens the membrane along the grain boundaries. SEM images of the fracture faces are shown in **Figure 75**a and b. **Figure 75**b is a magnification view of a grain boundary. EDS analysis of this region detected sulfur only within the grain boundary groove (**Figure 75**c), while no sulfur was detected in areas removed from the grain boundary (**Figure 75**d). This phenomenon has been previously observed for Fe exposed to H_2S environment (Ainslie et al. 1960). In the aforementioned study, exposure of the polycrystalline Fe to H_2S resulted in sulfur preferentially diffusing to the grain boundaries. Ainslie et al. suggested that exposure of the metal to the sulfur environment results in more rapid diffusion of sulfur along the grain boundary than through the bulk of the grains. This process results in a much higher sulfur concentration at the grain boundary region, compared to elsewhere on the metal sample, ultimately resulting in grain boundary embrittlement (Grabke 2006). Therefore, the tendency of sulfur to preferentially adsorb at the grain boundary of the Pd membrane in this study compromised the mechanical integrity of the MR by resulting in grain boundary embrittlement, as evidenced by the clean fracture of the Pd MR along the grain boundary.

Figure 76 and **Figure 77** show SEM-EDS images of the inlet and outlet regions of the ruptured Pd MR tube, respectively. **Figure 76**a reveals a relatively smooth surface at the inlet region, while the outlet region (**Figure 77**a) was observed to be moderately

pitted. EDS analysis of the inlet (**Figure 76**b) and outlet (**Figure 77**b) regions detected no sulfur presence on the membrane surface.

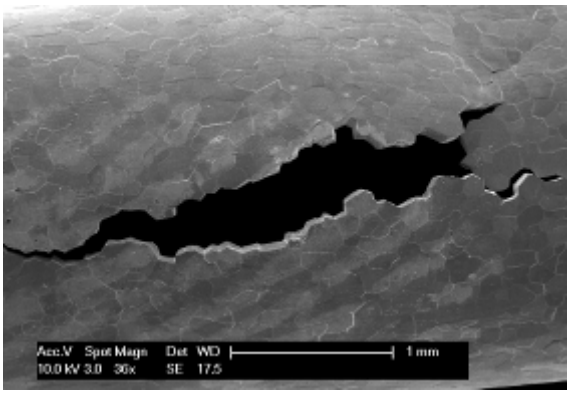

(a)

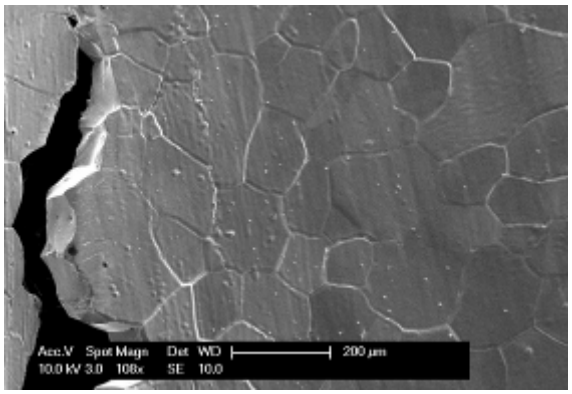

(b)

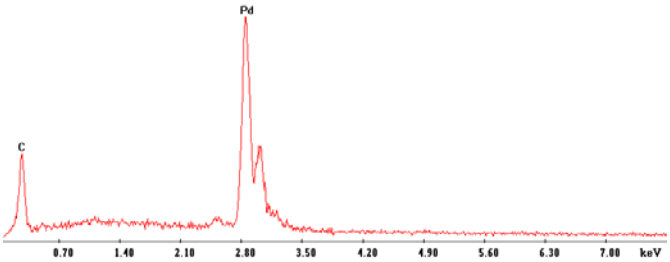

(c)

Figure 74. SEM-EDS images of ruptured Pd MR tube depicting the outer (permeate) surface (a), the inner (retentate) surface (b) of the Pd MR after 3 days of WGSR with H_2S-containing syngas feed at 1173K and 0.5s residence time. EDS analysis (c) of the inner surface of the ruptured region shown in (b) revealed negligible sulfide presence.

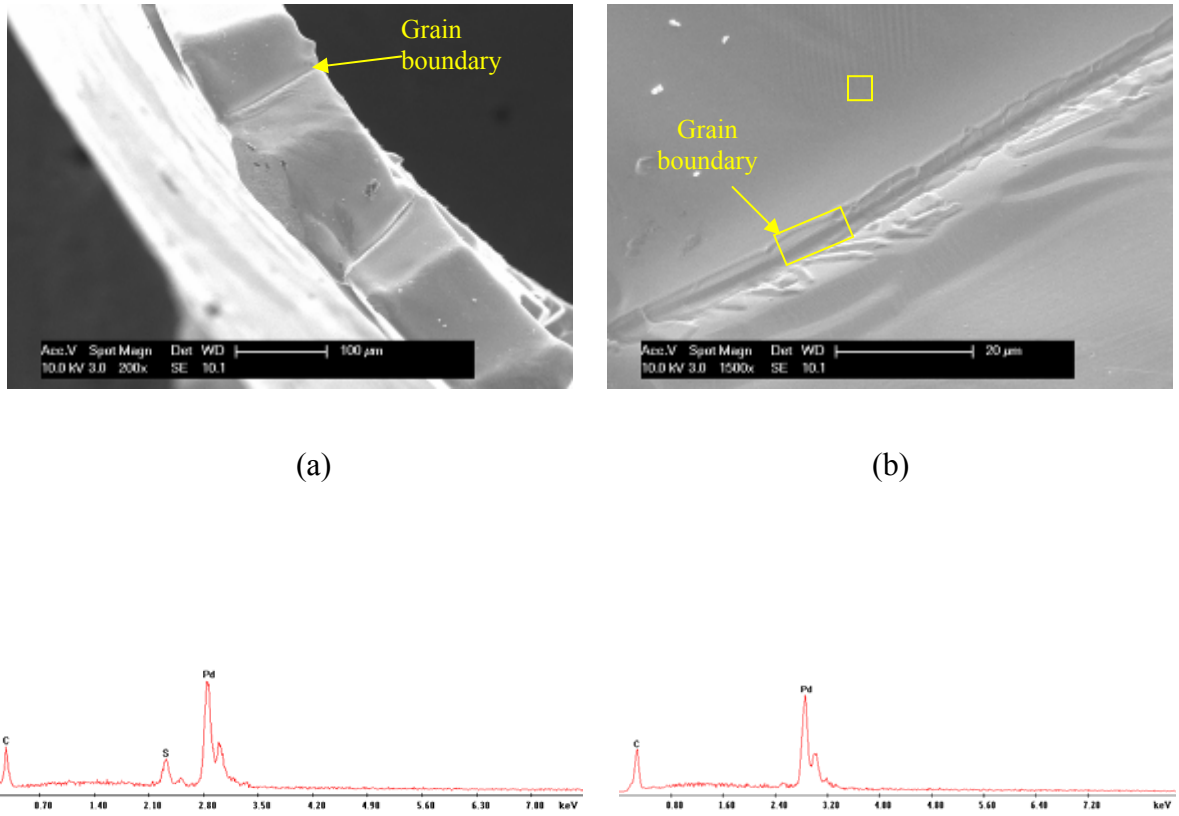

(a) (b)

(c) (d)

Figure 75. SEM-EDS images of fracture faces of ruptured Pd MR tube (a) after 3 days of WGSR with H_2S-containing syngas feed at 1173K and 0.5s residence time. EDS analysis of the magnified grain boundary region (b) detected sulfur within of the grain boundary groove (c), while no sulfur was detected in areas removed from the grain boundary (d).

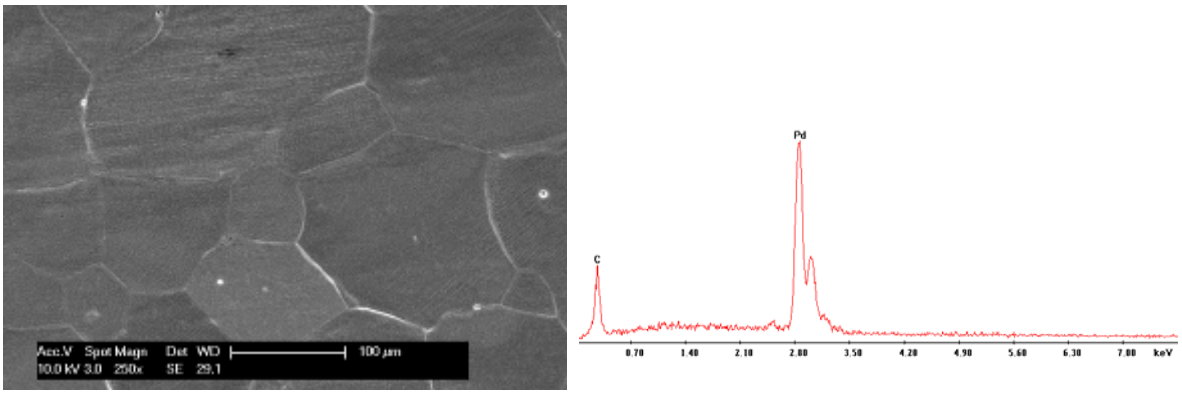

(a) (b)

Figure 76. SEM (a) and EDS (b) inner (retentate) surface image of inlet region of Pd MR after 3 days of WGSR with H_2S-containing syngas feed at 1173K depicting relatively smooth surface and negligible sulfide presence, respectively.

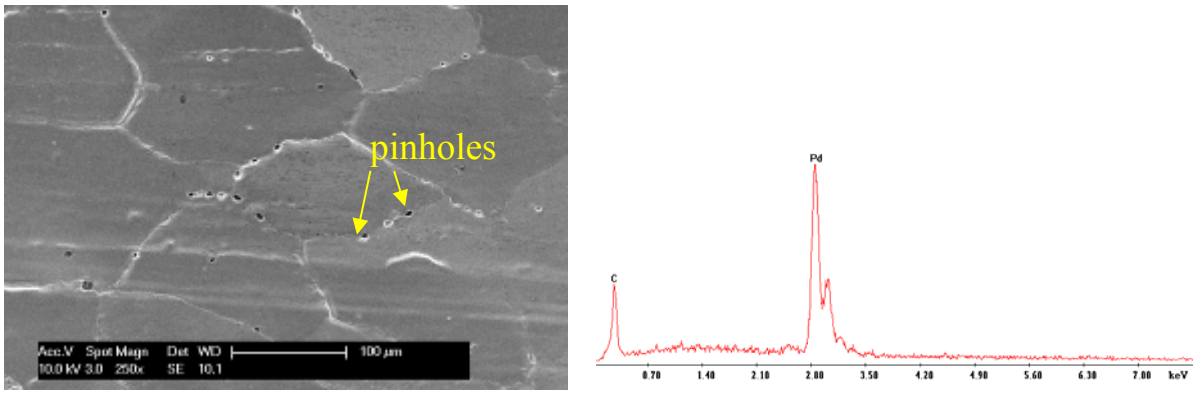

(a) (b)

Figure 77. SEM (a) and EDS (b) inner (retentate) surface analysis of outlet region of Pd MR after 3 days of WGSR with H_2S-containing syngas feed at 1173K depicting pitted surface and negligible sulfide presence, respectively.

6.3.3.4 SEM-EDS Analyses of $Pd_{80wt\%}Cu$ MRs After H_2S-containing Syngas Exposure

Figure 78 to **Figure 81** show SEM and EDS analyses of various regions of the $Pd_{80wt\%}Cu$ MR after WGS reaction testing for a total of about 6 days. **Figure 78** shows images of the inlet region of the ruptured $Pd_{80wt\%}Cu$ MR, an depicts a relatively smooth surface (**Figure 78**a) with significantly smaller grains (on the order of 10 μm wide) than those observed on the Pd MR sample. EDS analysis of this region (**Figure 78**b) revealed no sulfur presence on the membrane sample. However, in stark contrast to the relatively smooth inlet region of the MR, SEM analysis of the middle of the tube where failure occurred (~30 mm from the reactor inlet) (**Figure 79**a) revealed a significantly modified surface. Increased magnification of this region (**Figure 79**b) revealed an appreciably roughened surface with apparent valleys and nodules on the membrane surface. The markedly different surface observed in **Figure 79**a and b compared to the $Pd_{80wt\%}Cu$ surface in **Figure 69** may be attributed to the presence of sulfur in the gas mixture. The presence of sulfur at the membrane surface is known to decrease the metal surface energy, thereby stabilizing and accelerating the growth of defects (i.e. pits)(Grabke 2006) which, in this case, were influenced by the WGSR environment. Similar to the Pd membrane surface, EDS analysis of this region, however, showed no detectable sulfide (**Figure 79**c).

Figure 80a and b show SEM-EDS analysis of the fractured faces of the $Pd_{80wt\%}Cu$ MR. Similar to the Pd membrane, the $Pd_{80wt\%}Cu$ MR was also observed to preferentially fracture along the grain boundary. EDS analysis of this region, however, did not detect any sulfur. It is possible that the amount of sulfur present at the smaller grain boundaries

of the $Pd_{80wt\%}Cu$ membrane was significantly less than the sulfur present at grain boundaries of the larger Pd grains, since sulfur in known to segregate to much lesser extents to grain boundaries of smaller grains (Ainslie et al. 1960). Therefore, the low sulfur signal, if any, may have been below the detection limit of the SEM.

The outlet region of the $Pd_{80wt\%}Cu$ MR was also observed to be severely pitted at the exit region (**Figure 81**). The contrast between the exit region of the $Pd_{80wt\%}Cu$ MR (**Figure 81**a) compared to that of the Pd MR (**Figure 77**a) may be the result of the higher H_2S concentration of the syngas in the $Pd_{80wt\%}Cu$ MR and the presence of Cu in the alloy. An earlier study by Kulprathipanja et al. (Kulprathipanja et al. 2005) observed a similar pitting phenomenon when $Pd_{80wt\%}Cu$ membranes were exposed to a mixture of 30%H_2O-40%H_2-100 ppm H_2S-balance N_2 mixture at 723K. Kulprathipanja et al. observed the formation of micron sized pores in the membrane within 3 minutes, and attributed this to the presence of steam in the gas mixture enhancing H_2S dissociation to form S^{2-} which reacts more readily with Pd and Cu, than H_2S molecules.

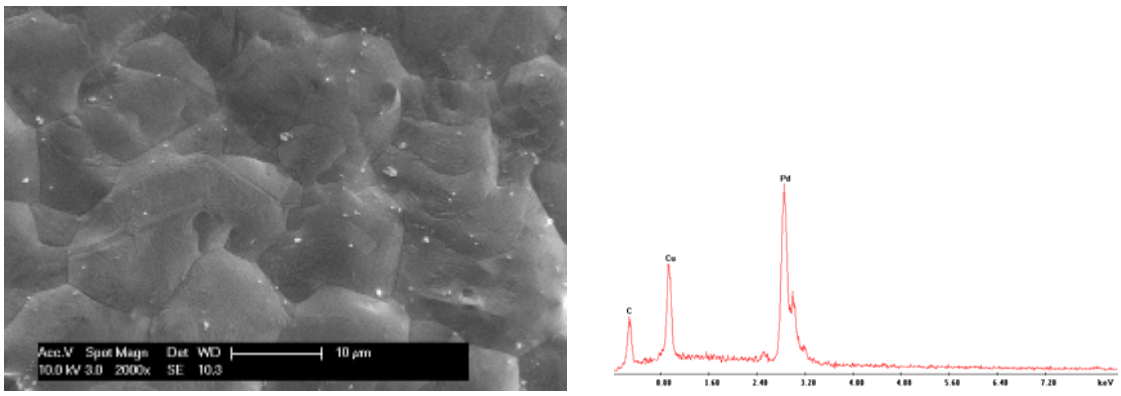

(a) (b)

Figure 78. SEM (a) and EDS (b) inner (retentate) surface image of inlet region of $Pd_{80wt\%}Cu$ MR after 6 days of WGSR with H_2S-containing syngas feed at 1173K depicting relatively smooth surface and negligible sulfide presence, respectively.

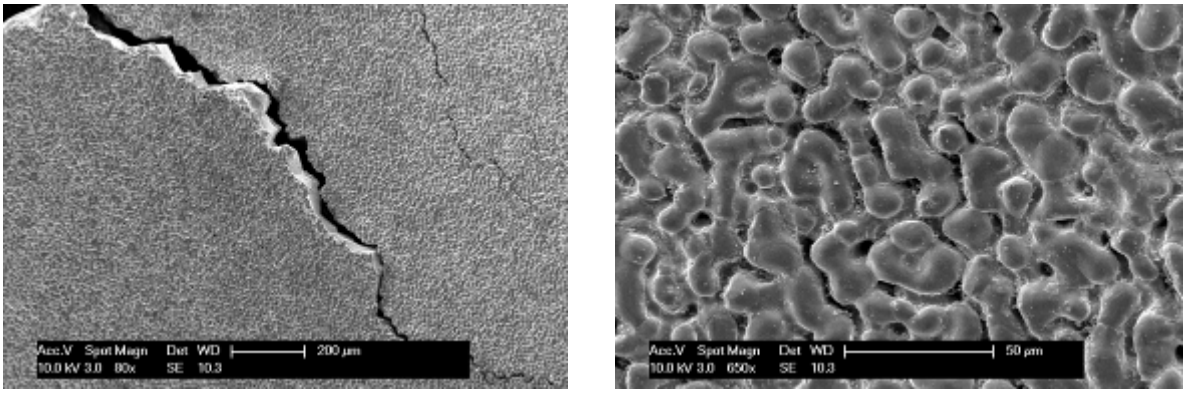

(a) (b)

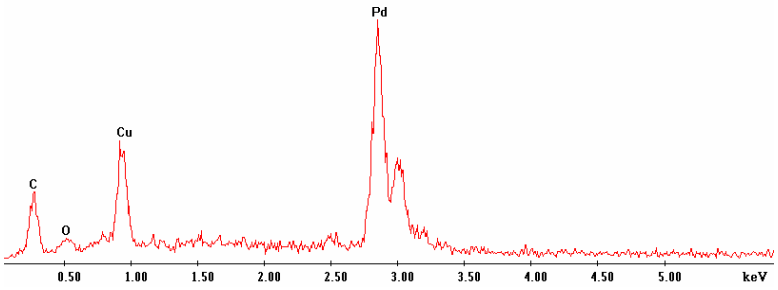

(c)

Figure 79. SEM-EDS images of inner (retentate) surface analysis of the ruptured $Pd_{80wt\%}Cu$ MR where failure occurred after exposure to 90 ppm H_2S-containing syngas feed, after 6 days of testing at 1173K depicting cracked surface (a). A magnified section of surface (b) revealed a highly modified surface. EDS analysis of the surface did not detect any sulfur presence (c).

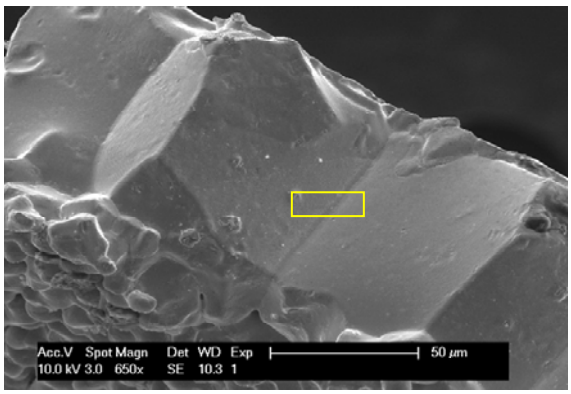

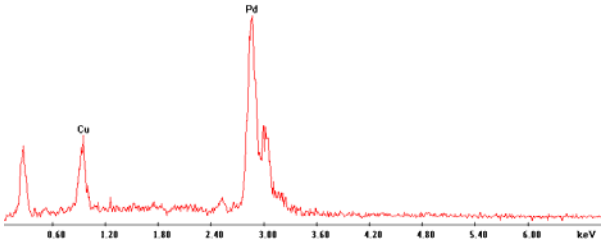

(a) (b)

Figure 80. SEM-EDS images of fracture faces (a) of ruptured $Pd_{80wt\%}Cu$ MR where failure occurred after exposure to 90 ppm H_2S-containing syngas feed, after 6 days of testing at 1173K. EDS analysis (b) detected no sulfur presence.

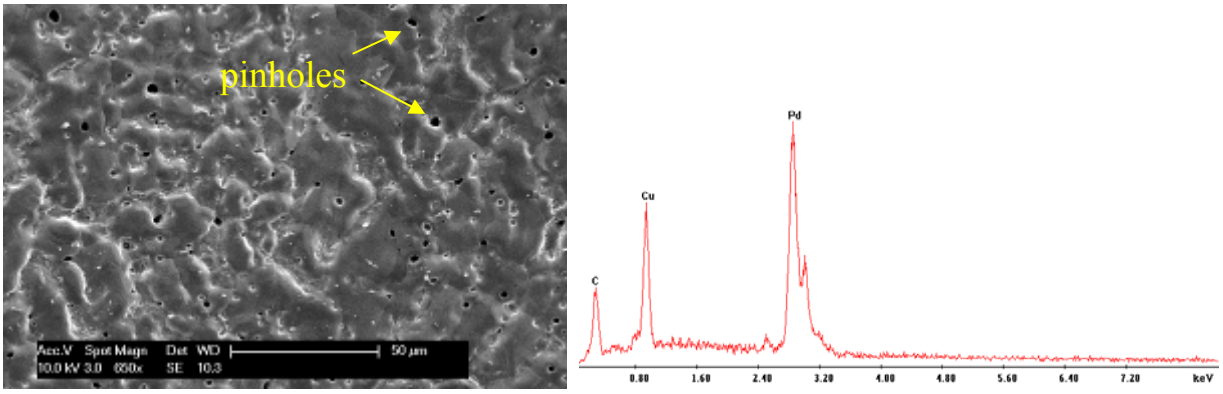

(a) (b)

Figure 81. SEM (a) and EDS (b) inner (retentate) surface analysis of outlet region of the ruptured $Pd_{80wt\%}Cu$ MR after 7 days of WGSR with H_2S-containing syngas feed at 1173K depicting severely pitted surface and negligible sulfide presence, respectively.

6.4 CONCLUSION

99.7% conversion of CO contained in a simulated syngas feed consisting of 53%CO, 35%H_2 and 12%CO_2 (dry basis) was attained in a 125-μm Pd four-tube membrane reactor at 1173K with a steam-to-CO ratio of 1.5 and 2s residence time. Furthermore, nearly complete H_2 recovery was also attained through the Pd membrane reactor module.

The $Pd_{80wt\%}Cu$ membrane reactor also effectively enhanced CO conversions above the equilibrium value of 32% (associated with non-membrane reactors) over the conditions of the study. However, the maximum conversions attained were appreciably lower than those obtained in the Pd membrane reactor, reaching maximum CO

conversions of 62% and 78% at 2 and 2.8s residence times, respectively. This was primarily attributed to the lower H_2 membrane permeance compared to that of Pd. The H_2 recovery was also observed to always be lower for the $Pd_{80wt\%}Cu$ MR.

Exposure of both membrane reactors to syngas mixtures containing H_2S levels such that the H_2S-to-H_2 ratio was less than ~0.0011 (a value less than the 0.0014 value expected to form stable sulfides at 1173K) did not appear to affect the H_2 permeance, mechanical integrity, and H_2 selectivity of the membrane reactors at 1173K. However, a steep drop in CO conversion was observed. This reduction in CO conversion was attributed to sulfur deactivating the catalytic activity of the Pd membrane surface towards the WGSR (Control experiments with H_2S-to-H_2 ratio of 0.001 at this same conditions demonstrated that there was no loss in H_2 permeance). When the H_2S-to-H_2 feed ratio was increased to 50 and 90 ppm H_2S for the Pd and $Pd_{80wt\%}Cu$ membrane reactor systems equivalent to 0.0014 and 0.0012 H_2S-to-H_2 ratios, respectively (values equal to or just below ratios expected for stable sulfides to form), the membrane reactors were observed to fail within minutes.

SEM-EDS analysis of the membrane reactors after H_2S-containing syngas exposure showed no presence of a sulfide layer on the membrane surfaces. The Pd membrane, however, exhibited sulfur presence within the fractured grain boundary groove. This suggests that the sulfur preferentially attacks the grain boundary location, compromising the mechanical integrity of the membrane reactor by resulting in grain boundary embrittlement.

In summary, our results show that at high temperatures, with no added catalyst particles, it is possible to enhance CO conversions significantly above the equilibrium

value and attain high H_2 recovery from simulated syngas in the absence of H_2S. The results also show that it is possible to stably operate (with respect to H_2 selectivity, H_2 permeance, and mechanical integrity) the Pd and $Pd_{80wt\%}Cu$ MRs in the presence of H_2S-to-H_2 ratios below 0.0011. However, the deactivation of the catalytic activity of the Pd and $Pd_{80wt\%}Cu$ membranes towards the WGSR by the H_2S will reduce CO conversions when H_2S is present in the feed.

7.0 CHAPTER SEVEN: SUMMARY & RECOMMENDATIONS

7.1 INTRODUCTION

In this final chapter, a summary of the main innovations obtained in the studies presented in this thesis will be given. Recommendations for future research will also be provided.

7.2 SUMMARY OF MEMBRANE REACTOR PROJECT

The main objective of this thesis was to evaluate the efficacy of Pd and $Pd_{80wt\%}Cu$ membrane reactors for enhanced CO conversion via the water-gas shift reaction, and simultaneous high-purity H_2 recovery through the selective membrane walls, in the absence and presence of H_2S. This work was conducted at 1173K to be representative of a membrane reactor placed immediately downstream of a coal gasifier to produce high-purity H_2 from coal-derived syngas.

This thesis shows that is possible to attain CO conversions significantly higher than the equilibrium value in catalyst free, Pd and $Pd_{80wt\%}Cu$ membrane reactors, while simultaneously producing a high-purity H_2 stream, and removing the produced CO_2 at

high pressure. This enhancement is attributed to the synergy between the rapid rate of H_2 extraction from the reaction zone by the H_2 selective Pd and $Pd_{80wt\%}Cu$ membranes, the modest inherent catalytic activity of the membrane reactors for enhancing the WGSR, and the high rate of WGSR at the elevated operating temperature.

In an attempt to understand how H_2S contamination present in coal-derived syngas would affect membrane reactor performance, the mechanism of H_2S sulfidization of Pd-based membrane reactors was studied from a thermodynamic and experimental approach. This work shows that sulfidization of Pd-based membranes is based on the activity of the elements in the alloy and the H_2S-to-H_2 ratio, not merely the inlet H_2S concentration. Results at 1173K showed that both Pd and $Pd_{80wt\%}Cu$ membrane reactors retained their mechanical integrity in the presence of 0.0011 H_2S-to-H_2 ratios (equivalent to 1,000 ppm H_2S-10%He-H_2 mixture), in agreement with thermodynamic analysis which suggested that the Pd and $Pd_{80wt\%}Cu$ membrane reactors should not form stable sulfides when exposed to H_2S-to-H_2 ratios below 0.0014 (equivalent to 1,400 ppm H_2S-in-H_2 mixture) at 1173K. Furthermore, control experiments showed negligible H_2 permeance losses at 1173K when Pd and $Pd_{80wt\%}Cu$ membranes were exposed to a feed mixture with a H_2S-to-H_2 ratio of about 0.0011.

. A COMSOL Multiphysics model developed to analyze and predict membrane reactor performance accurately reproduced experimental results. Simulations suggest that the CO conversion could be further increased at short residence times if bona fide WGS catalysts are used in the reactor. Also, increasing the H_2 permeance of the membrane was shown to result in increased CO conversion. This model was used to predict the performance of a Pd membrane reactor for H_2 generation and separation from a syngas

mixture containing H_2S. The model showed that at the conditions of interest, the Pd membrane reactors would be stable in the presence of syngas mixtures containing about 10 ppm H_2S. The simulations also show that possible deactivation of the catalytic membrane surface by H_2S would, however, affect the rate of H_2 production, resulting in an elevated H_2S-to-H_2 ratios which may result in membrane reactor failure at conditions which otherwise would be innocuous to the membrane reactors.

Finally, the efficacy of the membrane reactor for H_2 generation and separation from simulated coal-derived syngas in a post gasifier environment was evaluated in the absence and presence of H_2S. Results indicate that both membrane reactor systems significantly enhanced CO conversions above the equilibrium value of 32%. Specifically, the Pd membrane reactor was observed to result in CO conversion and H_2 recovery greater than 98%, while the $Pd_{80wt\%}Cu$ membrane reactor resulted in CO conversion and H_2 recovery of about 76% at 3 seconds residence time. However, when H_2S was introduced along with the syngas in both reactor systems, a precipitous reduction in CO conversion was observed. This decrease in conversion was attributed to deactivation of the catalytic Pd walls by the H_2S. Further, the results suggest that when the H_2S concentration in the reactor was controlled such that the H_2S-to-H_2 ratio remained below the equilibrium value of ~0.0014 required to sulfidize Pd at 1173K, the membrane reactors were observed to maintain their structural integrity and H_2 selectivity. When the ratio increased above this value, however, both membrane reactors were observed to fail within minutes, as evidenced by a rupture of a membrane tube in each system.

7.3 RECOMMENDATIONS

From work presented in this thesis, it is clear that integration of membrane reactors to the coal gasification process appears to be a promising technology to enhance simultaneous H_2 production and separation from coal-derived syngas. However, the success of this technology is dependent on the future developments of the membrane materials. For example, a major limitation of the membrane reactors in this study was their susceptibility to loss of H_2 selectivity after exposure to the water-gas shift environment for a few days. As a result, further research should be directed towards improving the stability of the membrane reactors in the WGSR environment. Specifically, the mechanism of pitting of the Pd-based membranes in the presence of the WGS atmosphere at high temperatures would have to be understood to develop more robust alloys for high-temperature WGSMR application.

Additionally, to successfully integrate the membrane reactor down stream of the coal gasifier, membranes capable of tolerating higher H_2S-to-H_2 ratios compared to the Pd and $Pd_{80wt\%}Cu$ membrane reactors presented in this study will have to be developed. Ternary Pd-based membranes containing Pd and either Au, Pt or Ag should be investigated. The latter three metals were recommended as a result of them being more noble metals compared to Pd, hence, they require appreciably higher H_2S-to-H_2 partial pressure ratios to form stable sulfides. Ternary alloys are proposed because of the potential to further reduce the activity of each component in the alloy, thereby further increasing the sulfur tolerance of the alloy.

Advances in membrane materials which exhibit tolerance to higher H_2S-to-H_2 ratios may allow the successful operation of MRs at conditions explored in this thesis.

Although experiments in the presence of H_2S resulted in appreciable decreases in CO conversion due to the deactivation of the catalytic membrane surface, this phenomenon may be circumvented by utilizing bona fide, sulfur-tolerant WGSR catalysts, i.e Co-Mo/Al_2O_3.

Simulation results presented in this thesis suggest that increasing the membrane H_2 permeance may further enhance CO conversions at shorter residence times. In light of this, it may be worthwhile investigating the catalyst free, WGSR at elevated temperatures (i.e. 1173K) in membrane reactors constructed from alloys such as Pd-Ag and Pd-Y which exhibit higher H_2 permeance values relative to pure Pd.

The COMSOL model developed in this work used a modified version of the gas-phase water-gas shift reaction to describe the catalytic effect of the Pd walls on the WGSR. To accurately model and predict membrane reactor performance at conditions of interest, detailed rate expressions for the WGSR over Pd and $Pd_{80wt\%}Cu$ membranes should be developed.

Pd alloys containing small amounts of boron (i.e. ~0.1 – 0.5%) should be investigated to mitigate the embrittlement fracture phenomenon observed for the Pd and $Pd_{80wt\%}Cu$ membrane reactors exposed to the syngas-H_2S environment. Unlike sulfur impurities which severely degrades mechanical properties of metallic alloys at the grain boundary, boron segregation to the grain boundary has been observed to result in a strengthening effect across the grain boundary (Krasko 1997; Grabke 2006). This is because boron in the grain boundary has a very low energy, and thus would tend to displace other impurity atoms which may result in grain boundary embrittlement (i.e. sulfur) from the grain boundary region (Krasko 1997).

APPENDIX A

COMSOL MULTIPHYSICS MEMBRANE REACTOR MODELING

Start by setting up the mass balance for species in the system (i.e. CO, H_2, CO_2, H_2O, H_2S and He). Note that an extra species (He) was added in this model to compensate for the unwanted influx of the N-1 (last species added to mass balance) species which results when H_2 is extracted from the reaction zone. This phenomenon is as a result of the intrinsic formulation of the Maxwell-Stefan application mode which solves the mass balances for each component except the last component which is calculated by taking the fact that

$$\sum_i \omega_i = 1$$

The mass balance is coupled to the momentum balance using the Non-isothermal Flow application mode which accounts for variation of gas density as a result of the loss of H_2 from the reactor. This leads to a reduction in the flow rate of the gas mixture as the reaction proceeds along the length of the membrane reactor.

The reactor parameters and component inputs used in the simulation are listed in the Tables below.

Membrane H_2 permeance and inlet mass fraction compositions used in the simulations

Case	per ($mol/m^2/s/Pa^{0.5}$)	ωCO	ωH_2O	ωCO_2	ωH_2	ωH_2S
Case 1 (CO+steam)	$1.5*10^{-5}$	0.491	0.519	-	-	-
Case 2 (syngas+steam)	$4.4*10^{-5}$	0.4278	0.4125	0.1395	0.0202	-
Case 3 (syngas+steam+H_2S)	$4.4*10^{-5}$	0.4278	0.4125	0.1394823	0.0202	$1.77*10^{-5}$

Retentate pressures used in the simulations

P ($*10^5$Pa)	τ (s)
2.70355	0.7
3.1509	0.82
4.45737	1.16
7.01197	1.81
7.74802	2.0
11.5625	3.0
19.1467	4.96

MODELING IN COMSOL MULTIPHYSICS

1. Start COMSOL Multiphysics.
2. Click the **Multiphysics** button in the **Model Navigator**.
3. In the **Space dimension** list select **Axial symmetry (2D)**.
4. In the dialog box below Space dimension, double-click the **Chemical Engineering Module** folder to expand it
5. **Select Chemical Engineering Module>Momentum balance> Non-isothermal Flow** from the list of application modes.
6. Click the **Multiphysics** button.
7. Click the **Add** button.
8. Select the application mode **Chemical Engineering Module>Mass balance>Maxwell-Stefan Diffusion and Convection.**

9. In the Dependent variables field, enter the species **wCO wH2O wH2 wCO2 wH2S wHe**, making sure to insert them in this order, with a space between each component.
10. Click the **Add** button**.**
11. Click **OK**.

REACTOR GEOMETRY MODELING

1. Click on the **Rectangle/Square** button while pressing the **shift** button. Type in the values in the table below in the corresponding fields.

Object Dimension	Expression
Width	0.0014625
Height	0.130175

2. Click **OK**.
3. Double-click on the **Equal** tab on the bottom of the screen.
4. Click the **Zoom Extends** button on the main toolbar to expand the model.

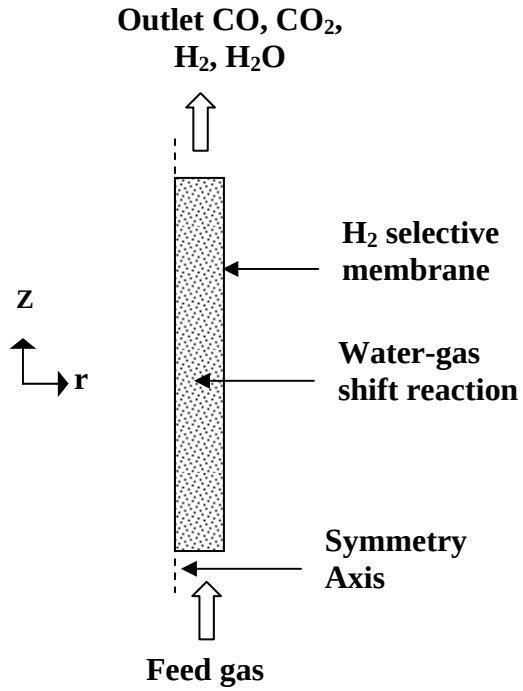

Figure 50. Geometry of membrane reactor depicting modeled domain.

OPTIONS AND SETTINGS

1. Define the reactor model constants in Options menu (**options>Constants**) according to the table below. Variables listed as inputs are given in Tables 9 and 10 in Chapter 5 (reproduced above).

Name	Expression	Description
T	1173	Reactor temperature (K)
P	*Input* (variable to specify residence time)	Reactor Pressure (Pa)
P_atm	1.01e5	Atmospheric pressure
R	8.314	Universal gas constant
velo	V2/A/4	Gas inlet superficial velocity entering one of four tubes
A	6.72e-6	Reactor tube cross sectional area (m^2)
V1	3.33e-6	Inlet gas vol. flow rate at STP (m^3/s) based on 200

Name	Expression	Description
		sccm total reactant flow
V2	V1*T*P_atm/273/P	Inlet gas vol. flow rate at reaction T & P (m^3/s)
k	0.002093	Forward WGS reaction rate constant ($((m^3/mol)^{0.5}s^{-1})$)
Keq	0.65	WGSR equilibrium constant at 1173K
wH2O_in	*Input*	Mass fraction of feed H2O
wCO_in	*Input*	Mass fraction of feed CO
wH2_in	*Input*	Mass fraction of feed H_2
wCO2_in	*Input*	Mass fraction of feed CO2
wH2S_in	*Input*	Mass fraction of feed H2S
wHe_in	1-(wH2_in+wH2O_in+wCO_in+wCO2_in+wH2S_in)	Mass fraction of feed He
M_H2	2e-3	Molecular weight of H_2 (mol/Kg)
M_H2O	18e-3	Molecular weight of H_2O (mol/Kg)
M_CO	28e-3	Molecular weight of CO (mol/Kg)
M_CO2	44e-3	Molecular weight of CO_2 (mol/Kg)
M_H2S	34e-3	Molecular weight of H_2S (mol/Kg)
M_He	100	Arbitrary weight used to prevent influx of unwanted species
W_tot	wH2O_in*M_H2O+wH2_in*M_H2+wCO_in*M_CO +wCO2_in*M_CO2+wH2S_in*M_H2S+(1-wH2O_in-wCO_in-wCO2_in-wH2_in-wH2S_in) *M_He	Total mass flow into reactor
m_H2_in	wH2_in*W_tot/M_H2	inlet H_2 molar flow rate
m_H2O_in	wH2O_in*W_tot/M_H2O	inlet H_2O molar flow rate
m_CO_in	wCO_in*W_tot/M_CO	inlet CO molar flow rate
m_CO2_in	wCO2_in*W_tot/M_CO2	inlet CO_2 molar flow rate
m_He_in	(1-wH2O_in-wH2_in-wCO_in-wCO2_in-wH2S_in)*W_tot/M_He	inlet He molar flow rate
m_H2S_in	wH2S_in*W_tot/M_H2S	inlet H_2S molar flow rate
m_tot	m_H2_in+m_H2O_in+m_CO_in+m_CO2_in+m_H2S_in+m_He_in	Total molar flow rate
x_H2O	m_H2O_in/m_tot	Inlet H_2O mole fraction
x_CO	m_CO_in/m_tot	Inlet CO mole fraction
x_CO2	m_CO2_in/m_tot	Inlet CO_2 mole fraction
x_H2	m_H2_in/m_tot	Inlet H_2 mole fraction
x_He	m_He_in/m_tot	Inlet He mole fraction
x_H2S	m_H2S_in/m_tot	Inlet H_2S mole fraction
x_tot	x_H2O+x_CO+x_CO2+x_H2+x_H2S	Total mole fraction
F	50	Correction factor used to

Name	Expression	Description
		reproduce experimental results
Per	*Input*	Membrane H_2 permeance ($mol/m^2/s/Pa^{0.5}$)
W	Per*R^0.5*T^0.5	R & T used to convert H2 partial pressure in H2 flux calculation to concentration (i.e. P=C*R*T)
eta_H2	2.31e-5	Viscosity of H_2 (Kg/(m·s))
eta_CO	4.44e-5	Viscosity of CO (Kg/(m·s))
eta_CO2	4.47e-5	Viscosity of CO_2 (Kg/(m·s))
eta_H2S	4.10e-5	Viscosity of H_2S (Kg/(m·s))
eta_H2O	4.44e-5	Viscosity of H_2O (Kg/(m·s))
eta_He	4.5e-5	Viscosity of He (Kg/(m·s))

SCALAR EXPRESSIONS

1. Define the scalar expressions in the scalar expressions dialogue box by selecting **Options>Expressions>scalar Expressions** from the **Options** menu:

Name	Expression	Description
cCO2	x_wCO2_chms*P/R/T	Concentration of CO_2
cCO	x_wCO_chms*P/R/T	Concentration of CO
cH2	x_wH2_chms*P/R/T	Concentration of H_2
cH2O	x_wH2O_chms*P/R/T	Concentration of H_2O
cH2S	x_wH2S_chms*P/R/T	Concentration of H_2S
cHe	x_wHe_chms*P/R/T	Concentration of He
rho_mix	M_CO*cCO+M_H2O*cH2O+M_H2*cH2+M_CO2*cCO2+M_He *cHe+M_H2S*cH2S	Mixture density
rCO	F*k*((cCO>0.001)*cCO)^0.5*cH2O*(1-B)	WGS reaction rate expression

Name	Expression	Description
B	(cCO2*cH2)/(cCO*cH2O*Keq)	Approach to equilibrium
eta_mix	x_wCO_chms*eta_CO+x_wCO2_chms*eta_CO2+x_wH2_chms*eta_H2+ x_wH2O_chms*eta_H2O+x_wH2S_chms*eta_H2S+x_wHe_chms*eta_He	Mixture viscosity
xH2	x_wH2_chms	H_2 mole fraction
xH2O	x_wH2O_chms	H_2O mole fraction
xCO2	x_wCO2_chms	CO_2 mole fraction
xCO	x_wCO_chms	CO mole fraction
xHe	x_wHe_chms	He mole fraction
xH2S	x_wH2S_chms	H_2S mole fraction
X	(x_CO*velo-xCO*U_chns)/x_CO/velo*100	CO conversion
H2S_H2	xH2S/xH2	H_2S-to-H_2 partial pressure ratio
V_n	U_chns/velo	Normalized velocity
X2	(xCO2-x_CO2)/(xCO+xCO2-x_CO2)*100	CO conversion based on mole fractions

2. Click **OK**.

PHYSICS SETTINGS – NON-ISOTHERMAL FLOW

1. Select the **Non-Isothermal Flow** application mode from the **Multiphysics** menu.
2. Select **Subdomain** settings from the **Physics** menu.
3. In the **Subdomain** selection list select **1**.
4. Make sure the **Active in this domain** box is checked.
5. In the **Density** edit field enter rho_mix.
6. In the **dynamic viscosity** edit field enter eta_mix.
7. Click the **Init** tab.

8. In the **pressure** edit field enter P_atm.
9. Click **OK**.

PHYSICS SETTINGS – MAXWELL-STEFAN

1. Select the **Maxwell-Stefan Diffusion and Convection** application mode from the **Multiphysics** menu.
2. Select **Subdomain Settings** from the **Physics** menu.
3. Highlight **1** in the **Subdomain** selection list.
4. Enter **rho_mix**, **P** and **T** in the **density**, **pressure** and **temperature** edit fields, respectively.
5. Enter **u** and **v** in the **r-velocity** and **z-velocity** edit fields, respectively.
6. Click the **Edit** button for the **Maxwell-Stefan Diffusivity matrix**.
7. Enter 2e-5 in all the edit fields.

Note that this constrains the interdiffusivity coefficients of the various species in this model to the value $2*10^{-5}$. This was done to mitigate the rapid diffusion of H_2 out of the reaction zone observed when the calculated binary interdiffusivity coefficients of H_2 and the various components was used. Although not a completely accurate representation of the diffusion phenomena of the multi-component species in this process, this approximation was determined to adequately capture the reaction-diffusion membrane reactor process.

8. Click **OK** in the **Maxwell-Stefan diffusivity matrix** dialog box.
9. Click the **wCO** tab. Enter **M_CO** and **–rCO*M_CO** in the **Molecular weight** edit field and the **Reaction rate** edit fields, respectively.

10. Click the **wH2O** tab. Enter **M_H2O** and **–rCO*M_H2O** in the **Molecular weight** edit field and the **Reaction rate** edit fields, respectively.
11. Click the **wH2** tab. Enter **M_H2** and **rCO*M_H2** in the **Molecular weight** edit field and the **Reaction rate** edit fields, respectively.
12. Click the **wCO2** tab. Enter **M_CO2** and **rCO*M_CO2** in the **Molecular weight** edit field and the **Reaction rate edit** fields, respectively.
13. Click the **wH2S** tab. Enter **M_H2S** in the **Molecular weight** edit field.
14. Click the **wHe** tab. Enter **M_He** in the **Molecular weight** edit field.
15. Click **OK**.

BOUNDARY CONDITIONS – NON-ISOTHERMAL FLOW

1. From the **Multiphysics** menu select **Non-Isothermal Flow**.
2. In the **Physics menu** select **Boundary Settings**.
3. Select boundary **#1** from the **Boundary selection** list and select the **Axial symmetry** boundary condition in the list.
4. Highlight boundary **#2**. From the **Boundary condition** list, select the **Inflow/outflow velocity** boundary condition. In the u_0 and v_0 edit fields enter **0** and **velo*(1-s^2)**, respectively.
5. Highlight boundary **#3**. From the **Boundary selection** list, select the **Normal flow/Pressure** boundary condition and enter **P_atm** in the $\mathbf{P_0}$ edit field.
6. Highlight boundary **#4** and select the **No Slip** Boundary condition.
7. Click **OK**.

BOUNDARY CONDITIONS – MAXWELL-STEFAN

1. Select **Maxwell-Stefan Diffusion and Convection** in the **Multiphysics** menu.
2. Select **Boundary Settings** from the **Physics** menu.
3. Highlight boundary **1** and select **axial symmetry** from the **Boundary condition** list. Make sure to click the tab for each component and select the axial symmetry for each one.
4. Highlight boundary **2** and select **Mass fraction** from the **Boundary condition** list. In the Mass fraction edit field (wCO_0), enter wCO_in. Repeat this process for the respective species by clicking on the various species tabs, selecting the mass fraction boundary condition, and entering wH2O_in, wH2_in, wCO2_in, wH2S_in, and wHe_in, in the corresponding edit fields.
5. Select **3** in the **Boundary selection** list and in the **Boundary condition** list and select the **convective flux** boundary condition**.** Repeat this process for all the species.
6. Select **4** in the **Boundary selection** list. Select **wH2** and select the **Flux** boundary condition from the **Boundary condition** list. Enter "**-W*M_H2*((cH2>0.001)*(cH2)^0.5)**" in the flux edit field.
7. Click **OK**

MESHING GEOMETRY

Because of the reactor's rectangular shape, a mapped mesh is a good choice for this model. The mapped mesh offers total control of the dimension and number of elements to be solved for.

1. From the **Mesh** menu select **Mapped Mesh Parameters**.
2. Click the **Boundary** tab.
3. In the **Boundary selection** list, highlight **1**, then select the **Constrained edge element distribution** checkbox. Enter 20 in the Number of edge elements edit field.
4. In the **Boundary selection** list, highlight **2**, then select the **Constrained edge element distribution** checkbox. Enter 10 in the Number of edge elements edit field.
5. Click **Remesh**, then click **OK**.

SOLVING MODEL

1. From the **Solve** menu select **Solver Parameters**.
2. Click the **Advanced** tab.
3. In the **Type of scaling** list select **Initial value based**.
4. Click **OK**.
5. Click the **Solve** button (=) on the Main toolbar.

PROCESSING AND VISUALIZATION

The default plot shows the velocity field in the domain. To generate the CO conversion plot as a function of residence time in Figure 51 of Chapter 5 (Case 1), the CO conversions at the exit of the reactor were plotted versus the corresponding residence times. The CO conversion at the exit of the reactor can be attained in two ways:

Line Plot of CO conversion

1. Select **Cross-Section Plot Parameters** from the **Postprocessin**g menu.
2. Click the **Line/Extrusion** tab.
3. Enter X in the **Expression** field.
4. Set the **Cross-section line data** according to the table below:

Property	Value
r0	0
r1	0
z0	0
z1	0.14

5. Click the **Line Settings** tab to select the line color.
6. Select the line color by clicking on the color tab.
7. Click **OK**.
8. Click **OK** again to generate the plot.
9. For the next condition, change the residence time by changing the reaction pressure (i.e. according to .Table 10 in Chapter 5 (Retentate pressures used in the simulations)).
10. To plot the CO conversions for the other residence times, repeat the previous steps by selecting **Cross-Section Plot Parameters** from the **Postprocessin**g menu.
11. In the **General** tab, check the **keep current plot** box
12. Click the **Line/Extrusion** tab.
13. Click the **Line Settings** tab to select the line color.
14. Select the line color by clicking on the color tab.
15. Click **OK**.

Surface plot of CO conversion

1. Open the **Plot Parameters** window from the **Postprocessing** menu.
2. On the **General** page, select **Surface** as **plot type**.
3. On the **Surface** page, type X2 in the **Expression** field.

Note that X calculates CO conversion based on the CO molar flow rates. Although this expression accurately calculates the conversion along the center axis of the reactor, it results in an erroneous surface CO conversion plot because of the no-slip boundary condition used in the Navier-Stokes equation which results in zero-velocity at the reactor walls. To generate a more realistic surface CO conversion, plot X2.

To generate the axial concentration profiles of the WGSR components shown in Figure 52 a to d in Chapter 5, take the following steps:

16. Select **Cross-Section Plot Parameters** from the **Postprocessing** menu.
17. Click the **Line/Extrusion** tab.
18. Enter xCO in the **Expression** field.
19. Set the **Cross-section line data** according to the table below:

Property	Value
r0	0
r1	0
z0	0
z1	0.14

20. Click the **Line Settings** tab to select the line color.

21. Select the line color by clicking on the color tab.
22. Click **OK**.
23. Click **OK** again to generate the plot.
24. To plot the concentration profile for the other species, repeat the previous step by selecting **Cross-Section Plot Parameters** from the **Postprocessin**g menu.
25. In the **General** tab, check the **keep current plot** box
26. Click the **Line/Extrusion** tab.
27. Type xH2 in the expression field.
28. Click **OK**.
29. Repeat this process for CO2 and H2O
30. For the next condition, change the residence time by changing the reaction pressure (i.e. according to .Table 10 in Chapter 5 (Retentate pressures used in the simulations)).
31. After the calculation is complete, repeat steps 1 to 14.
32. To plot the CO conversion along the length of the membrane reactor, select **Cross-Section Plot Parameters** from the **Postprocessin**g menu.
33. Type X in the **Expression** field.
34. Click the **Line Settings** tab.
35. Select the line color by clicking on the color tab.
36. Click **OK**.
37. Click **OK** again to generate the plot.
38. To generate the normalized velocity plot, go back enter V_n in the **Expression** field.

APPENDIX B

NOMENCLATURE

A	cross-sectional area [$6.72*10^{-6}$ m^2]
c_i	concentration of species i [mol/m^3]
E_A	activation energy [kJ/mol]
k_f	forward WGSR rate constant [$(m^3/mol)^{0.5}s^{-1}$]
k	H_2 permeance [$mol/m^2/s/Pa^{0.5}$]
k′	apparent H_2 permeance [$mol/m^2/s/Pa^{0.5}$]
K_{eq}	WGSR equilibrium constant
k_0	preexponential constant of WGSR [$(m^3/mol)^{0.5}s^{-1}$]
J_{H2}	rate of H_2 permeation [$mol/m^2/s$]
L	membrane reactor length [m]
M_i	molecular weight of component i [kg/mol]
N_{H2}	H_2 mass flux [$kg/m^2/s$]
P	reactor pressure [Pa]
P_atm	atmospheric pressure [Pa]
R	universal gas constant [J/mol · K]
rCO	WGSR rate expression [$mol/m^2/s$]
T	temperature [K]
T_{std}	standard temperature [K]
u	velocity vector (m/s)
velo	reactant superficial velocity in reaction zone [m/s]
v_1	reactant feed flow rate at STP [$3.33*10^{-6}$ m^3/s]
V_n	normalized gas velocity
x_i	mole fraction of component i

Greek symbols

β	approach to equilibrium factor

$$\beta = \frac{cCO_2 \; cH_2}{cCO \; cH_2O \; K_{eq}}$$

μ	viscosity [Kg/m·s]
υ_i	stoichiometric coefficient of species i
ρ	gas density [kg/m3]
$\omega_{i,}$	mass fraction of component i [kg_i/kg]
τ	residence time (s)

BIBLIOGRAPHY

Aasberg-Petersen, K., C. S. Nielsen and S. L. Jorgensen (1998). "Membrane reforming for hydrogen." Catalysis Today **46**(2-3): 193.

Abdalla, B. K. and S. S. E. H. Elnashaie (1993). "A membrane reactor for the production of styrene from ethylbenzene." Journal of Membrane Science **85**(3): 229.

Ainslie, N. G., R. E. Hoffman and A. U. Seybolt (1960). "Sulfur segregation at α–iron grain boundaries -- I." Acta Mettallurgica **8**: 523.

Ali, J. K., E. J. Newsom and D. W. T. Rippin (1994). "Exceeding equilibrium conversion with a catalytic membrane reactor for the dehydrogenation of methylcyclohexane." Chemical Engineering Science **49**(13): 2129.

Ali, J. K., E. J. Newson and D. W. T. Rippin (1994). "Deactivation and regeneration of Pd-Ag membranes for dehydrogenation reactions." Journal of Membrane Science **89**(1-2): 171.

Amandusson, H., L. G. Ekedahl and H. Dannetun (2000). "The effect of CO and O2 on hydrogen permeation through a palladium membrane." Applied Surface Science **153**(4): 259.

Anton, R., H. Eggers and J. Veletas (1993). "Auger electron spectroscopy investigations of segregation in Au-Pd and Ag-Pd alloy thin films." Thin Solid Films **226**: 39-47.

Antoniazzi, A. B., A. A. Haasz and P. C. Strangeby (1989). "The Effect of Adsorbed Carbon and Sulphur on Hydrogen Permeation Through Palladium." Journal of Nuclear Materials **162-164**: 1065.

Assabumrungrat, S., K. Suksomboon, P. Praserthdam, T. Tagawa and S. Goto (2002). "Simulation of a palladium membrane reactor for dehydrogenation of ethylbenzene." Journal of Chemical Engineering of Japan **35**(3): 263-273.

Barin, I. (1993). "Thermochemical data of pure substances."

Basile, A., G. Chiappetta, S. Tosti and V. Violante (2001). "Experimental and simulation of both Pd and Pd/Ag for a water gas shift membrane reactor." Separation and Purification Technology **25**(1-3): 549.

Basile, A., A. Criscuoli, F. Santella and E. Drioli (1996). "Membrane reactor for water-gas shift reaction." Gas. Sep. Purif. **10**(4): 243-254.

Basile, A., E. Drioli, F. Santella, V. Violante and G. Capannelli (1996). "A study on catalytic membrane reactors for water gas shift reaction." Gas. Sep. Purif. **10**(1): 53-61.

Basile, A., V. Violante, F. Santella and E. Drioli (1995). "Membrane integrated system in the fusion reactor fuel cycle." Catalysis Today **25**(3-4): 321.

Bracht, M., P. T. Alderliesten, R. Kloster, R. Pruschek, G. Haupt, E. Xue, J. R. H. Ross, M. K. Koukou and N. Papayannakos (1997). "Water gas shift membrane reactor for CO2 control in IGCC systems: techno-economic feasibility study." Energy Conversion and Management **38**(Supplement 1): S159.

Breckenridge, W., A. Holiday, J. Ong and C. Sharp (Feb. 2000). "Use of SELEXOL process in Coke Gasification to Ammonia Project." Presented at the Laurance Reid Gas Conditioning Conference.

Bryden, K. and J. Ying (2002). "Nanostructured palladium-iron membranes for hydrogen separation and membrane hydrogenation reactions." Journal of Membrane Science **203**: 29-42.

Burke, M. L. and R. J. Madix (1990). "Hydrogen on Pd (100)-S: the effect of sulfur on precursor mediated adsorption & desorption." Surface Science **237**(1-3): 1-19.

Bustamante, F., R. M. Enick, A. V. Cugini, R. P. Killmeyer, B. H. Howard, K. S. Rothenberger, M. V. Ciocco, B. D. Morreale, S. Chattopadhyay and S. Shi (2004). "High-Temperature Kinetics of the Homogeneous Reverse Water-Gas Shift Reaction." AIChE Journal **50**(5): 1028.

Bustamante, F., R. M. Enick, R. P. Killmeyer, B. H. Howard, K. S. Rothenberger, A. V. Cugini, B. D. Morreale and M. V. Ciocco (2005). "Uncatalyzed and wall-catalyzed forward water-gas shift reaction kinetics." AIChE Journal **51**(5): 1440.

Castro, F. J., G. Meyer and G. Zampieri (2002). "Effects of sulfur poisoning on hydrogen desorption from palladium." Journal of Alloys and Compounds **330-332**: 612-616.

Chen, F. L., Y. Kinari, F. Sakamoto, Y. Nakayama and Y. Sakamoto (1996). "Hydrogen permeation through palladium-based alloy membranes in mixtures of 10% methane and ethylene in the hydrogen." International Journal of Hydrogen Energy **21**(7): 555.

Chiesa, P., T. Kreutz and G. Lozza (2005). CO_2 sequestration from IGCC power plants by means of metallic membranes. ASME Turbo Expo. Reno-Tahoe, Nevada.

Copperthwaite, R. G., F. M. Gottschalk, T. Sangiorgio and G. J. Hutchings* (1990). "Cobalt Chromium Oxide: A Novel Sulphur Tolerant Water-Gas Shift Catalyst." Applied Catalysis **63**(1): L11.

Criscuoli, A., A. Basile and E. Drioli (2000). "An analysis of the performance of membrane reactors for the water-gas shift reaction using gas feed mixtures." Catalysis Today **56**(1-3): 53.

Dean, V. and M. Frenklach (1988). "Catalytic etching of Platinum Foils and Thin Films in Hydrogen-Oxygen mixtures." J. Phys. Chem. **92**: 5732-5738.

Dorris, S. E., T. H. Lee, S. J. Song, L. Chen and U. Balachandran (2006). "Development of dense cermet membranes for hydrogen separation." AIChE Spring National Meeting, Orlando Fl. April 23 – 27.

Edlund, D. (1996). A Membrane Reactor for H_2S Decomposition. Advanced Coal-Fired Power Systems '96 Review Meeting. Morgantown, West Virginia**:** 1-9.

Edlund, D., D. Friesen, B. Johnson and W. Pledger (1994). "Hydrogen-permeable metal membranes for high-temperature gas separations." Gas Separation & Purification **8**(3): 131.

Edlund, D. J. and W. A. Pledger (1993). "Thermolysis of hydrogen sulfide in a metal-membrane reactor." Journal of Membrane Science **77**(2-3): 255.

Ferreira-Aparicio, P., I. Rodriguez-Ramos and A. Guerrero-Ruiz (2002). "On the applicability of membrane technology to the catalysed dry reforming of methane." Applied Catalysis A: General **237**: 239.

Flytzani-Stephanopoulos, M., J. Meldon, Q. Fu, X. Qi and K. Kapoun (2003). "Water-gas shift with integrated hydrogen separation process." Annual Report to DOE, Grant # DE-FG2600-NT40819.

Flytzani-Stephanopoulos, M., X. Qi and S. Kronewitter (2004). "Water-gas Shift with Integrated Hydrogen Separation Process." Final Report to DOE, Grant # DE-FG2600-NT40819: 1-38.

Gaskell, D. (2003). "Introduction to the thermodynamics of materials." (4th edition).

Gobina, E. and R. Hughes (1994). "Ethane dehydrogenation using a high-temperature catalytic membrane reactor." Journal of Membrane Science **90**(1-2): 11.

Gobina, E. and R. Hughes (1996). "Reaction assisted hydrogen transport during catalytic dehydrogenation in a membrane reactor." Applied Catalysis A: General **137**(1): 119.

Golden, T. C., T. H. Hsiung and K. E. Snyder (1991). "Removal of Trace Iron and Nickel Carbonyls by Adsorption." Industrial & Engineering Chemistry Research **30**: 502.

Grabke, H. J. (2006). "Segregation and oxidation." Materiali in Technologije **40**(2): 39.

Grashoff, G. J., C. E. Pilkington and C. W. Corti (1983). "Purification of Hydrogen: A Review of the Technology Emphasizing the Current Status of Palladium Membrane Diffusion." Platinum Metals Review **27**(4): 157-169.

Gray, D. and G. Tomlinson (July 2002). "Hydrogen from coal."

Gryaznov, V. M. (1986). "Hydrogen permeable palladium membrane catalysts: An aid to the efficient production of ultra pure chemicals and pharmaceuticals." Platinum Metals Review **30**(2): 68.

Hara, S., K. Sakaki and N. Itoh (1999). "Decline in Hydrogen Permeation Due to Concentration Polarization and CO Hindrance in a Palladium Membrane Reactor." Industrial & Engineering Chemistry Research **38**: 4913.

He, G., Y. Mi, P. L. Yue and G. Chen (1999). "Theoretical study on concentration polarization in gas separation membrane processes." Journal of Membrane Science **153**: 243-258.

Hou, K. and R. Hughes (2002). "The effect of external mass transfer, competitive adsorption and coking on hydrogen permeation through thin Pd/Ag membranes." Journal of Membrane Science **206**(1-2): 119.

Howard, B. H., R. P. Killmeyer, K. S. Rothenberger, A. V. Cugini, B. D. Morreale, R. M. Enick and F. Bustamante (2004). "Hydrogen permeance of palladium-copper alloy membranes over a wide range of temperatures and pressures." Journal of Membrane Science **241**(2): 207.

Hurlbert, R. C. and J. O. Konecny (1961). "Diffusion of hydrogen through palladium." The Journal of Chemical Physics **34**(2): 655.

Itoh, N. (1995). "Limiting conversions of dehydrogenation in palladium membrane reactors." Catalysis Today **25**(3-4): 351.

Itoh, N., W.-C. Xu and K. Haraya (1992). "Basic experimental study on palladium membrane reactors." Journal of Membrane Science **66**(2-3): 149.

Jung, S. H., K. Kusakabe, S. Morooka and S.-D. Kim (2000). "Effects of co-existing hydrocarbons on hydrogen permeation through a palladium membrane." Journal of Membrane Science **170**(1): 53.

Kajiwara, M., S. Uemiya and T. Kojima (1999). "Stability and hydrogen permeation behavior of supported platinum membranes in presence of hydrogen sulfide." International Journal of Hydrogen Energy **24**: 839.

Kamakoti, P., B. Morreale, M. Ciocco, B. Howard, R. Killmeyer, A. Cugini and D. Sholl (2005). "Prediction of hydrogen flux through sulfur-tolerant binary alloy membranes." Science **307**: 569.

Kikuchi, E. (2000). "Membrane reactor application to hydrogen production." Catalysis Today **56**(1-3): 97.

Kikuchi, E., S. Uemiya, N. Sato and H. Inoue (1989). "Membrane reactor using microporous glass-supported thin film of palladium. Application to the water gas shift reaction." Chemistry Letters: 489.

Krasko, G. L. (1997). "Effect of impurities on the electronic structure of grain boundaries and intergranular cohesion in iron and tungsten." Materials Science and Engineering A **234-236**: 1071-1074.

Kulprathipanja, A., G. Alptekin, J. Falconer and D. Way (2005). "Pd and Pd-Cu membranes: inhibition of H_2 permeation by H_2S." Journal of Membrane Science **254**: 49-62.

Lee, W. H. (2002). "Oxidation and sulfidation of Ni_3Al." Materials Chemistry and Physics **76**: 26.

Li, A., W. Liang and R. Hughes (2000). "The effect of carbon monoxide and steam on the hydrogen permeability of a Pd/stainless steel membrane." Journal of Membrane Science **165**(1): 135.

Li, Y., Q. Fu and M. Flytzani-Stephanopoulos (2000). "Low-temperature water-gas shift reaction over Cu- and Ni-loaded cerium oxide catalysts." Applied Catalysis B: Environmental **27**(3): 179.

Lin, W.-H. and H.-F. Chang (2004). "A study of ethanol dehydrogenation reaction in a palladium membrane reactor." Catalysis Today **97**(2-3): 181.

Lin, Y.-M. and M.-H. Rei (2001). "Study on the hydrogen production from methanol steam reforming in supported palladium membrane reactor." Catalysis Today **67**(1-3): 77.

Lüdtke, O., R.-D. Behling and K. Ohlrogge (1998). "Concentration polarization in gas permeation." Journal of Membrane Science **146**: 145 - 157.

McKinley, D. L. (1967). Metal alloy for hydrogen separation and purification. U.S.A. **US Patent 3,350,845**.

Michaels, A. S. (1968). Chemical Engineering Progress **64**: 31.

Moe, J. M. (1962). "Design of water-gas shift reactors." Chemical Engineering Progress **58**(3): 33.

Morreale, B. (2006). "The influence of hydrogen sulfide on palladium and palladium-copper alloy membranes." Ph.D. Thesis, The University of Pittsburgh, Department of Chemical Engineering.

Morreale, B. D., M. V. Ciocco, R. M. Enick, B. I. Morsi, B. H. Howard, A. V. Cugini and K. S. Rothenberger (2003). "The permeability of hydrogen in bulk palladium at elevated temperatures and pressures." Journal of Membrane Science **212**(1-2): 87.

Morreale, B. D., M. V. Ciocco, B. H. Howard, R. P. Killmeyer, A. V. Cugini and R. M. Enick (2004). "Effect of hydrogen-sulfide on the hydrogen permeance of palladium-copper alloys at elevated temperatures." Journal of Membrane Science **241**(2): 219.

Mundschau, M., X. Xie, C. R. Evenson and A. F. Sammells (2006). "Dense inorganic membranes for production of hydrogen from methane and coal with carbon dioxide sequestration." Catalysis Today **118**(1-2): 12-23.

Mundschau, M., X. Xie and A. Sammells (April, 2005). "Advances in hydrogen separation membrane technology for the separation of CO_2 and the purification of hydrogen produced from coal." Proceedings of the 30th International Technical Conference on Coal Utilization & Fuel Systems.

Musket, R. G. (1976). "Effects of contamination on the interaction of hydrogen gas with palladium: A review." Journal of the Less-Common Metals **45**: 173.

Myles, K. M. and J. B. Darby (1968). "Thermodynamic properties of solid palladium-copper and platinum copper alloys." Acta Mettallurgica **16**: 485.

Paglieri, S. N. and J. D. Way (2002). "Innovations in palladium membrane research." Separation and Purification Methods **31**(1): 1.

Piccolo, L., A. Piednoir and J. Bertolini (2005). "Pd-Au single-crystal surfaces: Segregation properties and catalytic activity in the selective hydrogenation of 1,3-butadiene." Surface Science **592**: 169-181.

Rodriguez, J. C., J. Santamaria and A. Monzon (1997). "Hydrogenation of 1, 3-butadiene on Pd/SiO_2 in the presence of H_2S deactivation & reactivation of the catalyst." Journal of Membrane Science **165**(1-2): 147-157.

Sakamoto, Y., F. L. Chen, Y. Kinari and F. Sakamoto (1996). "Effect of carbon monoxide on hydrogen permeation in some palladium-based alloy membranes." International Journal of Hydrogen Energy **210**(11&12): 1024.

Seok, D. R. and S. T. Hwang (1990). "Studies in surface science and catalysts, in: Future Opportunities in Catalytic and Separation Technology." 248-267.

Shah, Y. T. (1970). Chemical Engineering Science(25): 1947.

Swartzfager, D. G., S. B. Ziemecki and M. J. Kelley (1981). "Differential sputtering and surface segregation: The role of enhanced diffusion." Journal of Vacuum Science & Technology **19**(2) 185.

Taylor, J. (1985). "Phase relationship and thermodynamic properties of the Pd-S system." Metallurgical Transactions B **16B**: 143.

Tosti, S., A. Basile, G. Chiappetta, C. Rizzello and V. Violante (2003). "Pd-Ag membrane reactors for water gas shift reaction." Chemical Engineering Journal **93**(1): 23.

Tosti, S., V. Violante, A. Basile, G. Chiappetta, S. Castelli, M. De Francesco, S. Scaglione and F. Sarto (2000). "Catalytic membrane reactors for tritium recovery from tritiated water in the ITER fuel cycle." Fusion Engineering and Design **49-50**: 953.

Uemiya, S., N. Sato, H. Ando and E. Kikuchi (1991). "The water gas shift reaction assisted by a palladium membrane reactor." Industrial & Engineering Chemistry Research **30**(3): 585.

Wang, D., T. B. Flanagan and K. L. Shanahan (2004). "Permeation of hydrogen through pre-oxidized Pd membranes in the presence and absence of CO." Journal of Alloys and Compounds **372**: 158.

Wei, T. and J. Phillips (1995). "Thermal and catalytic etching mechanisms of metal catalyst reconstruction." Advances in Catalysis **41**: 359.

Wu, N. L. and J. Phillips (1985). "Catalytic etching of platinum during Ethylene oxidation." Journal of Physical Chemistry **89**: 591-600.

Xue, E., M. O'Keeffe and J. R. H. Ross (1996). "Water-gas shift conversion using a feed with a low steam to carbon monoxide ratio and containing sulphur." Catalysis Today **30**(1-3): 107.

Zhang, J., D. Liu, M. He, H. Xu and W. Li (2006). "Experimental and simulation studies on concentration polarization in H_2 enrichment by highly permeable and selective Pd membranes." Journal of Membrane Science **274**: 83-91.

Ziemecki, S. B., G. A. Jones, D. G. Swartzfager and R. L. Harlow (1985). "Formation of Interstitial Pd-Cu Phase by Interaction of Ethylene, Acetylen, and Carbon Monoxide with Palladium." Journal of the American Chemical Society **107**: 4547.